DYNAMIC BEHAVIOUR OF SOLIDS IN A SINGLE SCREW EXTRUDER:

ASPECTS OF HEAT TRANSFER

DYNAMIC BEHAVIOUR OF SOLIDS IN A SINGLE SCREW EXTRUDER:

ASPECTS OF HEAT TRANSFER

By

ABDULLAH S. ALOTAIBI, B. ENG.

(Mechanical Engineering)

King Saud University, Riyadh, Saudi Arabia

A Thesis

Submitted to the School of Graduate Studies

in Partial Fulfillment of the Requirements

for the Degree

Master of Applied Science

McMaster University

MASTER OF APPLIED SCIENCE (2008) McMaster University

(Chemical Engineering) Hamilton, Ontario

TITLE: Dynamic behaviour of Solids in a Single Screw Extruder: Aspects of Heat Transfer

AUTHOR: Abdullah S. Alotaibi, B.Eng. (King Saud University, Riyadh)

SUPERVISOR Dr. M. R. Thompson

NUMBER OF PAGES: xiv, 143

Abstract

Effective heat transfer through a bed of particulate solid largely affects the production rate and the process stability in an extrusion process. Most classical models in single screw extrusion treat the solids bed as a continuum behaving as an elastic plug or fluid while neglecting the discrete nature of the particles and the presences of the fluid. The heat transfer within the solids bed in these models is calculated based on thermophysical properties of the bulk system without consideration for the presence of the interstitial fluid. From a practical point of view, experimental measurements of solids bed heat transfer within a rotating screw, particularly cross channel, as the bed moves down the length of the solids conveying zone are impossible to perform.

A new device was designed to model the radial compressive stresses and shear stresses on a solids bed of plastics, similar to the environment within the screw channel of a single screw extruder. This device enables the user to visualize the nature of the solids bed under different experimental conditions through a transparent wall. Also, the device provides ways to explore the heat transfer in a solids bed under different conditions by embedded thermocouples on the top or through the front wall of the containing chamber.

The results reported in this study have shown that the discrete nature of the solid bed has a strong affect on the heat transfer within the bed. The rate of heat transfer within the different beds of polymer did not appear dominated by the thermophysical properties of the materials. Rather, the evidence supports that conduction through the pseudo-static interstitial fluid (i.e. air) dominated the rate at which a polymer bed heats up; a finding similarly found for the sintering of powdered metals and ceramics in the literature. This finding would imply that differences in melting rates found in extruders are not related to the heat transfer in the solids bed; however, this statement only holds true so long as the granules making up the bed remain static (i.e. plug-like) and do not circulate within the screw channel. Quite interestingly, pellet circulation within the solid bed was observed in LLDPE over a range of test conditions. This pellet circulation resulted in enhanced heat transfer within the bed of LLDPE (a raise of 10°C) compared to PS and PP. PP exhibited pellet circulation but only over a small window of operation.

Different ways to improve heat transfer within solid bed were subsequently tested in this project, such as starve feed, forced convection and spherical particle. From this work, improved understanding of heat transfer in the solids conveying zone of a single screw extruder was gained.

Acknowledgements

I wish to express my sincere appreciation to my supervisor, Dr. M. R. Thompson for his constant guidance, advice, encouragement, and support. I am grateful to Dr. John Vlachopoulos for his comments and valued assistance. I would like to thank my employer SABIC, Saudi Arabia for financial support. Mr. Pete Pelletier form Toshiba is acknowledged for his technical assistance.

Moreover, I would like to thanks to Elizabeth Takacs for providing me with training and for her help .I would like to thank Mr. Paul Gatt, Mr. Gordon Slater and Mr.Douglas Keller their support and help in designing and fabrication of the simulator. I would like to express my sincere thank to my friends Tayyab and Hashemi for their valued assistance and Junfeng for his assistance in discrete element modeling. Also, I would like to thank my colleagues in Mechanical Engineering McMaster University and especially Ahmed Omar for his comments and help. Thanks are also extended to my colleagues in polymer processing group and the staff in Chemical Engineering department and MMRI for their kind support.

Finally, I would like to thank my family: my wife, my little daughter and my parents for their support and help

Table of contents

List of Figures

List of Tables

Chapter 1

1. Introduction

1.1Single screw extruder

The single screw extruder is the most common polymer processing machine in the plastic industry. This machine can be a part of many extrusion processes such as film blowing, pipe and sheet extrusion. Also, it is a fundamental step in other processes such as blow molding and injection molding.

The single screw extruder consists of a hopper, a barrel enclosing a rotating screw, and a die at the end of extruder. One can divide the single screw extruder from the functional point of view into three main zones

1- The solid conveying zone
2- The melting zone
3- The melt conveying zone

A typical schematic diagram of a single screw extruder is shown in Figure1. The screw generally has a constant depth in the solid conveying zone and then the depth gradually decreases along the melting zone. This decrease in screw channel depth provides compressive forces which help in melting the polymer. In the melt conveying zone the channel depth becomes constant. The function of the solid conveying zone is to transport the pellets or powder from the hopper to the screw channel, compact them and form a solid bed. At the start of the melting zone, the polymer in contact with the hot barrel melts forming a thin film of molten polymer in the gap between the solid bed and the barrel. If this film gets thicker than the gap between the barrel and the wiping screw flight, a melt pool will form at the retreating side of the solid bed. The thin film, which usually has a high melt viscosity, is exposed to a high shear stress that results in high viscous dissipation and the generated heat is utilized to melt the solid bed. Then the melted polymer is mixed and homogenized in the melt convey zone and finally pumped through the die (Vlachopoulos and Strutt, 2003).

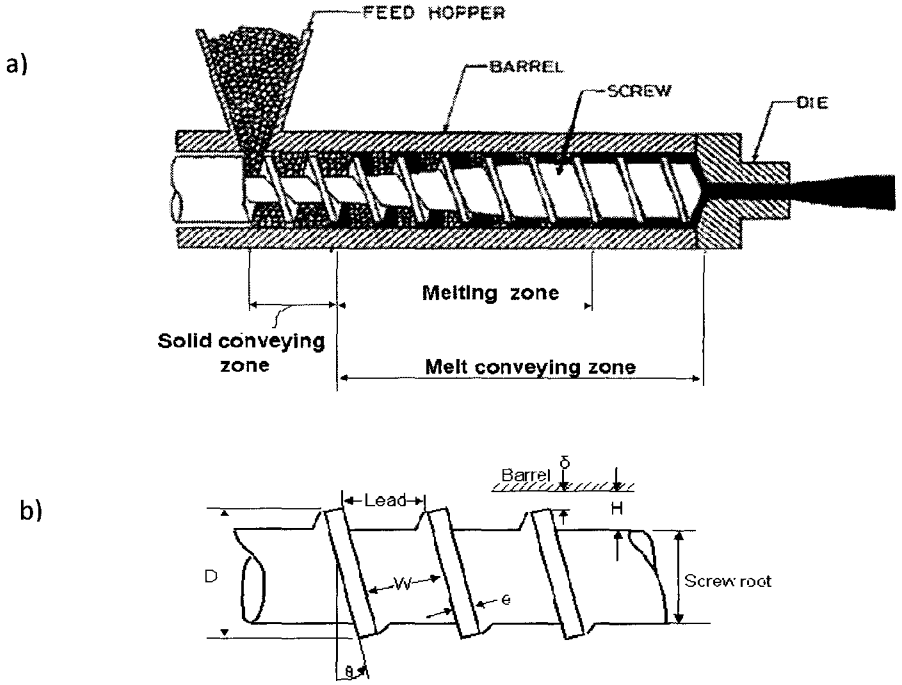

Figure 1.1 Schematic of single screw extruder A) schematic of single screw extruder b) a screw channel geometry ; **d** is the screw diameter, **w** is the channel width, **e** is flight width δ is the flight clearance, **θ** is the helix angle, and **h** is the channel depth (adapted from Vlachopoulos and Strutt,2003)

The output rate in single screw extruder is determined by the combined effectiveness of the three zones, so keeping a balance between these zones is essential to achieve a stable operation (Tadmor et al, 1967). Of the three zone, it is most commonly the case that melting is the rate limiting mechanism. In this context an understanding of the melting mechanism is essential for a designer. The melting mechanism in single screw extruder has attracted many researcher and scientists from both industry and academia. Earlier studies on melting in a single screw extruder (Maddock, 1956; Tadmor et al, 1967; Chung, 1970; Donovan ,1971; Sundstrom and Lo, 1978) and recent studies (Syrjala, 2000, Zitzenbacher and Langecker,2005) have improved and enhanced the science and design of single screw extruders. For instance, Figure 2 shows the development of melt throughput in Low Density Polyethylene (LDPE) blown film single screw extrusion as a function of screw diameter from 1955 to 1995 (White and Potente, 2002). The world's largest single screw extruder built so far has a screw diameter of 600 mm, and was designed to extrude 29 metric tonnes/h (Kruder,1985).

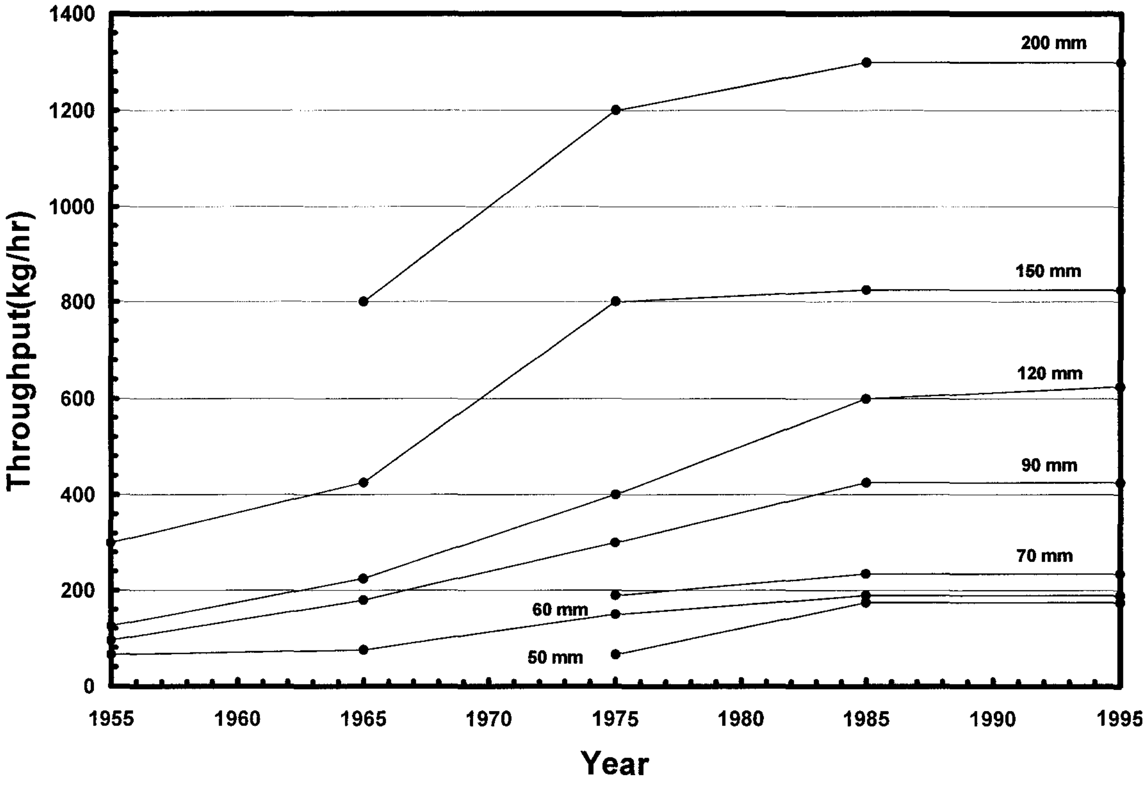

Figure 1.2 Development of melt throughput in LDPE blown film single screw extrusion as function of screw diameter (adapted from White and Potente, 2003)

A better understanding of melting mechanisms has led to radical changes in screw design from the classic metering screw. An example of this was the development of the barrier screw by Maillefer in the 1959 (Rauwendaal,1996). The then-novel concept of this screw was to split the screw channel by a barrier flight so that the unmelted plastic (i.e. solid) and melt were separated. The clearance between the barrel and barrier flight is larger than the main flight so that the melt plastic can more readily travel over the barrier flight into the melt channel. At the beginning of the barrier section, the solid channel width is larger than the melt channel. As the solids move along the screw towards the die the size of the melt channel increases compared to the solids channel until the solid channel disappear and the melt takes over the whole channel. This major development in screw design helped in improving the quality of the melt and the throughput by most notably minimizing the occurrence of solid bed breakup during melting. The solid bed break up may happen with conventional screws with a deep metering section and short length to diameter ratio (Rauwendaal, 2005)

The improvement in melting rate in recent times has been largely influenced by improved heat transfer through the solid bed. The solids bed in a single screw extruder typically consists of a granular bed of polymer pellets (or powder in some cases) and an interstitial fluid (typically entrained air). However, most of the developed models for single screw extrusion processes treat such a solid bed as a continuum assuming its behaviour can be described by an elastic plug or fluid (Tadmor et al,,1967; Darnell and Mol,1956) while neglecting the discrete nature of the particles and the presences of the fluid. These models consider the solid's thermophysical properties without taking into account the interstitial fluid or the limited contact area between touching particles.

Heat transfer studies within granular media in other fields such as steel, ceramic and glass (Argento and Bouvard, 1996) have shown that the influence of the fluid cannot be ignored in heat transfer. An effective thermal conductivity based on the solids and fluid thermal properties was found to improve the accuracy of continuum models (Gonzo, 2002). The effective thermal conductivity was found to be influenced by several factors such as: bed particle size, the fluid type and pressure, applied load, internal stress and the contact mechanism (Rao and Toor, 1987; Buonanno et al, 2003; Tehranian et al, 1994; Vargas and McCarthy, 2001).

Recent investigations (Moysey and Thompson, 2004) using discrete element modeling (DEM) have shown that the granular nature of the solid bed influences transport in the solid conveying zone of an extruder. The existence of dynamic behavior in the solid flow in the form of solid pulsing and recirculation in the feed throat was properly visualized by this modeling technique. More recently, using experimental and modeling methods it was found that an effective thermal conductivity calculated by taking into account the interstitial air in a solid bed predicts the temperature rise more accurately than assuming the thermal conductivity of the continuum (Moysey ,Ph.D. thesis, 2007). Hence, effective heat transfer is a major factor in the melting mechanism and improvement in it's modeling can help towards better design and operation of a single screw extruder. This is expected to have a considerable economic impact in the processing of polymers.

1.2 Research objective

The objective of this project is to investigate the heat transfer within the solid bed of selected semi crystalline and amorphous polymers under different operational modes. More specifically, the influence of varying barrel temperature, different feeding modes (starve vs. flood), influence of shear and consolidation forces, and the effect of forced convection on heat transfer within a solid bed were studied. For this investigation, a new apparatus capable of simulating two of the three principle forces (tangential shear and radial compression) on a solid bed within a screw channel was designed and built. All heat transfer data reported was collected using this device.

Effective heat transfer through a bed of particulate solid largely affects the production rate and the process stability in an extrusion process. Better understanding of heat transfer can positively impact modeling and design of a single screw extruder. This is expected to have a considerable economic impact in the processing of polymers.

1.3 Thesis Outline

This thesis is comprised of five chapters including the above introduction. Chapter 2 presents a literature review of different aspects of heat transfer and proposed melting mechanisms within a single screw extrusion process. A detailed description of the specially built device used in this study is described in Chapter 3. Chapter 4 presents the results along with meaningful discussion. This is followed by conclusions in the final chapter.

Chapter 2

2.Literature review

2.1 Mechanisms of heat transfer in granular media

Effective heat transfer through a bed of solids largely affects the production rate and the process stability in an extrusion process. The solids bed of a single screw extruder by its nature is a granular assembly that consists of solids (i.e. pellets) and an interstitial fluid (i.e. air). This bed is constrained top-to-bottom between the barrel and screw root, and in width between two flights walls, producing a rectangular cross-section. Researchers who have studied and modeled single screw extrusion processes have treated such a system as a continuum behaving as an elastic plug or fluid while neglecting the discrete nature of the particles and the presences of the fluid (Tadmor et al.,1967; Darnell and Mol, 1956). Classical models use the solid thermophysical properties of the bulk system without consideration for the presence of the interstitial fluid.

Modes of heat transfer within a packed bed with a stagnant interstitial fluid can be classified into (Yagi & Kunii, 1957; Morlerus, 1997): i) conduction through the solid particles, ii) conduction through the contact area between two touching particles, iii) radiation between adjacent voids, iv) conduction through the stagnant interstitial fluid and the solids, and v) convection due to fluid movement.

The first and the second mechanism will be dominant if the following assumption is valid (Batchelor and O'Brien, 1977):

$$\frac{k_s a}{k_f r} >> 1 \tag{2.1}$$

where $\mathbf{k_s}$ is the conductivity of the solid phase, the $\mathbf{k_f}$ is the conductivity of the fluid phase, **a** is the contact radius between two adjacent particles and **r** is the radius of the particle. This condition is true at high conductivity ratios ($\mathbf{k_s/k_f}$) or under vacuum conditions.

In general, experimental and numerical studies in the area of granular heat transfer for steel, ceramic and glass materials (Argento and Bouvard,1996,) have shown that the predicted heat transfer is largely affected by the presences of the fluid whether it's moving such as in the case of fluidized beds (Yusuf et al, 2005) or stagnant (Molerus, 1997). Only under excessive compression does this mode of heat transfer vanish as the voids in the bulk system become too small. The thermophysical properties of such systems which contain both fluid and solids are completely different from those of solids alone (Rao and Toor, 1987).

An effective thermal conductivity based on the solid and fluid thermal properties was found to improve the accuracy of modelling (Gonzo, 2002). Results in literature showed that the effective thermal conductivity is influenced by several factors such as; bed particle size, the fluid type and pressure, the applied load, the internal stress and the contact mechanism (Rao and Toor, 1987 Buonanno et al, 2003 Tehranian et al, 1994 Vargas and McCarthy,2001).

Toor and Rao (Rao and Toor, 1987) reported that the heat transfer rate from a hot particle to other discrete particles in bed of comparable particle size was half of the value described by classical continuum theory and only when the size of the hot particle is much larger than the bed particles the heat transfer can be described by the classical continuum theory. Beside particle size, the exterior roughness of a particle has an influence on the effective thermal conductivity. For example, it has been shown for a packed bed that the effective thermal conductivity was significantly higher for smooth steel spheroids than for rough ones due to diminishing of the thermal contact resistance between the spheroids (Buonanno et al, 2003).

The type and the pressure of the interstitial fluid influence the effective thermal conductivity of a bulk system. As the gas pressure within the bulk system increases, so too does the effective thermal conductivity (Vargas and McCarthy, 2002) and this increase is a function of the solid-gas ratio. On the other hand, the effective thermal conductivity of a bed of aluminum granular in the presence of air was lower than the same system in the presence of helium (Tehranian et al, 1994).

In addition to the above factors, the effective conductivity in a granular media is strongly influenced by the interparticle forces and whether the particles exhibited elastic, plastic, elasto-plastic and visco-elastic contact mechanisms. Hertzian mechanics stipulates that an elastic contact is defined by its contact radius (**a**) between two adjacent particles as (Vargas and McCarthy, 2001):

$$2a = \left[\frac{3F_n r}{4E}\right]^{1/3} \tag{2.2}$$

where $\mathbf{F_n}$ is the normal force acting between the particles centers, **E** is the effective Young's modulus and **r** is the radius of the particle. This indicates that the contact area increases with increasing load on the particles and thereby enhances the heat transfer. The effect of the applied load on the effective thermal conductivity was studied by Tehranian et al (1994) using a bed of aluminum particles in the presence of air. They found that the thermal conductivity increased by factor of 5.2 when the applied load was raised from 0 to 1.36 MPa.

Not only the load but also the distribution of load has been found to tremendously influence the heat transfer in a granular media (Vargas and McCarthy, 2001). Stress distributions within an assembly of granular bed demonstrated non-uniformity, in which the load is concentrated in some areas and not evenly distributed throughout the material as in the case of a continuum. These routes along which the load is supported are called stress chains (Roessing et al,2002). Vargas and McCarthy (2001) studied the effect of the stress on the conductivity within a particulate bed of stainless steel particles under uniaxial compression and vacuum experimentally and by discrete particle simulations. They observed that the conductivity of particles have an anisotropic behaviour. The heterogeneities in stress chains caused non-uniformity in heat transfer which subsequently affected the temperature distribution. For example, the stress chains in the horizontal direction acted as barriers to heat transfer hindering heat transfer in the vertical direction, as shown in Figure 2.1. However, they found that the degree of anisotropy decreased with increased applied load, primarily due to rearrangements of the particle packing.

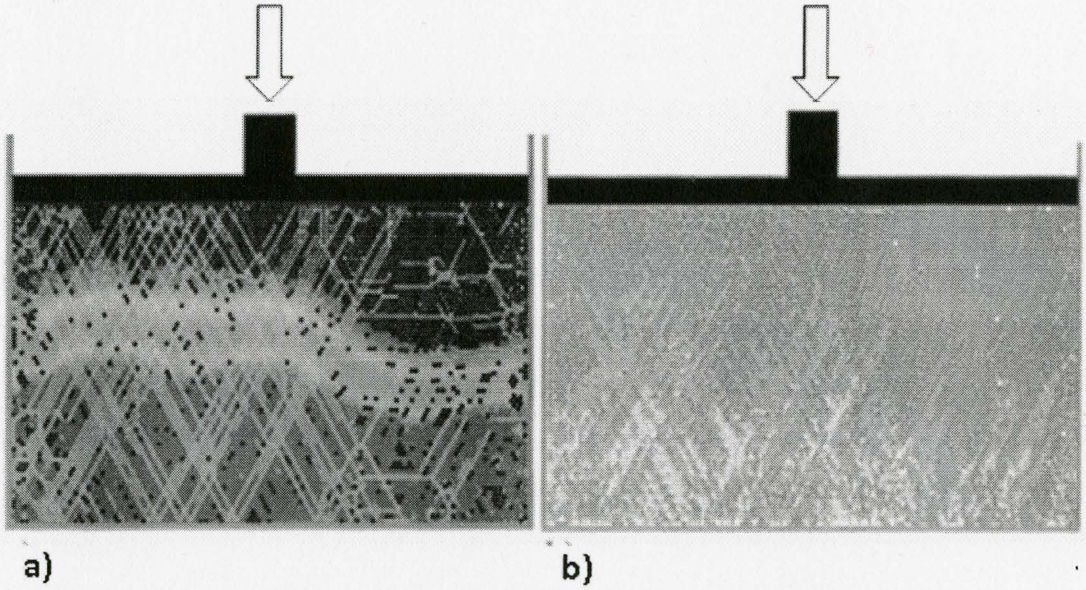

Figure 2.1 Effect of stress chains on heat propagation from bottom to top of a granular bed. (a) The temperature field where the white lines represent particle contacts which experience larger than average stress. Note the temperature in the left-hand side propagated further than the right-hand side. (b) Shows the heat flow through the particle bed. Heat flow is high in the left-hand side (Vargas and McCarthy, 2001).

Similarly, the stress distributions within a solid bed in single screw extruder have been found to exhibit anisotropic stresses which are a function of temperature (Spalding et al, 1997; Moysey, 2007). Obtaining efficient heat transfer and a uniform temperature distribution within the solid bed are important factors in determining the onset of melting and the rate of melting in a single screw extruder.

2.2 Melting of polymer

Conductive and convective heat transfer within a bed of polymer solids has vital importance to the operation of a single screw extruder. Heated from the barrel and screw as well as by the interstitial gas, the polymer bed increases in temperature and softens. Melting follows, and depending on the type of extruder this can be achieved by differing modes of thermal and mechanical energy transfer. Polymer melting is a fundamental step in polymer processing and critical for determining the output rate. Most of the mechanical power input (more than 50%) is consumed in assistance of this step. The homogeneity and stability of the end product greatly depend on melting (Gogos et al, 1998).

The thermal energy required to achieve melting of polymers can be estimated from specific enthalpy curves similar to those shown in Figure 2.2. Depending on whether the polymer is semi crystalline (ex. polypropylene, PP) or amorphous (ex. polystyrene PS) the required energy varies. In general, semi crystalline polymers need more energy to achieve melt state compared to their amorphous polymer counter partner. For example, the required thermal energy to heat up PP to 200 °C is about 600 kJ/kg while it is only 350 kJ/Kg for polystyrene to heat it up to the same temperature (Qian & Gogos, 2000)

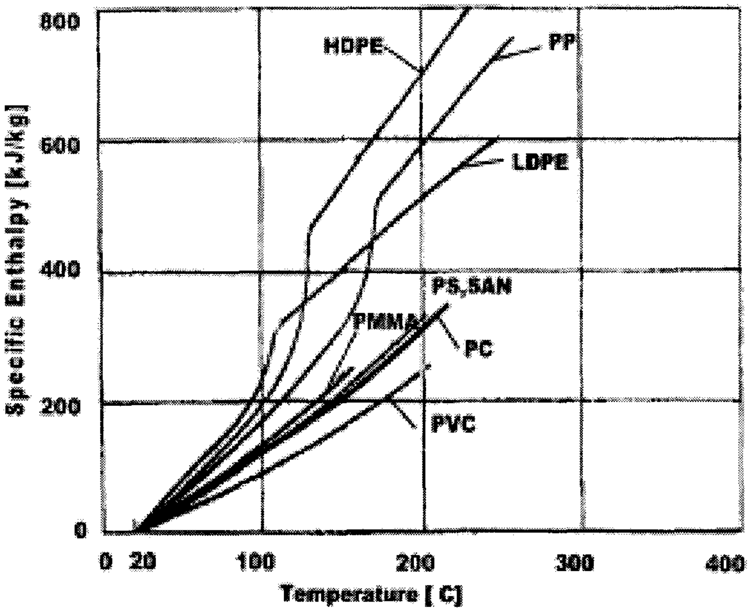

Figure 2.2 Specific enthalpy of different polymers (adapted from Qian & Gogos, 2000)

The melting of solid polymers against a hot moving surface was described by Tadmor and Gogos (2007) as follows: when the solid polymer is in contact with the hot surface a thin layer of molten polymer will form due to conduction. When this surface moves, the movement of this surface creates shear forces in the melt layer. The shearing of the molten layers (i.e. flow deformation) generates heat. This is known as viscous energy dissipation (VED) resulting from the irreversible dissipation of the mechanical energy.

VED has a major role in heating up the polymer since most polymers are highly viscous and are usually processed at high shear rates. The thermal energy equation that governs the melting can be written as (Qian & Gogos, 2000):

$$\rho C_p \frac{DT}{Dt} = (\nabla k.\nabla T) + (\tau : \dot{\gamma}) + \dot{S} \tag{2.3}$$

Where is **ρ** the density, **C_p** heat capacity ,**k** thermal conductivity of the solid polymer, τ is the shear stress tensor , $\dot{\gamma}$ is the shear rate tensor and the last term $\dot{S}$ is for any other thermal sources. The left hand side of this equation represent the increase in the internal energy, while the right hand side terms $(\nabla k.\nabla T)$ and $(\tau : \gamma)$ represent the heat conduction and the irreversible VED, respectively.

Other forms of mechanical energy dissipation have been recognized. Gogos et al (1998) reported energy dissipation in solids which significantly raised the feed polymer temperature. These dissipative losses could be in the form of plastic energy dissipation (PED) where individual particles are plastically deformed and/or by friction between solid particles defined as frictional energy dissipation (FED).

PED and FED can be written as (Gogos et al, 1998):

$$PED = \frac{d}{dt}\int_{\varepsilon}^{\varepsilon+\delta\varepsilon} \sigma_{\upsilon}(\dot{\varepsilon})\, d\varepsilon \tag{2.4}$$

where **σ_v** is the stress spent generating plastic and **ε** is the effective applied deformation.

$$FED = n\, p\, f\, F_n \Delta\upsilon \tag{2.5}$$

where **n** is the contact points per unit volume, **p** is the number of particles per unit volume, **f** is the interparticle kinematics frictional coefficient, **F_n** is the normal force and **Δv** is the average relative velocity of the particles in the unit volume.

The effect of PED in raising polymer temperature was evaluated by Gogos et al (1998). In their experiment, the evaluation was done on moulded cylindrical polymer samples (diameter 10 mm, height 7 mm) by uniaxial compression. Three different polymers, PS, PE and PP were used in this evaluation. The rise in temperature of the samples was measured by a thermocouple imbedded in the center of the sample. The recorded rise in the sample temperature from room temperature at engineering strain of 0.9 was 35°C for PS, 14 °C for PP and 5°C for LDPE. Qian and coworkers (Qian et al,2003) further expanded on this work with the assumption that all of the compression energy input contributed to temperature rise as PED. They found that the input energy at an engineering strain of 0.8 was enough to raise their Linear Low Density Polyethylene (LLDPE) sample to 40°C and their PS sample to 93 °C almost to its glass temperature.

Cheng et al (1977) observed the effect of FED for several polymers at conditions typical of extrusion using an instrument where a plug is pushed against a rotating roll. Their data showed that frictional energy dissipation at high roll speed and high pressure was enough to melt the polymer even at roll temperature below the thermodynamic melting point of the polymer.

PED and FED are assumed to be the dominant source of heat in intermeshing co rotating twin screw extruder. Experimental work carried out by Qian et al (2000) on a twin screw extruder showed the important role of these two modes of mechanical energy dissipation on the heating/melting of polymers. The experiments were conducted on a twin screw extruder with three barrel section. Only one heating unit was used and the others were kept off. The rise in barrel temperature was recorded against different feed rates of PP (powder and pellet) and PS (pellet), as shown in Figure 2.3. The low increase of temperature for PP powder compared to PP pellet was attributed to its smaller size which had less possibility to deform and be trapped in a kneading block element, resulting in lower PED.

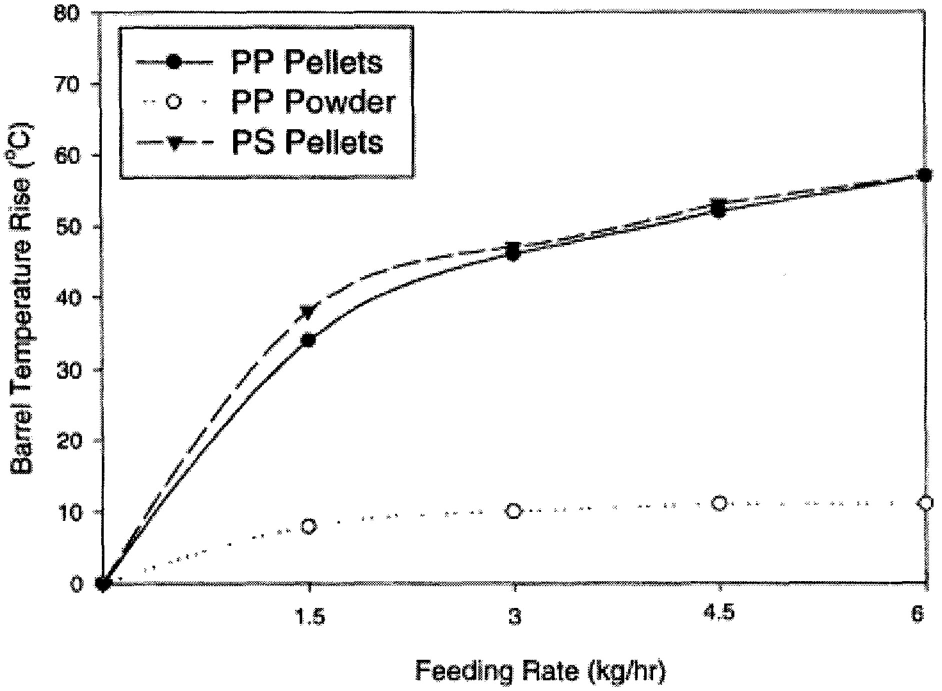

Figure 2.3 Barrel temperature raise for different materials at different rates (adapted from Qian et al , 2000)

In a single screw extruder the contribution of PED was suggested to be less effective compared to a twin screw extruder (Gogos et al, 2002). This was attributed to the formation of the melt film between the hot barrel and the solid bed within the single screw extruder which acted as a lubricant allowing slippage of the bed against the barrel surface, and therefore resulting in less deformation.

2.2.1 Melting in single screw extruder (melting under shear)

The first study aimed at understanding the melting mechanism within a single screw extruder dates back to 1959 when Maddock (1959) reported his visual observations based on screw freezing experiments. The procedure of these experiments involved stopping an extruder operating under steady state conditions and quickly cooling down the barrel and screw to solidify the molten polymer in the screw channel. The screw was later pushed out of the barrel and the solidified polymer unwrapped for analysis. In some cases there is a need to heat up the barrel to the melting point for this technique in order to help push out the screw. He observed that the solids were separated from the melt in the melting zone. The solid particles were segregated to a bed at the trailing flight while the melt phase accumulated at the leading flight creating a melt pool. The width of that solid bed gradually diminished whereas the melt pool width correspondingly increased in the down channel direction (Tadmor et al, 1967).

Based on these observations Tadmor (1967) developed the first quantitative model that predicts melting in a single screw extruder. The model predicts the solid bed profile (SBP) (i.e. width) in the screw channel of a typical single screw extruder. The main assumption of this model is that the solid particles are compacted together to form a solid plug which moves together as a continuous solid despite the granular nature of the bed. The melting rate was found to be proportional to the square root of screw channel width in other words to the available contact area between the solid bed and the barrel surface (Tadmor et al, 1976). However, further increases in the channel width may lead to solid bed break up which affects the quality of the product (Kruder G., 1985). The melting mechanism described is known as conductive melting with forced melt removal (i.e drag flow with forced melt removal) (Tadmor and Gogos,2006). The heat transfer source for melting/heating in this model is conduction through the solid-melt interface and viscous dissipation in the melt film.

The theory based on this assumption named as a continuous melting is more likely to occur in single screw extruder. The other melting theory is based on disperse melting where the solid particles are not continuous but dispersed in the melt phase (Rauwendaal, 1996). The disperse melting is more likely to be applicable in twin screw extruder. However, it may occur in a single screw extruder too. In fact, certain screw designs have been developed to initiate the dispersed of solids in the melting process such as the Double Wave™ screw (Rauwendaal, 2005).

2.2.2 Polymer sintering (melting under no shear)

The above section describes polymer melting of a bulk system (solid bed) in single screw extruder; however, evaluations of the solid bed from screw freezing experiments suggest that particles within its interior undergo coalescence (sintering) rather than any form of shear-induced melting. When polymer particles are in contact with each other at elevated temperature, above their melting/softening temperature, they tend to decrease in total surface area by coalescence and form a homogenous melt. This process, called sintering, starts with the development of bridges and interfaces between adjacent particles followed by densification in which the interparticle cavities are eliminated (Kontopoulo and Vlachopoulos, 2001). The polymer sintering process is a fundamental and controlling step in rotational moulding because it affects significantly the process time and the end product quality. This process is shear and pressure free, used to manufacture hollow plastic parts (Bellehumeur et al, 1996; Chaudhary et al, 2002). The sintering of a polymer results from competing effects of surface tension and viscosity. Surface tension drives coalescence between two particles whereas viscous lubrication of the particle surfaces resists the approaching particle (Kontopoulo and Vlachopoulos, 2001). Frenkel derived an analytical model that predicts the rate of sintering based on the balance of the surface tension and the viscosity which was corrected by Eshelby (Bellehumeur et al, 1996). This model was can be written as (Bellehumeur et al, 1996):

$$\frac{y}{a}=\left(\frac{\Gamma t}{\eta a}\right)^{1/2} \tag{2.6}$$

where **a, t, y, η** and **Γ** are the particle radius, sintering time, sintering neck radius, viscosity and surface tension, respectively. The validity of the above model is limited to Newtonian flow for the description of the early stages of sintering when the particle diameters remain relatively constant. It was found that the sintering rate increases when the zero shear viscosity decreases. Polymers with high zero shear viscosity may not coalescence to form a single circular particle (Bellehumeur et al, 1996). Addition of small amounts of low molecular weight additives to neat polymer enhances particles coalescence and bubble removal in sintering process. This effect was attributed to a decrease in the melt elasticity at low shear rate (Chaudhary et al, 2002)

Subsequent development have been by done by other researchers to predict the complete coalescence of the particles (Pokluda et al, 1997), however, the more important development was the inclusion of viscoelastic behaviour. For example, a polymer with a low zero shear viscosity but high elasticity (i.e. High G') has a lower sintering rate (Bellehumeur et al, 1996). Using the convected Maxwell constitutive equation Bellehuner et al (1997) included the viscoelastic nature of the polymeric materials to the Frenkel's model. Details of this model can be found in elsewhere (Bellehuner et al ,1997). Finally, since the sintering process between adjacent particles involves viscous flow, the rate of the process is greatly affected by the local temperature (Tadmor et al, 2006).

2.3 Single screw extrusion process

2.3.1 Effect of dynamic coefficient of friction and bulk density

The difference in the dynamic coefficient of wall friction between the solid polymer particles with the barrel and screw surfaces is considered to be the dominant factor influencing the solid conveying rate in a single screw extruder, as revealed by Darnell and Mol (1956). This external friction has been reported to be a function of temperature, pressure and the relative velocity of the polymer with respect to the metal surfaces in the extruder (Spalding et al,1993). Cheng et al (1977) indicated that these factors affecting the frictional behaviour can be quite different from one polymer to another. Under conditions typical of extrusion using a screw simulator, the coefficient of friction was calculated from the retarding force on a rotating roll as a plug of polymer (PS, PP, or LDPE) was pushed against it. Since these polymers match those studied in this thesis, their results bear close inspection. They found that the dynamic coefficient of friction for PS decreased slightly with increasing pressure or speed and was less sensitive to temperature than the other two polymers. However, they observed that PS samples exhibited an interesting behaviour, in which the surface of the sample in contact with roll was ground off although the roll surface was polished. This was attributed to the high adhesion between PS and the drum surface compared to the shear strength of the sample resulting in fracture. The coefficient of dynamic friction at low pressure and speed was found to increase with the rise of the roll surface temperature until it reached a maximum around 80 °C and then sharply it decreased. Unlike their observations for PS, LDPE samples left a very thin layer of the polymer on the roll surface even at room temperature and experienced large deformation when the roll temperature was 80°C. Finally, their experiment on PP showed that the dynamic coefficient of friction increased with temperature reaching a peak value, drop steadily over a temperature between 80 and 100 °C reaching a plateau and then sharply increased at a temperature close to the melting point. However, they observed less deformation in the PP sample compared to LDPE.

In addition to the coefficients of friction, another important factor that affects the solid conveying mechanism is the bulk density of the polymer (Darnell and Mol ,1956; Prentice and Qiu, 1998) which is a required parameter in designing the extruder screw or in the prediction of flow rate. Included in the 1956 paper by Darnell and Mol (Darnell and Mol ,1956), the authors included experimental data showing the dependency of the bulk density on the height of a solids bed. They showed that the bulk density of a polymer decreases with a decrease in channel depth. Temperature plays an important role on bulk density in the extruder. The temperature profile within an advancing solids bed starting from the feed zone is steadily increasing within an extruder to a point above the melting temperature. This changes the bulk phase morphology by initiating the fusion between the particles which eliminate the voids and increases the bulk density. Prentice and Qiu (1998) showed the sensitivity of polymeric solids bulk density to temperature and pressure in their compaction device. They found that the bulk density of different polyethylenes increased sharply with increasing temperature even at low pressure while PS showed a more gradual increase in bulk density with increasing temperature and pressure. The sharp increase in bulk density for the polyethylene was attributed to the significant plastic deformation compared to PS.

2.3.2 Effect of Feeding mode (starve vs. flood)

Most single screw extruders used in industry are flood fed where the screw channel in the solid conveying zone is completely filled with polymer particles emptying by gravity from a hopper (McKelvey, 1978). However, this type of feed is not always advantageous for achieving maximum output rates such as the case for resins of high molecular weight (McKelvey, 1978), low friction or with cohesive properties. Also, it was reported (Gale, 1997; Thompson et al, 2000) that this type of feed greatly reduces the mixing quality of solid additives if the single screw extruder is being used for mixing purpose. This was attributed to the formation of agglomerates which once formed, are difficult to disperse due to their strong binding forces.

To overcome these problems, starve feed mode can be used for a single screw extruder. Most twin screw extruders, which are known to be powerful melting and compounding devices compared to single screw extruders, are starve feed (Campbell et al, 1995). In this mode of feeding, the screw channel in the solid conveying zone is only partially filled with polymer using an external feeding device (ex. gravimetric feeder). In this mode of operation the output rate of the extruder is no longer dependent on the speed of the screw (Mckelvey, 1978).

The melting mechanism in starve feed mode was examined by Isherwood et al (1984) using the freezing experiment. At a moderate degree of starvation (2-10%) they found that the melting patterns showed a delay in the initiation of melting corresponding to the late formation of the solid bed. Although the initiation was delayed, the rate of melting was quite rapid so that the overall completion of melting corresponded with flood fed processes. They attributed this to the loose nature of the particles which allows a greater degree of particles mobility and more interparticulate friction that increased the bulk polymer temperature more efficiently than a tightly confined bed. The increased mobility of the particles in the solid conveying zone was also linked to efficient mixing of the additives prior to melting in these starve fed systems. A significant reduction in the size and the presence of powdered agglomerates results from only a small amount of starvation (Thompson et al, 2000; George et al, 1997).

Furthermore, the advantages of starve fed mode include enhanced power economy during extruder operation. It is important for the extrusion processing of high molecular weight needed at high rates (McKelvey, 1978). However, excessively high degrees of starvation can cause instability in extrusion process (i.e. fluctuation of die pressure) and can deteriorate the extruder performance (Isherwood et al, 1984). Therefore, there is an optimum feeding rate which results in stable operation and better extruder performance (George et al, 1997).

2.3.3 Single screw extrusion of homo PP vs. LLDPE

Homopolymer PPs generally known in the polymer processing industry to plasticate at lower specific rate compared to PE. Cheng (Cheng,1988) who characterized different PP resins with different melt flow rates concluded that the PP melting rate was the controlling factor for extrusion rate, and not the solid conveying or pumping rates. Thermal and rheological properties such as high melting temperature, high crystallinity, low pellet compressibility, and low shear viscosity were all suggested to contribute in the decrease of melting rate of PP. Stangland et al (2002) extensively examined the extrusion behaviour between PP and LLDPE. They examined the behaviour in a single screw extruder with a screw compression ratio of 2.8, screw diameter of 63.5 mm and screw length of 21 L/D. Both resins were extruded at different screw speeds but using the same barrel temperature profile. Their experiments indicated that the output rate of PP at 60 rpm was less than LLDPE by almost 30 %. With further increase in screw speed the quality of the melt deteriorated (i.e. some solid were observed in the melt). Also, they found that the axial pressure profile at the same screw speed was higher for LLDPE than PP especially at the early section of the screw. They believed this increase of pressure profile made the LLDPE resins to have adequate solids conveying and pressurization compared to PP. Using a rotating roll at conditions typical of extrusion process, they found that the melting flux and the shear stresses acting on the two resins (LLDPE and PP) were different. For example, although both resins showed a decrease in the shear stresses at the interface as a function of temperature, LLDPE exhibited higher shear stresses at interface compared to PP. The authors indicated that the lower in shear stresses at the interface of PP would reduce the solid conveying forces at the barrel wall and therefore the solid conveying rate. On the other hand, the melting flux of LLDPE was found to be higher than PP by 30% which was similar to their results in the single screw extruder. In addition to that, they measured other physical and rheological properties such as bulk density, thermal conductivity and specific heat to verify the cause of this reduction. However, none of the measured properties could be related to this problem.

2.4 Techniques used to study melting in single screw extruder

Visualization of plastic melting inside the metal barrel of an extruder is necessary to promote understanding of the process and to enhance the efforts to model and design in this machine. The overall understanding of the melting in single screw extruders has been promoted by many researchers using different techniques (Maddock, 1959; Cheng et al, 1977; Sundstrom and Lo, 1978; Zhue and Chen, 1991; Noriega et al, 2004). The pioneering investigation made by Maddock (1959) using freezing experiments was the first technique found to be helpful in understanding melting. However, this technique is time consuming and lacks the capacity for dynamic visual observation of the process.

Developments were made by using a modified barrel with glass windows to observe the dynamic behaviour of the process (Zhu and Chen, 1991). Others have used optical techniques to observe the melting process (Noriega et al, 2004). In the case of Noriega, their observations were made by using a rigid boroscope with rod lenses attached to a holder that goes in the barrel. Another way of studying the melting is by developing an instrument that can simulate the melting process in extrusion. Initially Sundstrom and Lo (1978) developed a screw simulator which utilizes the concept of a heated rotating roll against a forced plastic sample. However, their instrument was only capable of limited experimental conditions. Cheng and others (Cheng et al, 1977) developed a screw simulator utilizing the same concept of Sundstrom and Lo but with more flexibility in operating conditions. The testing specimens used in both equipment were prepared by compression molding. Spalding et al (1993) developed a similar instrument but with rectangular chamber utilizes solid particles. This instrument provides visual observation of the melting and the frictional mechanisms at the surface of the roll but not within the solid bed. Others (Gogos et al, 1985) used an annular cell with a rotating shaft to study the melting of polymer.

Chapter 3

3.Experimental Work

This chapter summarizes the experimental work. The first section describes a new device designed to represent a single screw extruder. The second section is about materials characterization which includes the physical, rheological, thermal and mechanical properties.

3.1 Drum simulator description

A drum simulator was designed to model the radial compressive stresses and shear stresses on a solid bed of plastics similar to the environment within the screw channel of a single screw extruder. Note – the axial compressive stresses produced on a solid bed due to upstream rate restrictions due to melting could not be approximated by this device. The device consisted of a sample chamber, a rotating drum and compression plunger. The side walls of the sample chamber contain the solids and provide heat similar to the screw flights. The back wall of the sample chamber, similar to the side walls was electrically heated while the front wall of the sample chamber was kept transparent for observation purposes.

The plunger acts as an adiabatic screw root and the rotating drum provides heat as well as tangential (shear) stresses.

For trials, the sample chamber was open from the top to allow sample charging. The plunger made from polytetrafluoroethylene (PTFE) was subsequently put into place above the granular bed to provide compressive forces and often contained two thermo-wells to measure bed temperature. Figure 3.1 shows a schematic of the drum simulator.

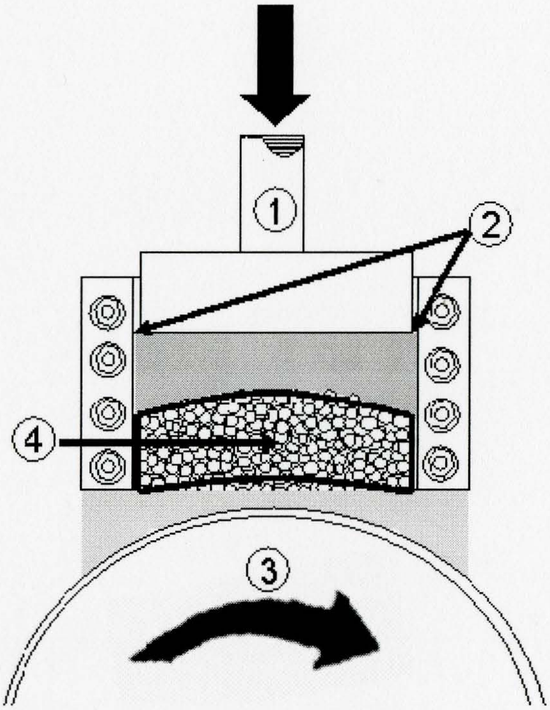

Figure 3.1Schematic of drum simulator whereas 1) plunger 2) side walls of sample chamber 3) rotating drum 4) solid bed

The sample chamber was a rectangular box 76 mm in length and 30 mm in width providing a contact are area of 2280 mm^2 (Figure 3.2a). Side and the back walls of the sample chamber were made of aluminum alloy type 6061-T6 with thicknesses of 13.25 and 9.75mm respectively. The materials used for the front wall were either a borosilicate glass or polycarbonate. The 6.3 mm borosilicate glass wall was used for high temperature experiments (~ 230°C) while the 12.6 mm polycarbonate wall was used for low temperature experiments (~140°C). Four rows each containing four holes of 1.5 mm dia. were evenly drilled into the lower end of the polycarbonate wall (closest to the rotating drum) to make internal temperature measurements of the solid bed. A PTFE gasket with curvature similar to that of the drum was fixed at the bottom of sample chamber to minimize materials leakage and avoid abrasive wear between the sample chamber and the drum. The sample chamber was firmly fixed in the center of a horizontal supporting plate which was held by two threaded rods of 19 mm in diameter (Figure 3.2b). A set of springs (Max. spring load 500 lb) were used to minimize vibration produced by drum rotation. The gap between the drum and sample chamber was always kept around 0.25mm.

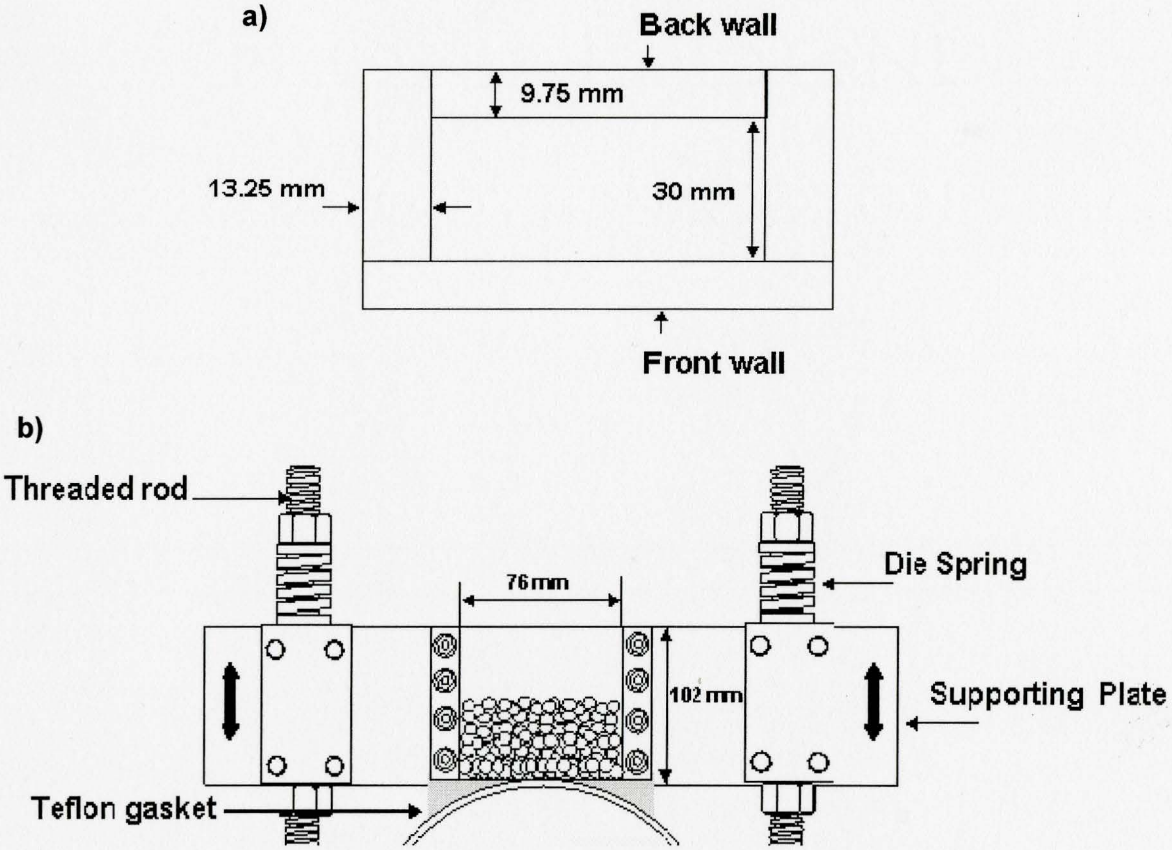

Figure 3.2 Solid chamber arrangement a) Solid chamber top view b) solid chamber fixed to the supporting plate by the threaded rods.

The heated drum consisted of a hollow cylinder made up of concentric layer of aluminium and steel. The outer layer was carbon steel (AISI 4140) with thickness of 3.13 mm while the inner layer was aluminium alloy type 6061-T6 with a thickness 3.8mm. Initially the drum had been made from aluminium alloy because of its excellent thermally conductivity. However due to the high wearing experienced against the PTFE gasket, the drum was covered with a carbon steel sleeve. The drum diameter and width were 208.0 and 89.0 mm, respectively. The drum was supported above the base by two ball bearings. The estimated weight of the whole assembly was 60 kg.

The side walls of the sample chamber were each heated using two slab heaters of 25 W while the back wall was heated by three cartridge heaters each of 150 W. A control thermocouple (type T) was located in the back wall close to the rotating drum; the position of the thermocouple was selected so that the wall temperature at the solid bed mid-height was known. Figure 3.3 shows the heater and the thermocouple locations of the sample chamber.

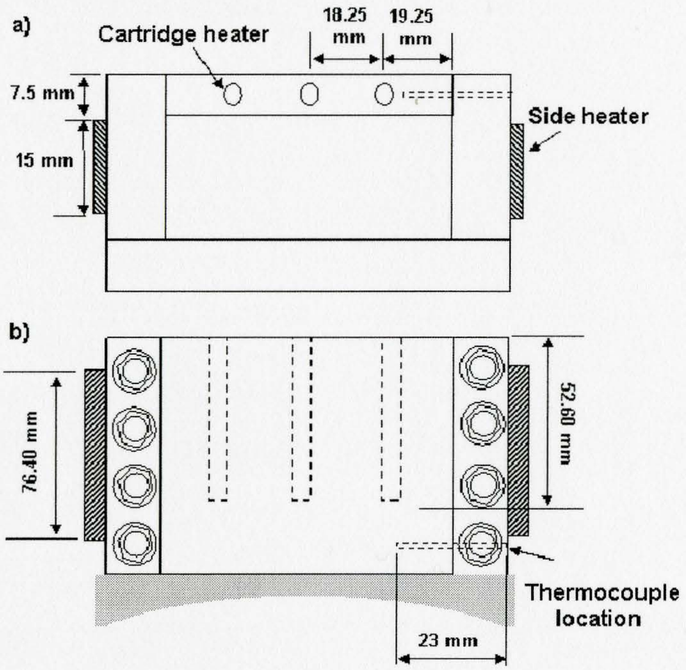

Figure 3.3 Solid chamber heaters a) top view b) front view

The drum was heated by two ring heaters each of 500 W. A thermocouple (type T) was positioned across the width of the drum at a distance of 5.3 mm from the outer surface. The power was provided to the drum heaters using a rotating electrical connector. Figure 3.4 shows heater locations of ring heaters in the drum. Both the drum and the sample chamber heaters were controlled by an Omega (CN 8241-R1) universal input temperature controller.

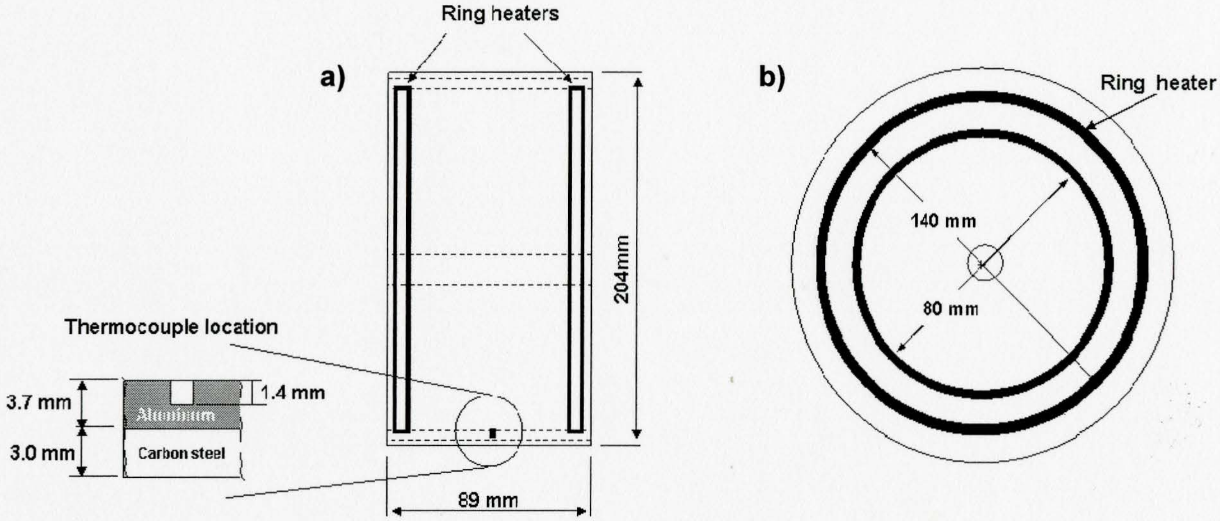

Figure 3.4 Location of ring heaters in the rotating drum a) side view b) inner view

The drum was direct coupled to 1.0 HP TOSHIBA alternative current (A/C) motor. Table 3.1 gives the specification of the motor. The motor speed was controlled by variable speed inverter type (VFNC1S-2022P) supplied by Toshiba. The inverter was capable of displaying the current load on the motor which could be used for torque calculation. Further details are described in the inverter manual.

Table 3.1 Motor specifications of the drum simulator

Motor specifications	
Motor Power	1 HP
Volts	230 V
Frequency	60 Hz
Full load speed	1150 RPM
Full load amperes	3.6 amp.
Full load efficiency	82.4 %

The heating controllers and the inverter were combined in a control box as shown in Figure 3.5. Two voltage supplies were used, 120 V to power the drum and sample chamber heaters, and 230 V to power the motor.

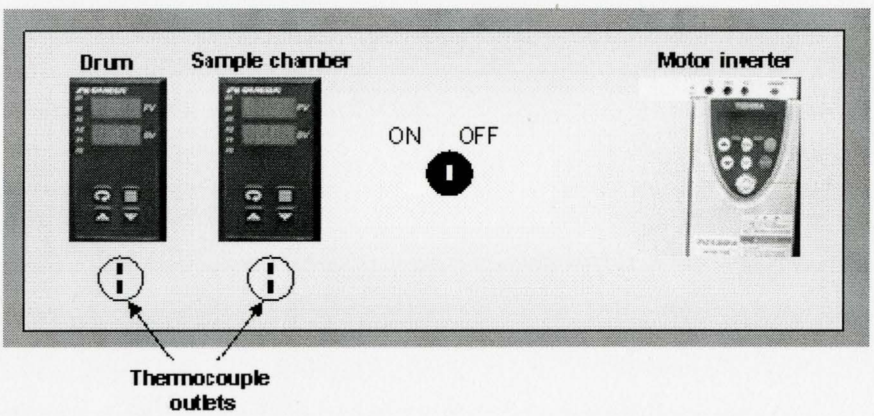

Figure 3.5Front view of the drum simulator control box

The whole assembly was constructed upon a sliding plate which allowed it to be positioned within a mechanical testing machine (MTS, Instron 3366 with 10

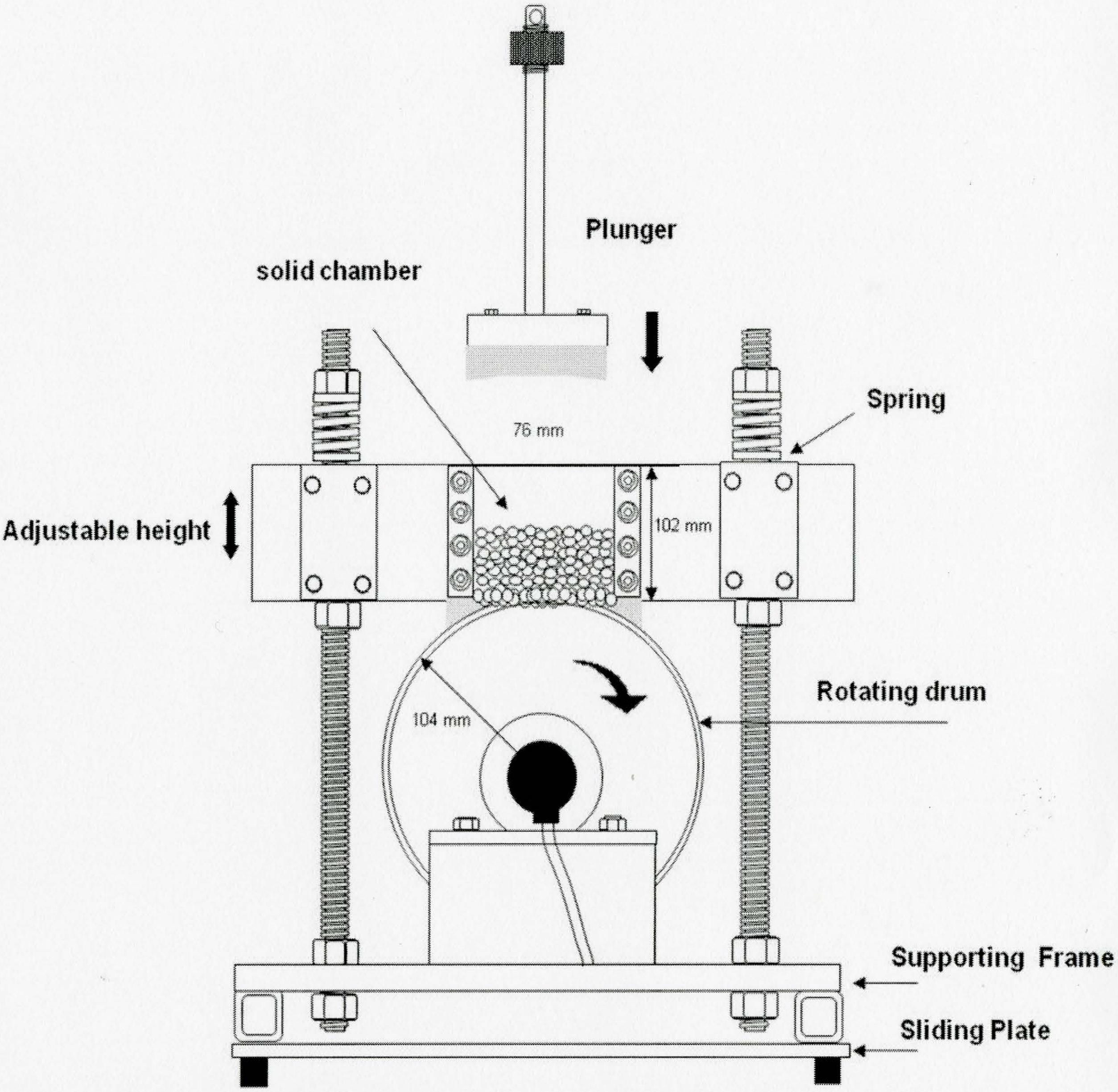

Figure 3.6 Schematic of drum simulator setting on the moving plate.

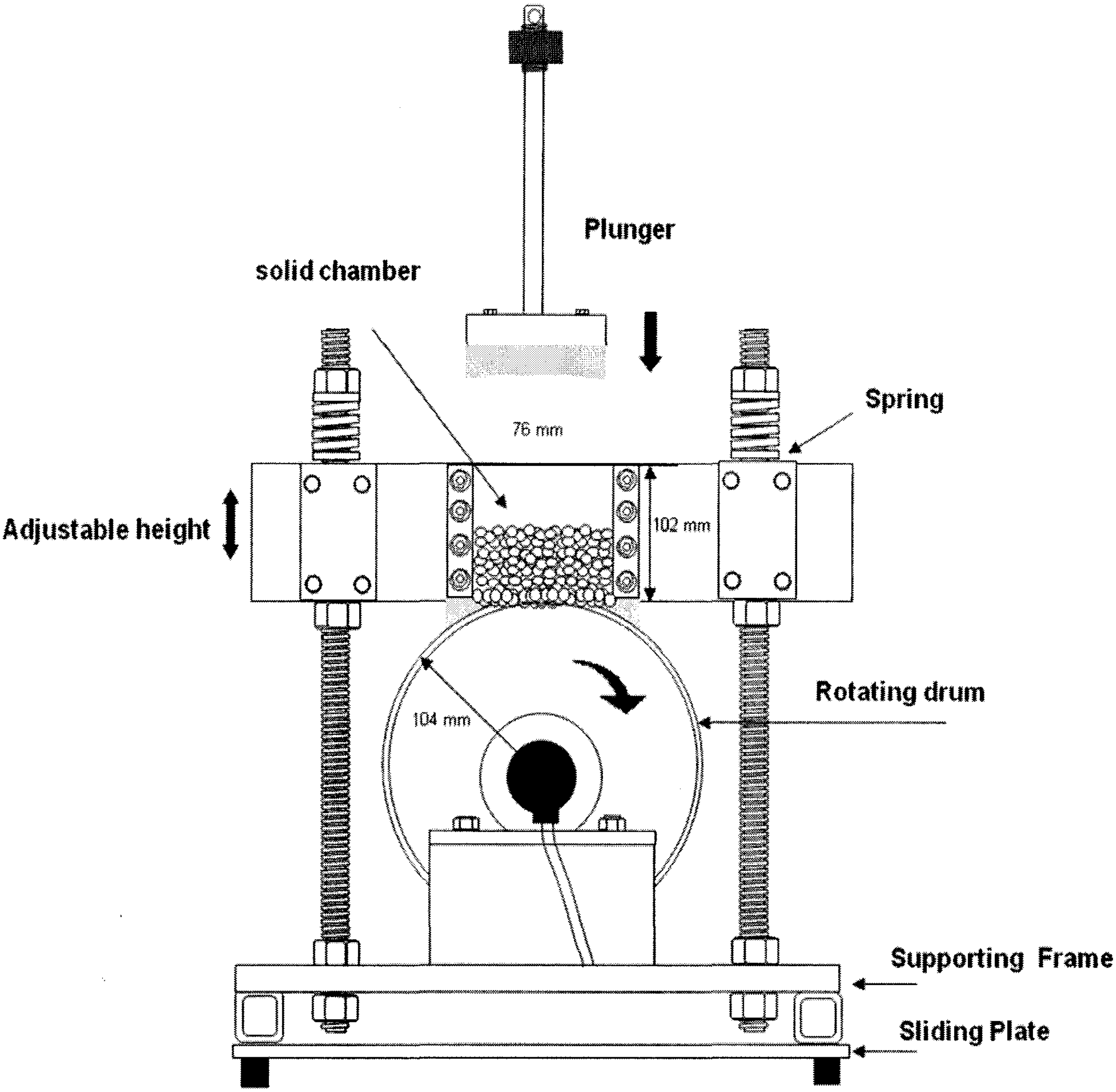

Figure 3.6 Schematic of drum simulator setting on the moving plate.

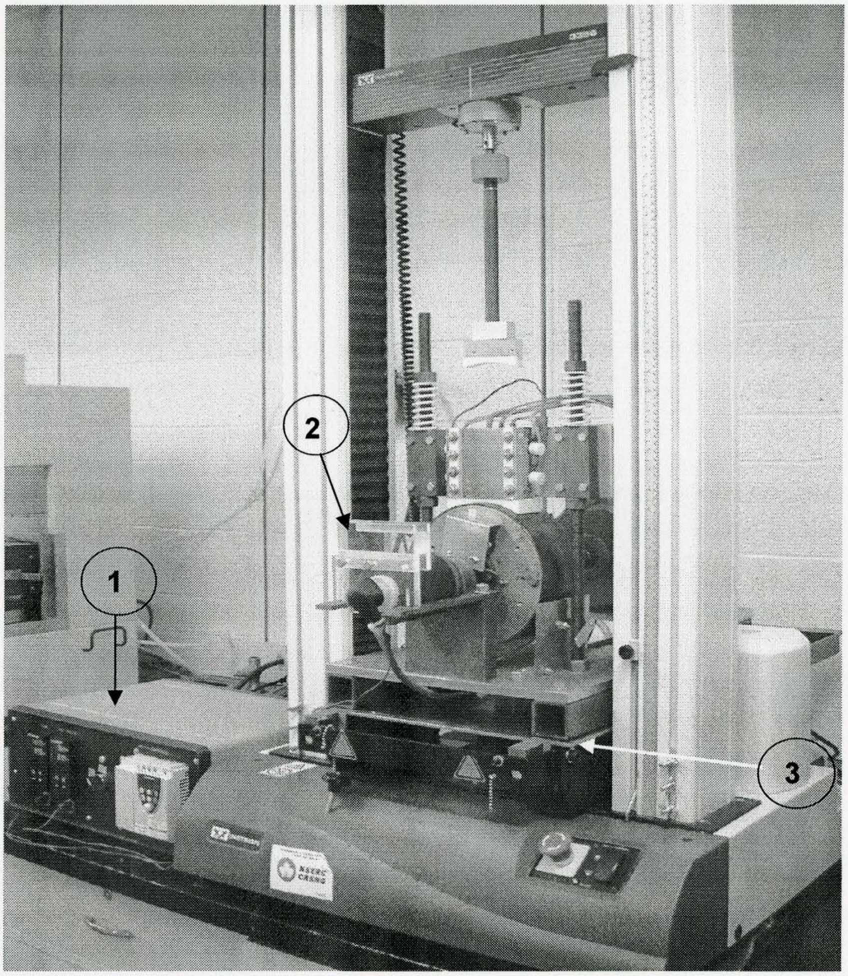

Figure 3.7 Overall drum simulator placed on Instron machine where is 1) control box 2) camera stand 3) sliding plate.

3.1.1 Temperature and speed calibration

The surface wall temperature of the sample chamber was determined using a hand-held surface thermocouple (Type K). It was found that the set-point wall temperatures reported by our controller were very close to the actual surface temperature exposed to the polymer bed, for example a set temperature of 80°C had a measured exterior temperature of 79.1°C with standard deviation of 0.8 °C. Similarly, the drum surface temperature was confirmed in the same manner.

The drum surface temperature value was generally below the set value which is believed to be a result of the heat loss between drum surface and the surrounding environment. Therefore, measurements of drum surface temperature were made against different set-point values. The set value was then adjusted so that the true surface temperature of the barrel corresponded to our desired conditions during our experiments. Figure 3.8 shows the relationship between the set temperature and the actual drum surface temperature.

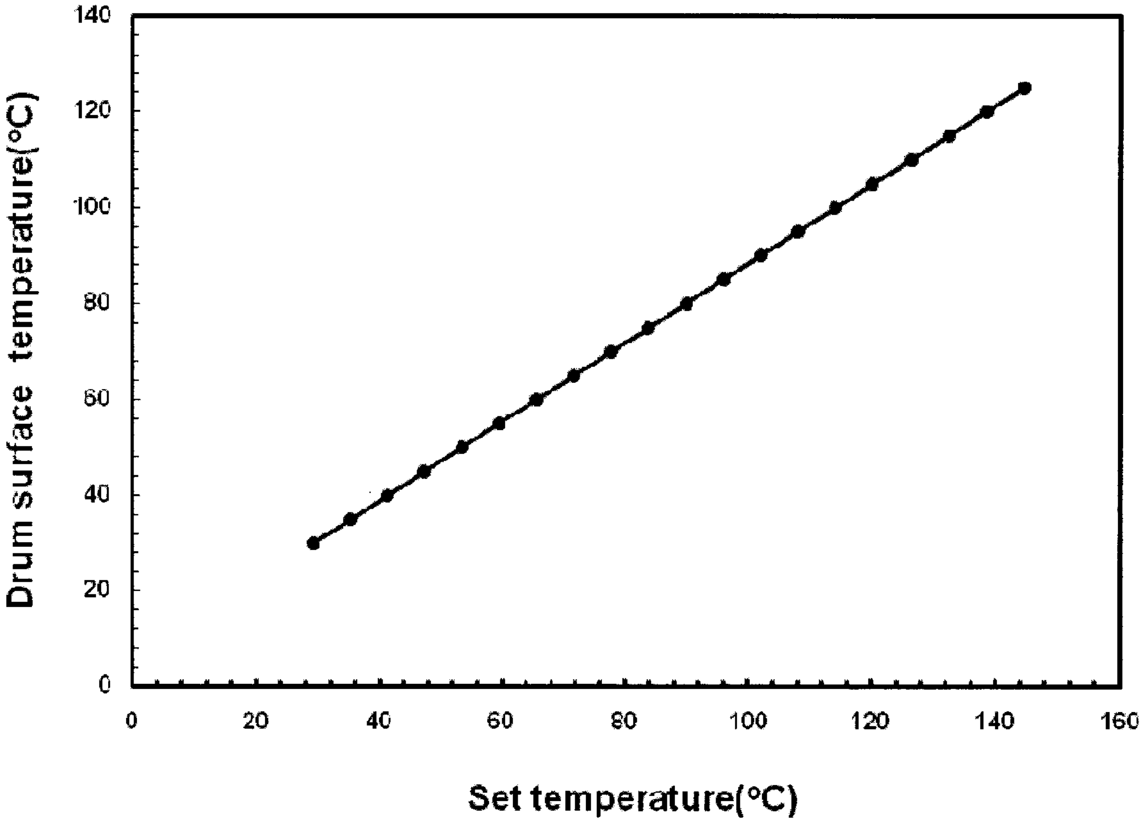

Figure 3.8 Drum surface temperature curve against the set value

The rotational speed of the drum was calibrated to the set-point frequency by a non-contact tachometer (AMETEK model 1726). Figure 3.9 shows the calibration curve of drum speed.

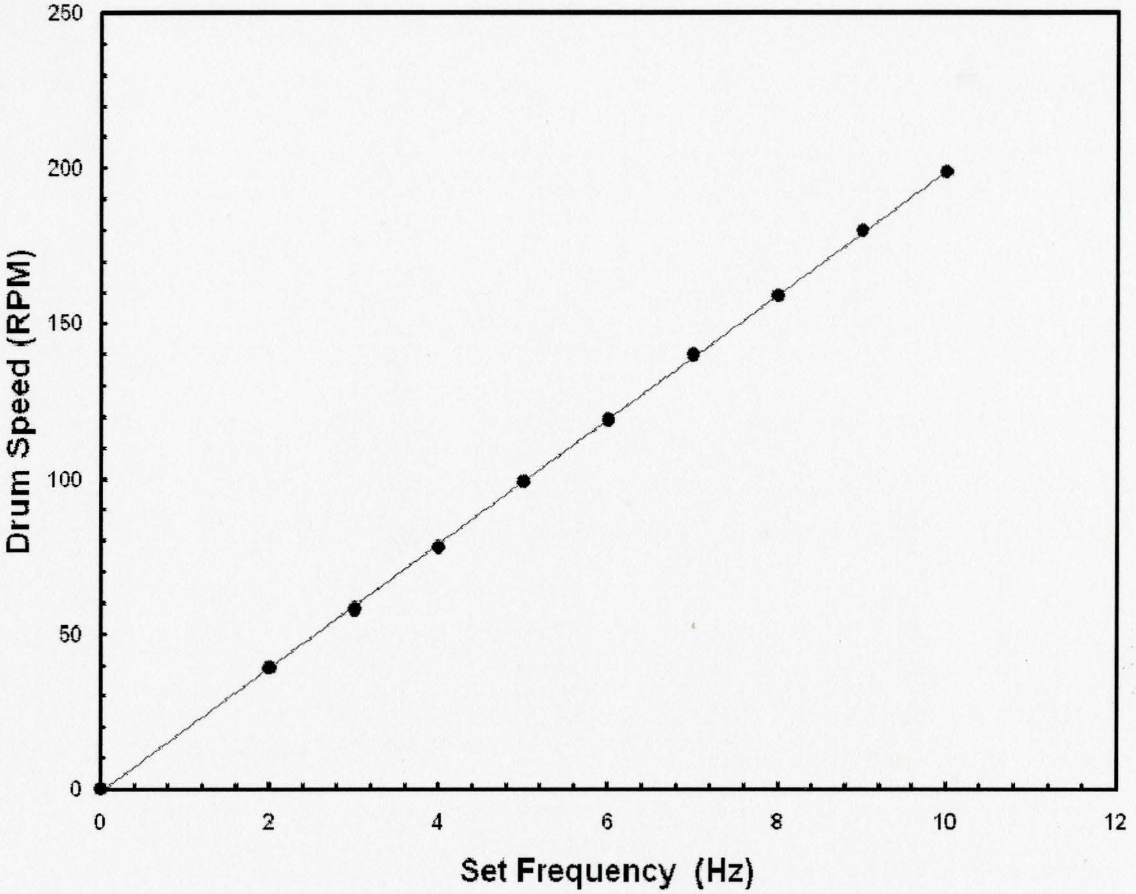

Figure 3.9 Calibration graph of drum speed of the drum simulator.

3.1.2 Experiment Procedure

Experiments were conducted at different conditions of temperatures, compressive deformation and drum speed. A constant sample weight (30 g) was used in each experiment. The drum and sample chamber temperatures were allowed to equilibrate for 35~45 min at set temperature before each experiment. Triplicate runs were performed in each experiment to ensure good reproducibility. The heat transfer experiments were made by type K thermocouples (fast response probe) with tip diameter of 1.5 mm and accuracy of 1.0 °C. The temperature was recorded every minute using Omega digital thermometer type HH82A and the experiment lasted for 20 minutes. Further details about each experiment will be described in chapter 4.

3.2 Materials

Both semi crystalline and amorphous polymers were investigated in this study. The semi crystalline polymers were linear low density polyethylene (LLDPE) and homopolymer polypropylene (PP) while polystyrene (PS) represented a typical amorphous material. LLDPE and PP pellets were obtained by underwater die face cutting of the extrudate, whereas, the PS pellets were strand cut. As a result of the different methods of pelletization and the inherent properties of the materials, the particle shape differed for each polymer.

The LLDPE was a blown-film extrusion grade while PP and PS were injection-moulding grades. Table 3.2 shows important physical properties of the materials. The data reported was obtained from the supplier data sheet except the values of the bulk densities which were measured in the solid chamber of the drum simulator.

Table 3.2 Physical properties of the used materials

Materials Name	Trade Name	Solid Density (kg/m^3)	Bulk Density (kg/m^3)	Melt flow index (g/10min) *	Supplier
LLDPE	LLDPE118 N	918	536.2 ± 1.5	1.0	SABIC
PP	HP1604	900	543.09 ± 2.17	12**	BP
PS	PS125	1050	589.05 ± 0.205	2	SABIC

****PP melt flow rate measured at 230°C**
*** Measured at 190°C**

3.3 Materials characterization

3.3.1 Bulk density

The bulk densities of the three polymers were measured in the solid chamber of the drum simulator since the value is sensitive to the container dimensions. The resin was poured into the solid chamber until the chamber was completely filled. Excess material was scraped by a blade. After that, the material inside the chamber was weighed. The bulk density was calculated by dividing the weight of the sample by the volume of the chamber. At least, five measurements were done for each polymer.

3.3.2 Pellets Shape analysis

Shape analysis of polymer particles was made using a sintering apparatus described in detail in another thesis (Bellehumer, 1997). Five different pellets were randomly selected from each material. The pellet shape of each sample from different orientations was captured using a digital camera. The diameter D, thickness t and width W of each pellet as shown in Figure 10 were determined using Sigma Scan TM Pro 3.0 (from Jandel scientific, 1992).. The average dimensions and standard deviation are reported in a later chapter.

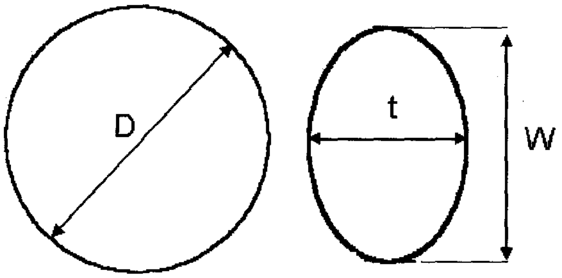

Figure 3.10 Measured particle dimensions

3.3.3 Direct shear test

Direct shear test is a well known test in soil mechanics which estimates the shear strength of the soil mass under shear. A linear relation between shear strength (τ) and normal stress (σ) on plane at any point was presented by Coulomb [Craig, R. F.,1997] as:

$$\tau = c + \sigma \tan\varphi \tag{3.1}$$

where c and φ are the shear strength parameter (apparent cohesion) and the angle of shearing, respectively. Shear strength of polymer pellets was evaluated by using a direct (translational) shear cell apparatus. The apparatus consisted of a square splitted metal box (60mmx60mm), a loading plate to apply normal load, an electrical motor with a gear box to provide a uniform shearing rate and a proving ring to read the shear force. Figure 3.11 shows the main features of the direct shear cell apparatus.

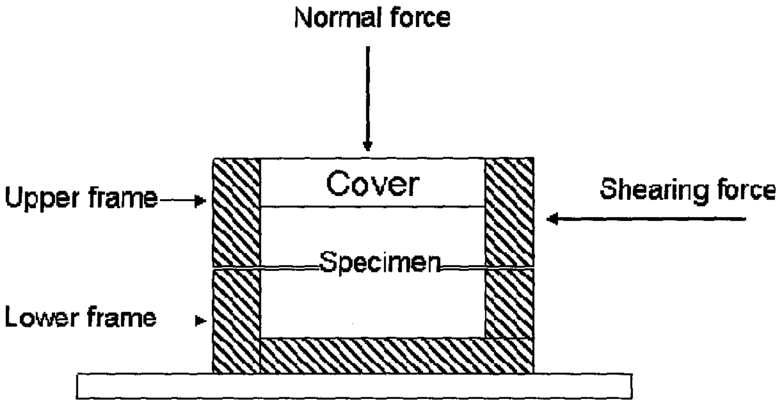

Figure 3.11 Schematic diagram of the direct shear cell

The sample was confined in the metal box with a small gap between the two halves. A constant shear rate was maintained by the electrical motor. Three normal loads of 6.273, 16.273 and 36.273 kg were applied on the sample. These loads correspond to normal stresses of 17.31, 44.91 and 100.11 kPa.

The resulting shear force was recorded by the proving ring and the corresponding shear strength was calculated by dividing the shear force by the sample area. The values of c and φ were obtained from linear fit of the shear strength versus the normal stress.

3.3.5 Melt density

The melt density is a required parameter in surface tension calculation. The value of the melt density of each sample was determined by KAYNESS melt indexer. The melt indexer is simply a capillary viscometer which consists of a heated barrel, piston rod and a standard die at the end of the barrel. According to ASTEM D1238, the dimensions of the standard die are 2.095 mm in diameter and 8 mm in length. Typically, 5 to 7 grams of each sample was loaded in the barrel at a specific temperature (190°C for LLDPE and PS while 230°C for PP). First the sample was packed using the piston rod and preheated for 5 minutes to get rid of the air pockets. Then, the piston rod was loaded with a standard weight of 2.16 kg to allow the molten polymer to flow through the die. At the same time, a plastic tape with flag length of 0.25" was hanged to the arm that attached to the piston rod. At least three extruded samples of each resin were collected and then weighed. The melt density was calculated from the weighed sample and the volume of the traveling strip as follow:

$$\rho_m = \frac{W}{\pi R^2 L} \tag{3.2}$$

Where W is the weight of the extruded sample (g), R is the radius of the barrel (4.775 mm) and L is the flag index length (6.35mm). Also, the melt indexer was used to prepare samples for surface tension and sintering experiments at similar conditions. Different dies were used to produce an extrudate that fit into the glass tube of the surface tension device.

3.3.6 Thermal proprieties

Differential scanning calorimetry (DSC) type 2910 made by TA instruments was used to determine the melting point for the semi crystalline polymers and the glass transition temperature for the amorphous polymer. A 5 to 6 mg sample of each polymer was weighed and encapsulated in a aluminum pan, then loaded into the instrument. At first, a thermal scan from 20 to 200°C at rate of 10 °C/minute was applied to remove the thermal history of the sample. This was follows by a cooling scan to 20°C at the same rate. Finally, a second heating scan was performed similar to the first one. The melting point and the heat of fusion of each sample were obtained from the first recorded heating curves.

3.3.7Rheological proprieties

Dynamic rheological measurements were made on ARES rheometer. The parallel-plate rheometer is equipped with two transducers to cover different torque ranges, i.e. 0.2-200 g-cm and 2.0-2000 g-cm, selected based on the materials being tested and whether dynamic or steady shear is being evaluated. Parallel plate geometry with 25 mm diameter plate was used in the measurements. Sample discs of 25 mm diameter were prepared by compression moulding at 190°C for each polymer. The overall preparation time was 7 min. The sample discs were placed between the plates and heated to the test temperature to eliminate any thermal stresses. The gap was then adjusted to 1.5 mm and any excess molten materials were trimmed off by spatula for maintaining a smooth edge surface.

Firstly, a dynamic strain sweep test was carried out to determine the linear viscoelastic region for each polymer at the test temperature. Then, a dynamic frequency sweep was performed with frequency varying from 0.1 -100 rad/s at an amplitude strain within the linear viscoelastic region.

The storage modulus G', the loss modulus G" and the complex viscosity η^* were calculated by the software as per the following equations [Dealy and Wissbrun, 1990]:

$$G' = \frac{2M_O h}{\pi R^4 \phi_O} \cos\delta \tag{3.3}$$

$$G'' = \frac{2M_O h}{\pi R^4 \phi_O} \sin\delta \tag{3.4}$$

$$\eta^* = \sqrt{\left(\frac{G'}{\omega}\right)^2 + \left(\frac{G''}{\omega}\right)^2} \tag{3.5}$$

where Φ_o is the oscillation strain amplitude, M_o is the measured torque, δ is the phase lag, R is the plate radius, h is the gap between plates and ω is the frequency.

Measurements for three different temperatures were performed with the three polymers. Zero shear viscosity was estimated by fitting the dynamic viscosity data using Cross Model. The Cross Model is given as follow [Dealy and Wissbrun, 1990]:

$$\eta = \frac{\eta_o}{1 + (\lambda\dot{\gamma})^{1-n}} \tag{3.6}$$

where η_0 is the zero shear viscosity, λ is a characteristic relaxation time, n is the power-law exponent, and $\dot{\gamma}$ is the shear rate.

3.3.8 Tensile strength testing

Tensile strength for each polymer was measured using an MTS (Instron 3366). Test bars were prepared on an ARBURG 320S injection moulding machine with dimensions according to Type I in ASTM D638. The average thickness measurements of each sample were obtained for each specimen. The sample gauge length was 50 mm and the cross head speed was 50 mm/min for LLDPE, 25 mm/min for PP and 5 mm/min for PS. An extensometer was attached to each sample for an accurate measurement of the Young's modulus. All tests were made at room temperature. The reported values were based on an average of at least 5 measurements.

3.4 Sintering experiment (particle coalescence)

Sintering experiments were conducted on the three polymers. The extrudates obtained from the melt indexer were used to get two identical particles. The size of a particle (obtained from the extrudate) for sintering experiments was approximately the same for all materials studied. The two particles that will undergo sintering were positioned at the center of a small glass cup so that they were making contact. The glass cup was then placed in the center of the heating chamber. The set temperature inside the chamber was 230°C for all the experiments. The set temperature was controlled by a thermocouple sitting inside the wall of the heated chamber. Also the temperature inside the glass cup (i.e. air inside the chamber) was recorded.

The experiments were recorded using a videocassette recorder connected to an optical microscope type Olympus SZ-60 equipped with video camera. After the completion of the experiment, the recording was transferred over to a personal computer equipped with frame grabbing hardware. The image grapping was made using HLImage ++97 software at intervals of 30 sec. The sintering neck radius (y) between the two particles and the projected particle area were measured using image analyzer software Sigma Scan Pro3.0. The particle radius (a) was estimated from the measurement of the sintering neck radius (y) between the two particles and the projected particle. Figure 3.12 shows a schematic of ideal sintering for two particles. The sintering time was calculated using an empirical model based on Frankel-Eshebly approach [Bellehumeur, et al. 1998]:

$$\frac{y}{a} = 1 - k * exp\left(\frac{-t}{\tau}\right) \tag{3.7}$$

All sintering experiments were repeated at least three times to ensure reproducibility.

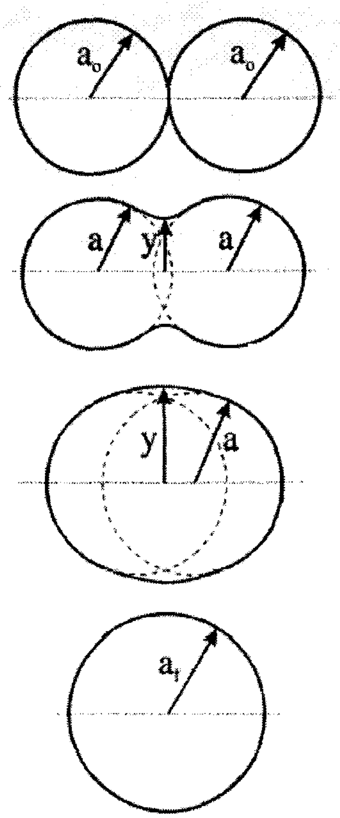

Figure 3.12 Schematic of neck growth of two particles, where a_0 and a_f are the initial particle and final radius, respectively adapted from [Bellehumeur et al. 1996].

3.5 Surface tension

Surface tension values for the three polymers were determined using a drop shape technique (i.e. pendant drop). A 6 mm filament was cut from the extrudate obtained from the melt indexer. The filament was inserted into a capillary glass tube so that half of it extended outside the tube. Then the glass tube was inserted into a heated chamber that had two quartz windows for illumination purpose. The chamber temperature was controlled by an electrical heater and the temperature around the pendant drop was measured by an exposed thermocouple placed close to the glass tube. The temperature measured by the external thermocouple was assumed to be the test temperature.

The sample filament was preheated in the chamber for 45 min to allow the formation of a drop. Once the drop was formed an image was obtained for calibration using Sanyo CCD camera attached to a microscope. The image was transferred over to a computer which was equipped with surface tension analysis software (First Ten Angstroms Inc.). The software prompts the user to input the melt density and the tube diameter. The tube diameter was obtained from the image and calibrated against the actual diameter of the tube measured by a digital calliper. The movie then was initiated, enabling images to be collected every 20 sec. The typical overall period for each experiment was around two hours. In all experiments a blanket of nitrogen gas was used to prevent polymer degradation. Experiments were repeated three times to ensure good reproducibility.

Chapter 4

4. Results and discussion

4.1 Materials characterizations

This first section outlines the substantial effort made to characterize the material properties of all three polymers used in this study. These data provided insights into the findings from the drum simulator.

4.1.1 Thermal properties

The results obtained from DSC of the three polymers (PS, LLDPE, PP) are summarized in Table 4.1. The data reported was obtained from first heating scan in order to capture the thermal history of the polymer as it would melt in extruder. PP and LLDPE showed peak melting temperature 164.0 and 119.0 °C, respectively. PS being an amorphous resin did not show any melting transition yet demonstrated a glass transition at 86.0 °C. In terms of heat of fusion, which is an indication for the energy required to completely disrupt the crystalline structure of a polymer, LLDPE had a higher value than PP.

Table 4.1 Thermal properties obtained from DSC.

Materials	Onset of melting (°C)	Peak melting point (°C)	Heat of fusion (J/g)
LLDPE	107.0	119.0	94.0
PP	154.0	164.0	85.0
PS	86.0*	90.0*	N.A

*Glass transition point
N.A Not applicable

The DSC melting curves for PP and LLDPE are shown in Figure 4.1. Both resins showed a single sharp melting point, however, LLDPE showed a broader melting range spanning 80°C as shown in Figure 4.1. Other properties important to consider in regards to the thermal behaviour of these polymers (i.e. specific heat capacity and thermal conductivity) were taken from (Tadmor and Gogos, 2006) and presented in Table 4.2

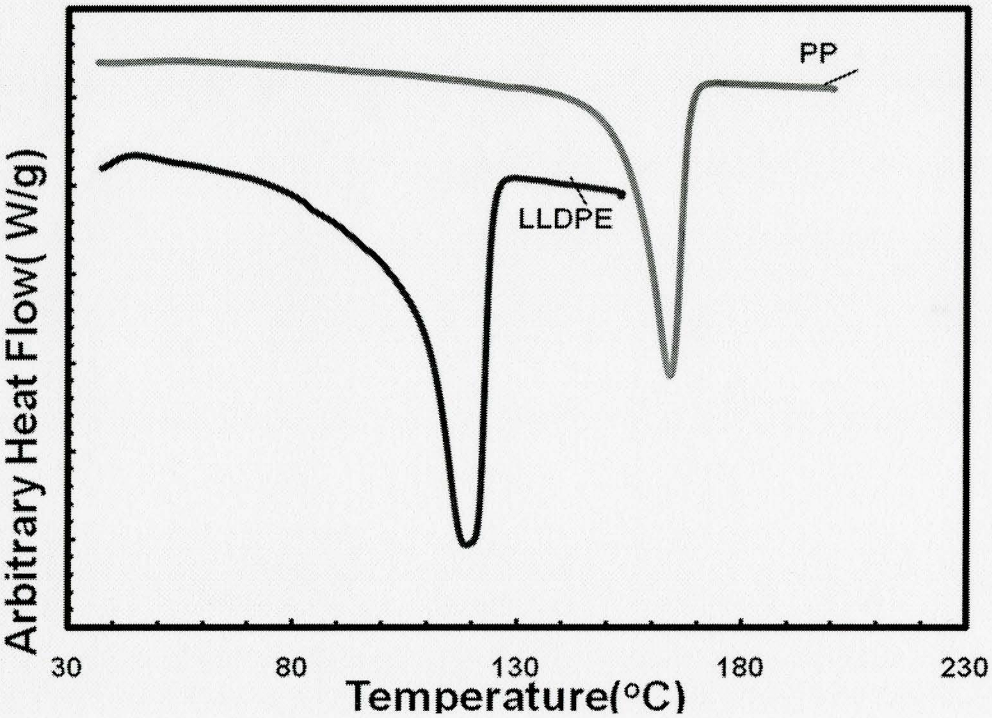

Figure 4.1 DSC curve for LLDPE and PP.

Table 4.2 Specific heat and thermal conductivity of the three resins (Tadmor and Gogos, 2006)

	Solid State		Melt state	
Materials	Specific heat C_p (J/kg-K)	Thermal Conductivity K (W/m^2-K)	Specific heat C_p (J/kg-K)	Thermal Conductivity K (W/m^2-K)
LLDPE	1884.1	0.368	2005.5	0.243
PP	1762.64	0.298	2800.96	0.234
PS	1239.29	0.153	2089.21	0.185

4.1.2 Rheological results

The dynamic rheological properties such as the viscosity, and storage and loss moduli were obtained for the three resins at three different temperatures. The measurements for LLDPE resin were taken at 140,170, 200 and 230°C , for PP at 175, 200 and 230 °C and for PS at 170, 200 and 230 °C. Properties of PS could not be determined closer to its transition temperature like the other two polymers as its solid-like behaviour in that range exceeded the measurement limits of our instrument. The dynamic viscosity data were used to estimate the zero shear viscosity by fitting the data to the Cross constitutive model (Dealy and Wissbrun, 1990). Figure 4.2 shows the zero shear viscosity of the three materials plotted as a function of temperature. It can be seen from the plot that PS has the highest drop in zero shear viscosity over the tested range of temperature compared with the other two materials. Such a drop is typical of an amorphous polymer as it transitions from its rubbery to viscous flow state. By 230°C both PP and PS demonstrated converging viscous properties while for LLDPE, its zero shear viscosity curve indicated far less sensitivity to temperature giving it a higher value at this temperature.

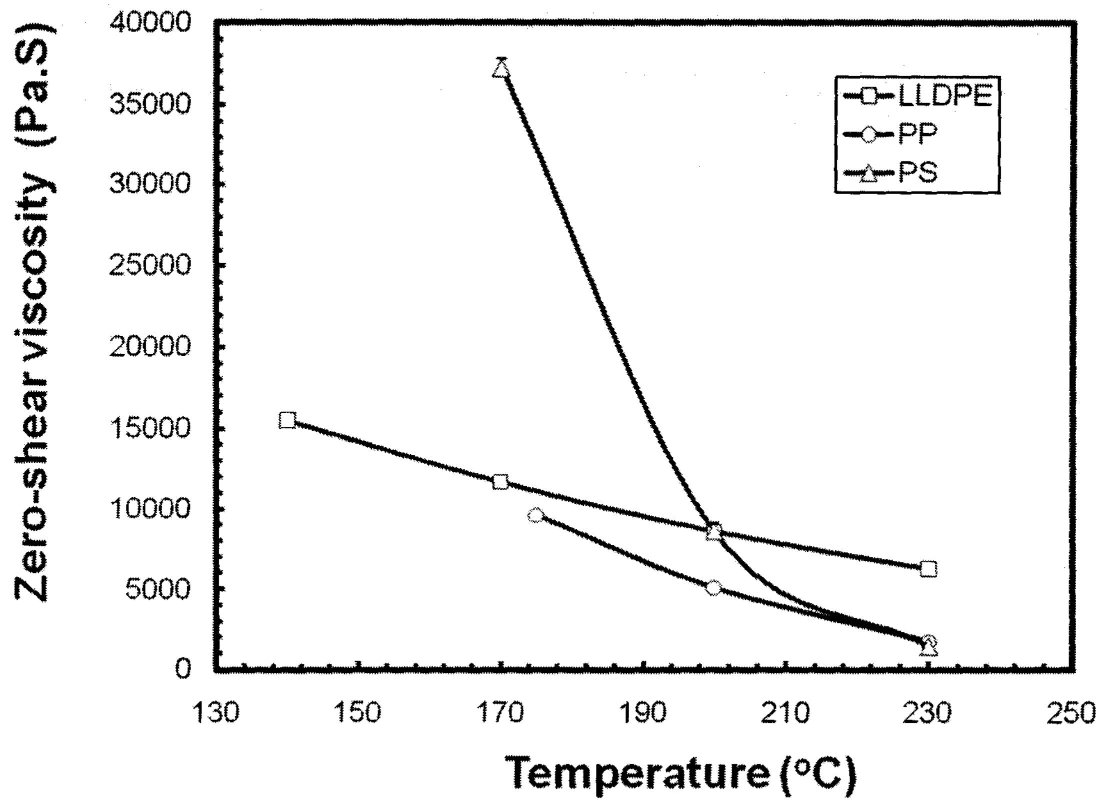

Figure 4.2 Zero shear viscosity of the three materials at different temperatures (lines included for clarity).

Plots of dynamic viscosity versus frequency for the three materials at 230°C are shown in Figure 4.3. It is clear from these curves that both polyolefins (i.e. LLDPE and PP) showed exclusive shear thinning behaviour over the frequency range for all the three materials and PS exhibited a Newtonian response to shear rates less than 1 rad/s. G' (storage modulus) and G" (loss modulus) at 230°C of the three materials are shown in Figures 4.4 and 4.5, respectively. PS and PP showed similar stiffness and viscous properties at this temperature. The substantial network of branches in LLDPE restricted chain segmental motion at these low frequencies

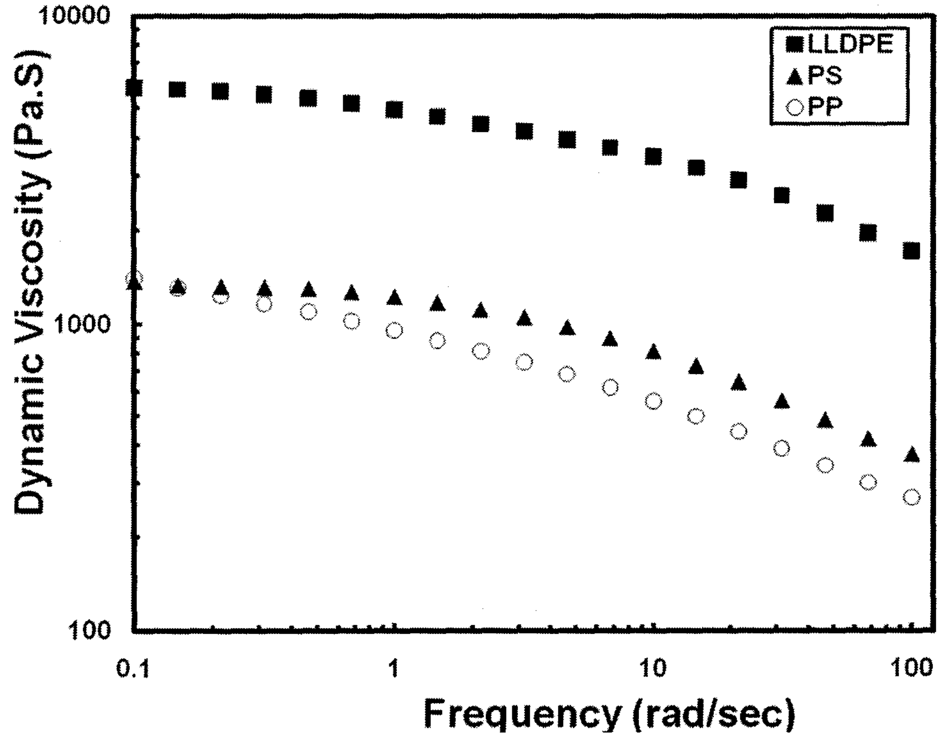

Figure 4.3 Dynamic viscosities of the three materials at 230°C.

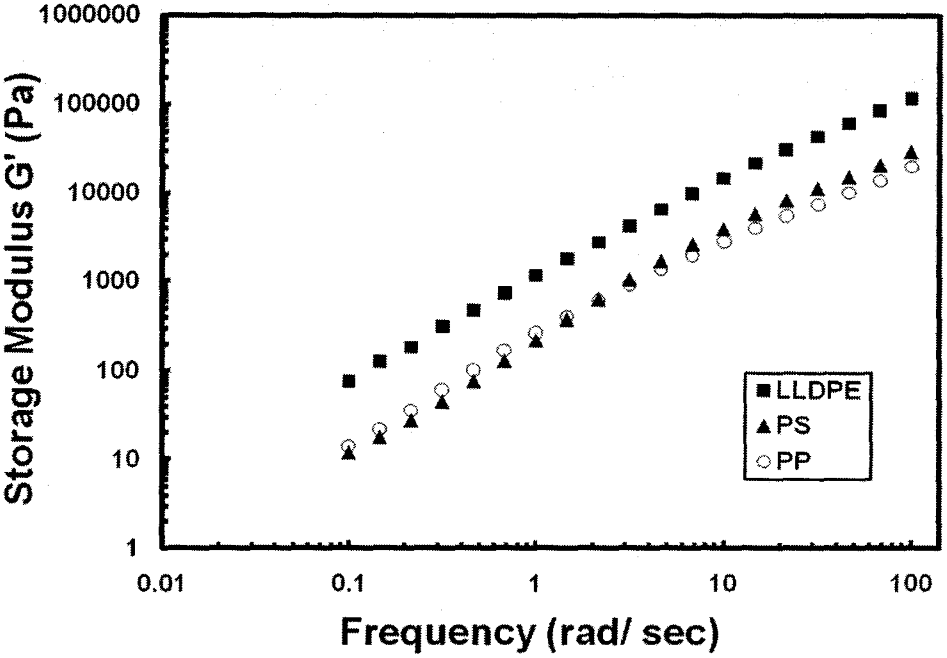

Figure 4. 4 Storage modulus (G') of the three materials at 230°C

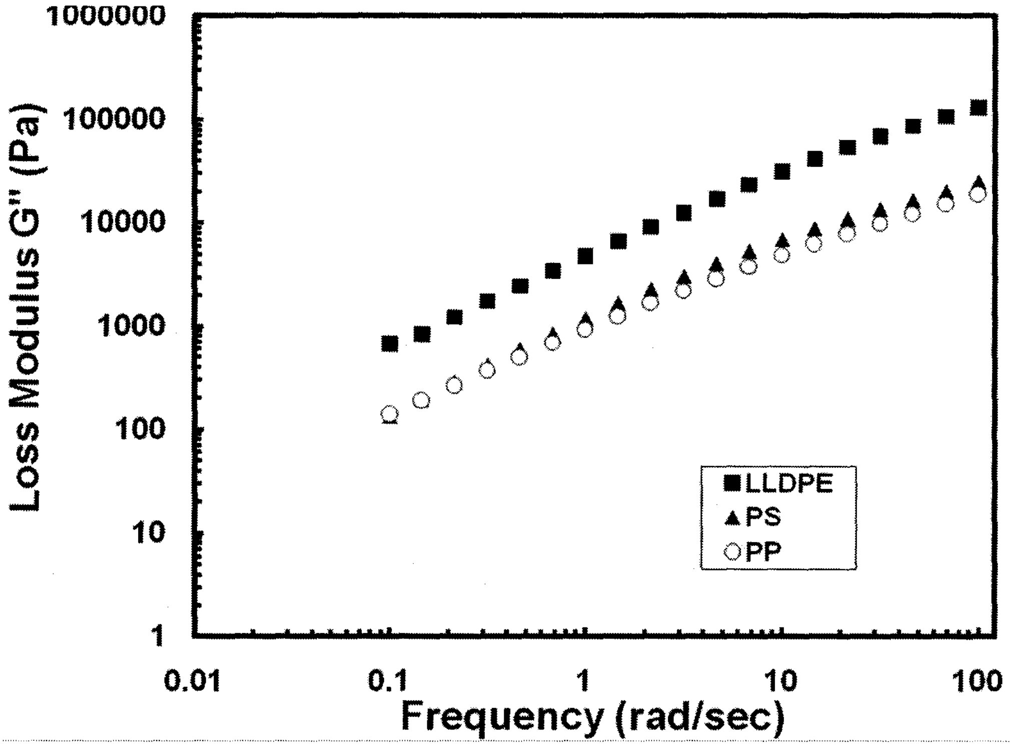

Figure 4.5 Loss modulus (G") of the three materials at 230°C

In general, the shear modulus (G’ + G”) of these polymers followed the same trends as the zero shear visocity data. Table 4.3 lists the G* values at 0.1 rad/s for 170°C and 230°C to give a sense of trend. PS showed the highest value of G’ at 170 °C compared with the other two resins, just as it was for the zero shear viscosity results. With the increase of temperature to 230 °C LLDPE has the highest storage modulus compared to PS and PP.

Table 4.3 Storage modulus for the three resins at 0.1 rad/s for 170°C and 230°C.

Complex shear Modulus G* (Pa)

Temperature (°C)	LLDPE	PP	PS
170	1180	578*	3102
230	675	140	136

*Measured at 175°C

4.1.3 Mechanical properties

Typical stress-elongation curves for the three resins at room temperature are presented in Figure 4.6 while average property values with their standard deviations are summarized in Table 4.4. LLDPE showed the lowest Young's modulus and ultimate tensile stress but the highest elongation at break compared to PP and PS.. Glassy PS showed the highest modulus and due to brittle failure, a low elongation at break was observed. A similar value (i.e. 3340 MPa) for the Young's modulus for PS was reported by Hahanfeld & Dalke (1985).

Table 4.4 Mechanical properties of the three resins

Materials	**Young's Modulus (MPa)**	**Ultimate tensile stress (MPa)**	**Elongation at break (%)**
LLDPE	308.70 ±32.81	13.65±0.31	977.80±92.84
PP	2145.50 ±18.79	36.20±0.23	38.02±7.38
PS	3462 ± 395.66	43.28± 0.73	3.80±1.52

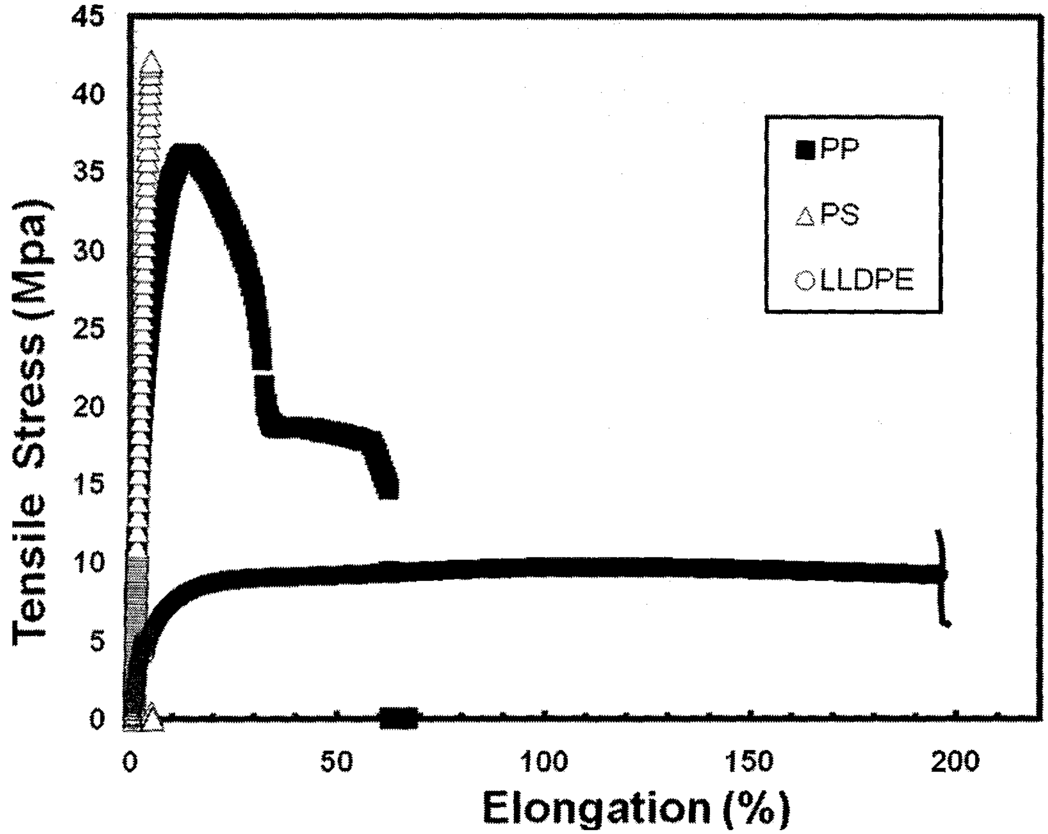

Figure 4.6 Tensile stresses versus the elongation for the three resins.

4.1.4 Pellet shape analysis

Shape analysis of polymer particles was made using Sigma Scan TM Pro 3.0. The average particle dimensions of the three materials with their standard deviations are shown in Table 4.5. LLDPE had the largest particle diameter compared to the other two materials. The side profiles (machine direction view with respect to how they were originally extruded) of particles for the three materials were almost the same. From the side view in Figure 4.7, LLDPE had a lens shape, PP had an elliptical shape and PS had a cylindrical shape. Further, the external shape of PS particle shows sharp edges.

The shape of the particles is mainly controlled by the type and the conditions of the pelletizing process and the rheological properties of the processed materials. This property is important to the porosity and shear strength of a granular bed made up of each polymer, which in turn affect the mobility and heat transfer. PS showed the highest bulk density compared to the other two resins (see Table 4.5). Conversely, the porosity of PS was lowest, i.e. $\varepsilon = 0.44$, which can be a related to its cylindrical shape. On the other hand, PP and LLDPE with their elliptical shape more closely packed resulting in porosities of 0.40 and 0.42, respectively. Overall, only marginal differences in the bed particulate arrangement was found between these three polymers.

Table 4.5 Summary of particles shape analysis of the three materials

Materials	**Average Diameter D (mm)**	**Thicknes s t (mm)**	**Top area (mm^2)**	**Side area (mm^2)**	**Bulk Density (kg/m^3)**
LLDPE	4.63 ± 0.25	2.57 ± 0.15	17.02 ± 0.47	9.12 ± 0.34	536.2 ± 1.5
PP	3.77± 0.33	3.47± 0.41	11.41 ± 1.19	10.47 ± 1.30	543.09 ± 2.17
PS	3.63 ± 0.32	2.65 ± 0.25	10.24 ± 0.89	11.35 ± 0.7	589.05 ± 0.205

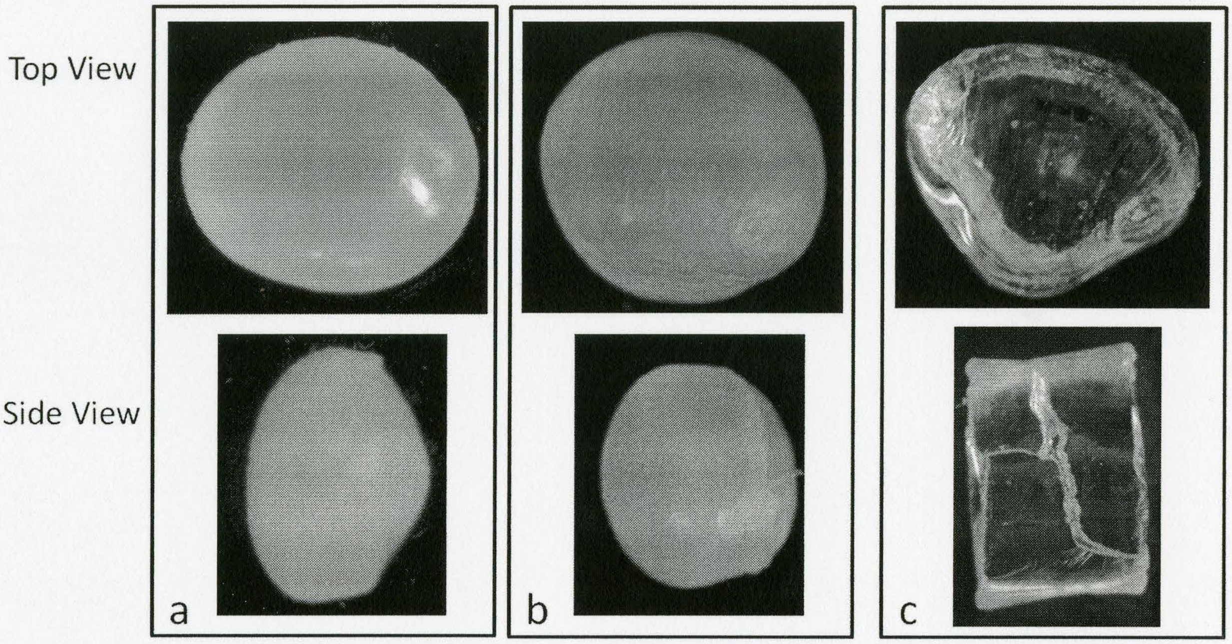

Figure 4.7 Pellet shape of the three materials a) LLDPE, b) PP and c) PS

4.2 Melting under zero shear stress

4.2.1 Sintering rate and surface tension of contacting, isolated particles

Images of sintering for the three resins were captured to evaluate the change in the dimensionless neck radius (y/a). Selected images showing the neck growth for the three resins at 230°C are shown in Figures 4.8 - 4.10. The dimensionless neck radius started to change when the temperature reached the melting point of the polymer. Sintering images showed complete coalescence of

PP and PS by the end of the experiments while LLDPE bridging was noted but complete coalescence was not observed even after 510 sec. The sintering rates of the three resins were determined by images analysis of the experimental data and an empirical model (Equation 3.7) was used to fit the data as shown in Figure 4.11. It can be seen from the plot that the sintering rates of PP and PS were rapid and the coalescence was completed when the neck radius approached one while in the case of LLDPE, the maximum dimensionless neck radius achieved was 0.8. This is an interesting result considering the melting temperature of LLDPE, as determined by DSC, is much lower than PP and its viscosity drops much more quickly than PS for temperatures immediately above its melting point. For all intensive purposes, LLDPE should have been expected to sinter the most quickly of the three materials. Sintering rate for the three resins are shown in Table 4.6.

The observed sintering rates are explained according to the viscoelastic properties (Section 4.1.2) and surface tension values for the three resins. The surface tension results were measured at 185°C and are summarized in Table 4.6. The temperature used for the surface tension measurement was considerably below that of the sintering experiments (45°C less); however, for conditions much higher or lower it was not possible to obtain a good droplet shape for all three materials. Therefore, we are simply using the surface tension values in the table to show relative differences between the three materials, with the assumption that these differences were similarly found at 230°C. LLDPE and

PS have comparable surface tension values while PP has the lowest. Knowing that surface tension is the driving force in sintering process, higher values help to facilitate fast sintering. However, this is true if the zero shear viscosity is also low. From the dynamic rheological measurements at 230°C, LLDPE has the highest zero shear viscosity compared with the other resins which was seen as largely contributing to the lower sintering rate. Also, the storage modulus of LLDPE, which represents the melt elasticity, is higher than the two resins. This is important since the sintering rate is not only function of the zero shear viscosity and surface tension but also affected by the viscoelastic nature of the polymer (Bellehumeur et al, 1996).

It should be noted that unlike extrusion which involves high shear rate, the sintering experiments are characterized as zero shear processes. So, faster sintering rate does not imply faster melting in single screw extruder. However, while forced melting is indicative of extrusion, within the interior of the solid bed of polymer and away from the shear field, sintering is viewed as an integral contributor to the overall extent of melting.

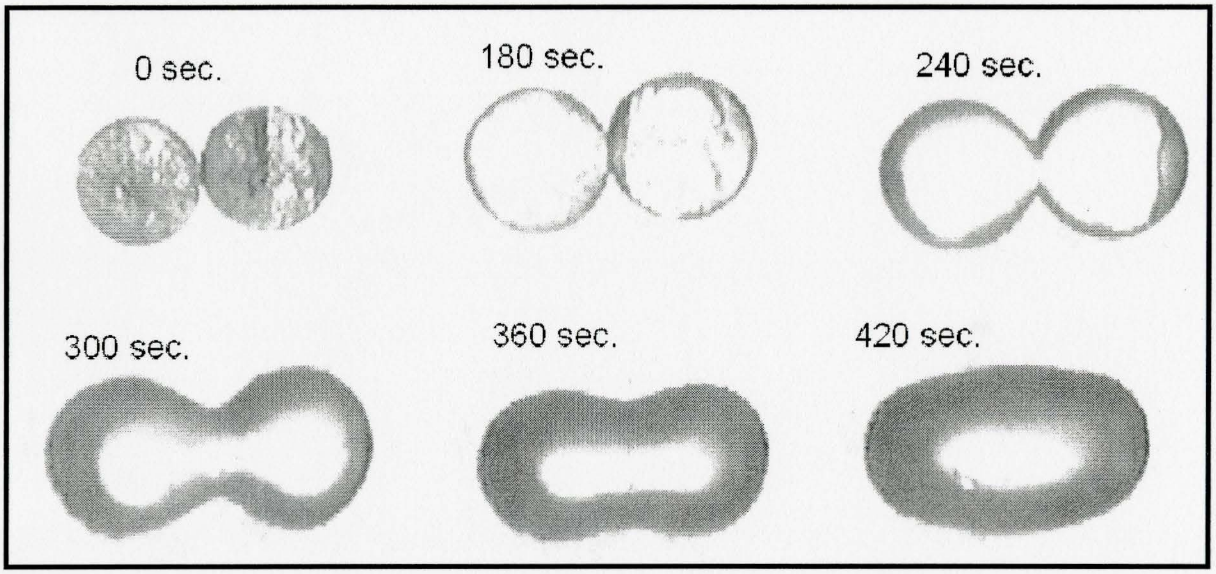

Figure 4.8 PS particle coalescence over time at 230°C.

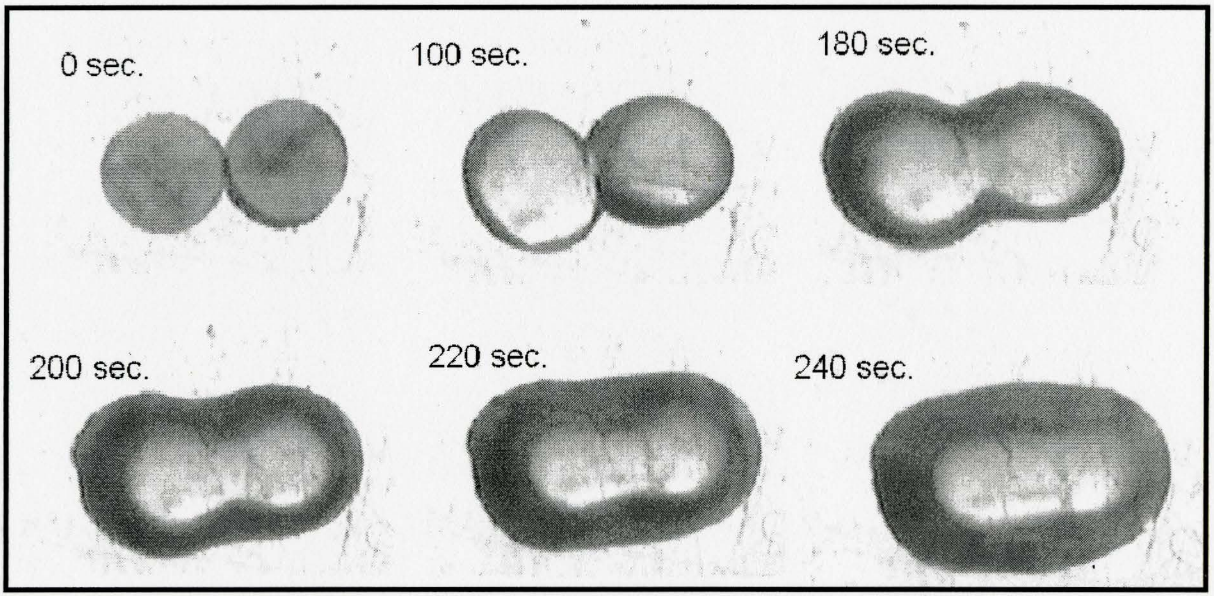

Figure 4.9 PP particle coalescence over time at 230°C.

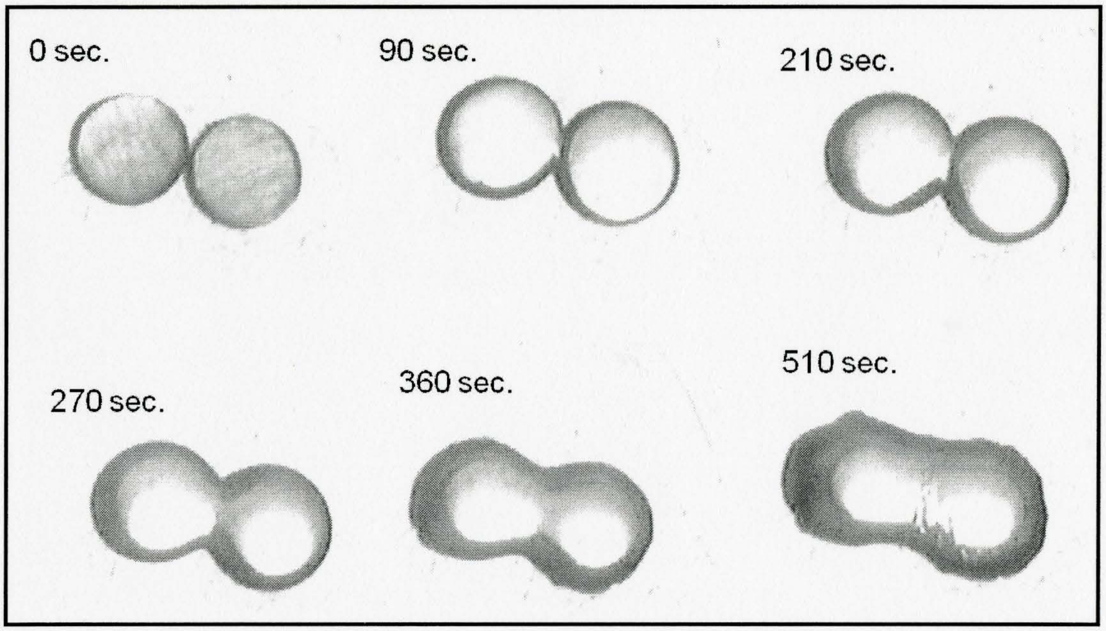

Figure 4.0010 LLDPE particle coalescence over time at 230°C.

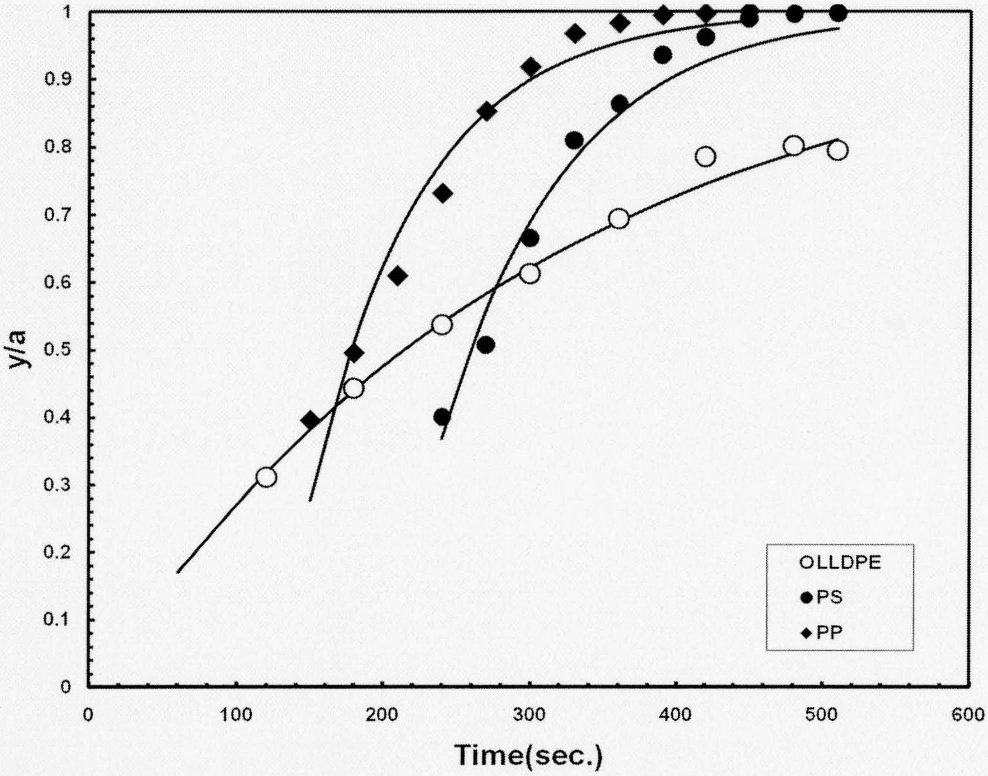

Figure 4.11 Dimensionless neck growth (y/a) of particles over time for the three resins. The solid lines represent the best fit using Equation 3.7.

Table 4.6 Results summary of sintering rate, surface tension and zero shear viscosity of the three resins.

Materials	Zero shear viscosity η_o @230 °C (Pa.s)	Surface tension Γ (mN/m)	Sintering rate (sec)
PS	1480±35.4	22.38 ± 0.89	504.6 ±17.1
PP	1750.77± 65	17.65 ± 0.13	562.4 ± 14.2
LLDPE	4944.05 ± 270	21.99 ±0.23	1840 ±41

4.2.2 Sintering of a dense granular bed (no compression forces)

Melting of the three resins was examined in the solids chamber without rotation of the drum or significant compression by the plunger. Photos of changes in the solid bed over time were captured every four minutes. A constant mass (30 g) of polymer was used each time. The solids chamber walls and the drum were maintained at 235 °C. The total time of each experiment was 16 minutes. The plunger was allowed to move down every four minutes with minimal force on the bed (10 N) in order to record the bed height. Unlike, the observation in sintering experiments, LLDPE solid bed showed more particle coalescence over the period of an experiment compared to PS and PP as shown in Figure 4.12. The LLDPE bed in contact with the hot drum formed a homogenous melt and the melt homogeneity decreased as the distance from the drum surface increased. Some unmelted LLDPE remained close to the plunger after the experiment run. The percentage of melt for PS, similar behaviour was observed though the melt layer in contact with the drum appeared less homogeneous and soft non-coalesced particles next to the plunger. On the other hand for PP, a thin layer melt was observed next to the drum and unmelted solid particles could be seen throughout the majority of the bed at the end experiment as shown in Figure 4.12 (c). The average percentages of melt estimated from Figure 4.12 for LLDPE, PS and PP were 79.45, 72.70 and 47.25 %, respectively. In all cases, melting progressed fastest close to the drum and side walls of from the solids chamber.

The more efficient melting of LLDPE compared to PP and PS puts into sharp contrast the sintering experiments above. While melting of individual particles revealed the importance of viscosity, viscoelasticity, and surface tension, it would seem under bulk conditions that other factors become far more important. Thermal and rheological properties would tend to favour LLDPE melting into a homogeneous pool fastest than the other two polymers; however, as shown already in the sintering experiments these continuum properties do not directly dictate the behaviour of discrete systems. From Equation 2.2 (Vargas and McCarthy, 2001) it is understood that the particle-particle and particle-wall contact area developed under an applied normal force (even body forces), and the relationship of the contact area to the shape of the particles and the material's Young's modulus are important factors for heat transfer within a dense granular bed. Looking at the bed melting rate in the context of these variables and with the expectation that the modulus would decrease with time, it becomes easier to explain the observations made in the drum simulator. From the mechanical results and particle shape analysis above, LLDPE showed the lowest Young's modulus and had the largest particle diameter compared to the other two resins. It can be inferred from these attributes that a bed of LLDPE solids should experience the largest contact area compared to PP and PS. Heat transfer plays a strong role in melting within the granular bed; a topic that needs greater study as the open literature is quite sparse. Subsequent sections will cover this topic in detail.

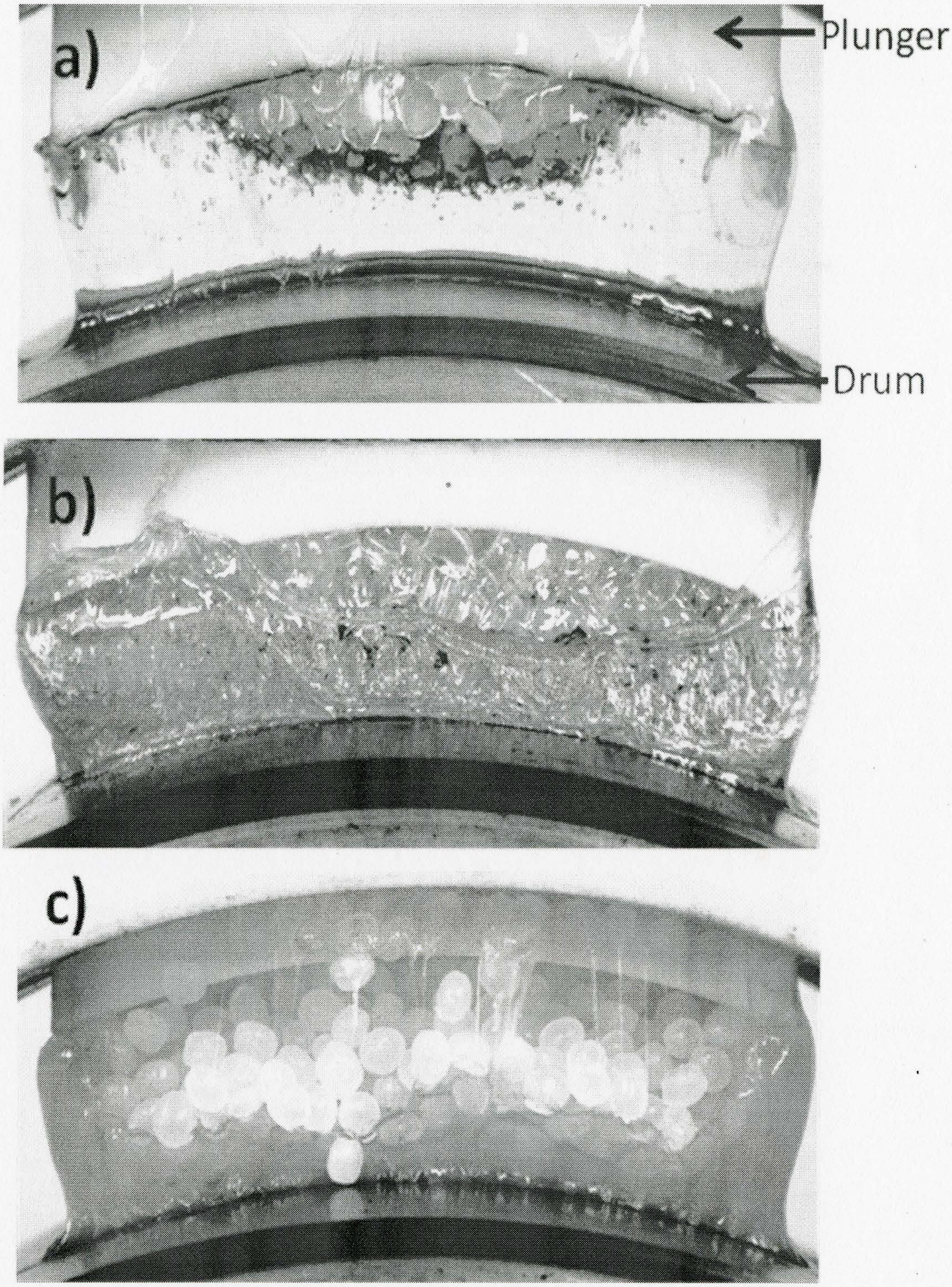

Figure4.12 Images of solid bed melting at 235 °C after 16 min. under no applied load or shear stresses at the drum, a) LLDPE, b) PS and c) PP

4.2.3 Melting under compression

The melting behaviour of LLDPE, PP, and PS was also examined under compression. In this case, melting was expected to occur much more rapidly due to the greater contact area developed within the bed due to the applied compressive force. The temperatures of both solids chamber and the drum were set at 235°C and the drum speed kept at zero, similar to the previous section. Once again the chamber was filled with 30 g of resin, which due to differences in bulk density meant differing initial bed heights for the experiments between the three polymers. The cross head speed of the plunger was 1.73 mm/min and the resulting force from compression was recorded. The plunger speed was selected with consideration for the rate of height shrinkage in a screw channel for a polymer in a 50mm extruder operating at 0.5 kg/h/RPM and using a metering screw with a 3:1 compression ratio. Each experiment was continued until a plateau in the force versus solid bed height curve was noticed, or complete melting of solid bed was observed. Images of the solids bed for each resin were taken over the span of the experiment, as shown in Figure 4.13.

Only PS showed a completely homogenous melt at the end of the experiment (elapsed time 369 s). This was faster than when melting with no compressive forces (i.e. sintering of granular bed), where even after 960 s complete homogenous melting was not achieved. The fast and complete melting observed under compression was related to the plastic dissipation energy (PED) within the individual particles. Gogos et al (1998) found that PED resulting from compression forces at engineering strain of 0.9 can rise the initial temperature of polystyrene (PS) pellets by 35°C. Due to the irregular particle shape and random arrangement of individual granules within the PS bed, and recognizing that both consolidation and compaction occurred as the plunger compressed the bed, the actual strain during our experiments cannot be estimated. We merely stated Gogo's findings in order to recognize a heat source for PS which was not as strongly present for the other two polymers.

The LLDPE and PP beds showed less melt homogeneity with unmelted solids present next to the plunger. Further, in the case of LLDPE and PP, a large quantity of polymer melt leakage was found from the gap between the drum and the solid chamber gasket. No leakage was observed in the case of PS. The leakage by the PP bed was noticed at early time of the experiment (224 sec.) while in the case of LLDPE, leakage had only begun to occur near the end of the experiment (329 sec.). The total time of each experiment was around 400 sec. The degree of leakage noticed for LLDPE and PP appeared to be the same, as shown in Figure 4.13.

The recorded force versus bed height from comparison of the three resins is shown in Figure 4.14. It could be seen that the PP bed built up force very rapidly compared to the other two resins. For example, the time needed to reach 0.2 kN for the PP, LLDPE and PS resins were 128.0, 241.0 and 280 sec respectively.

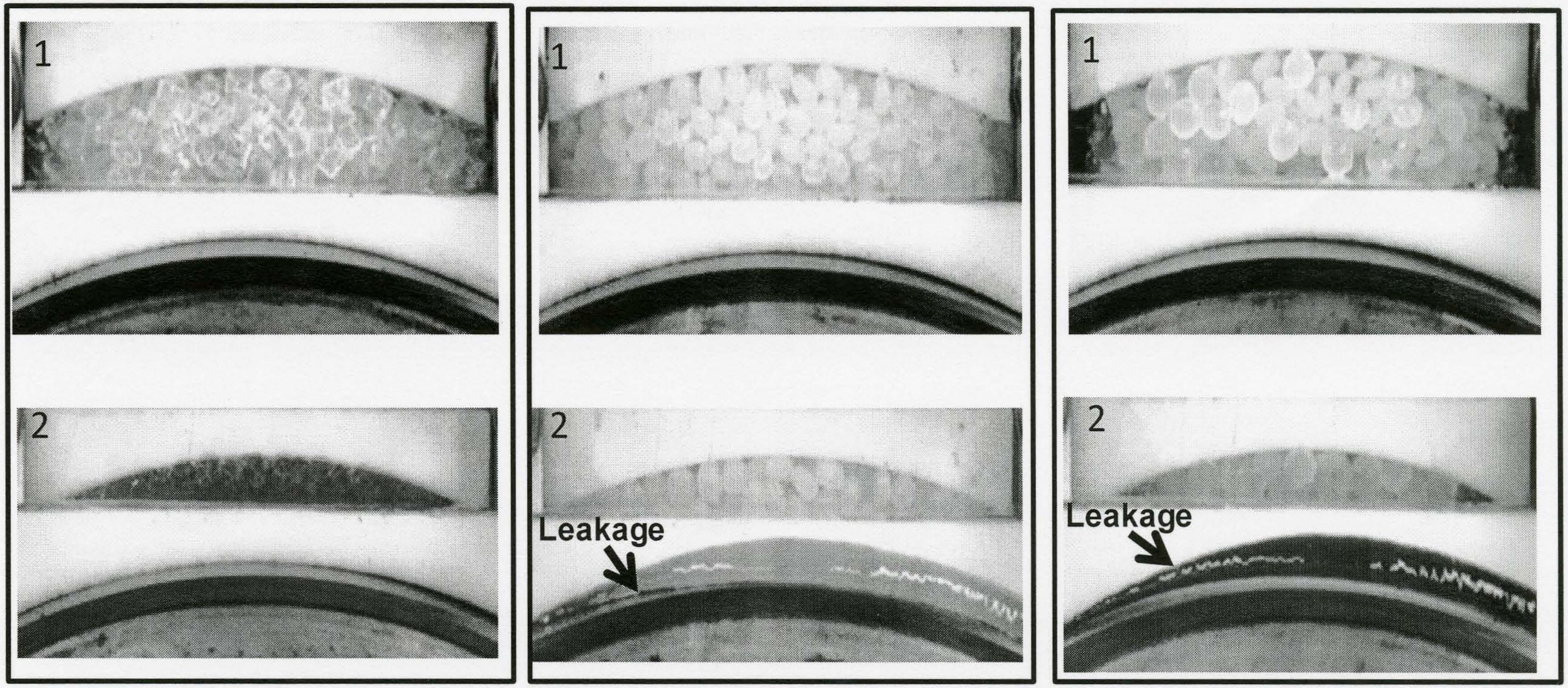

a)

b)

c)

Figure 4.13 Solid bed melting for the three resins under compression at temperature of 235°C for both the drum and the solid chamber. a)PS ,b)PP and c) LLDPE; 1) at the start of the test 2) at the end of the test

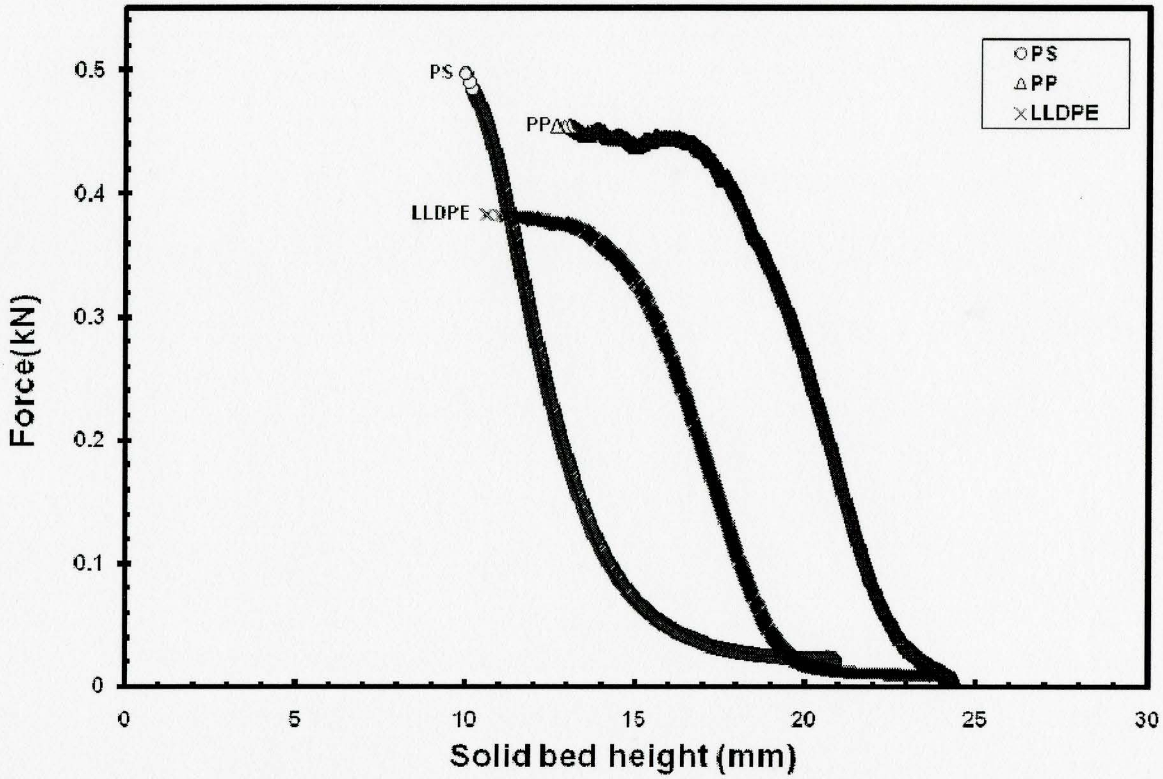

Figure 4.14 Solids bed melting for the three resins under steady compaction at 235°C for both the drum and the solid chamber.

The delay in building force for PS and LLDPE was attributed to particles rearrangement (consolidation) during the compression. No studies of melting under shear were conducted in the drum simulator. The minor leakage noted under compaction and no shear became unmanageable once the drum rotated. This made it impossible to interpret the relevance of recorded data during preliminary shear trials. Evaluation of the performance of the drum simulator showed that its greater contribution to our knowledge of melting would come out of understanding how the solids heated up prior to the onset of melting.

4.3 Heat transfer in the solids bed (Top of solid bed measurement)

The ultimate culmination of this research is intended to provide a better explanation of observed differences in the melting rate of these three polymers found in an extruder. It is evident from the results in Sections 4.2.2-4.2.3 that knowledge of the modes of heat transfer within a dense granular bed is important to understanding its rate of melting. The efficiency of heat transfer will define the onset and the rate of melting during extrusion. From a practical point of view, experimental measurements of solids bed heat transfer within a rotating screw, particularly cross channel, as the bed moves down the length of the solid conveying zone are impossible to perform. The drum simulator provides ways to explore the heat transfer in a solids bed under different conditions by embedding thermocouples from the top or through the front wall.

Temperature measurements made from the top of solid bed (which represents the screw root in a real extruder) were made at two points A and B as shown in Figure 4.15, by placing two thermocouples through the top of the plunger. The drum temperature was the only variable in these tests. The two points were at a distance of 18 mm from each side wall while the gap between the two probes was 37.7 mm. The tip of the thermocouple was located a vertical distance of 8.0 mm from the plunger surface and the distance from the front wall to the thermocouple tip was 13.60 mm. The drum was set at speed of 100 RPM and then a constant mass of 30g of each resin (23°C) was poured into the solids chamber. A constant force of 10 N was applied on the sample during the experiment which corresponded to an apparent pressure of 4.385 kPa. The walls of the solids chamber were maintained at 80°C

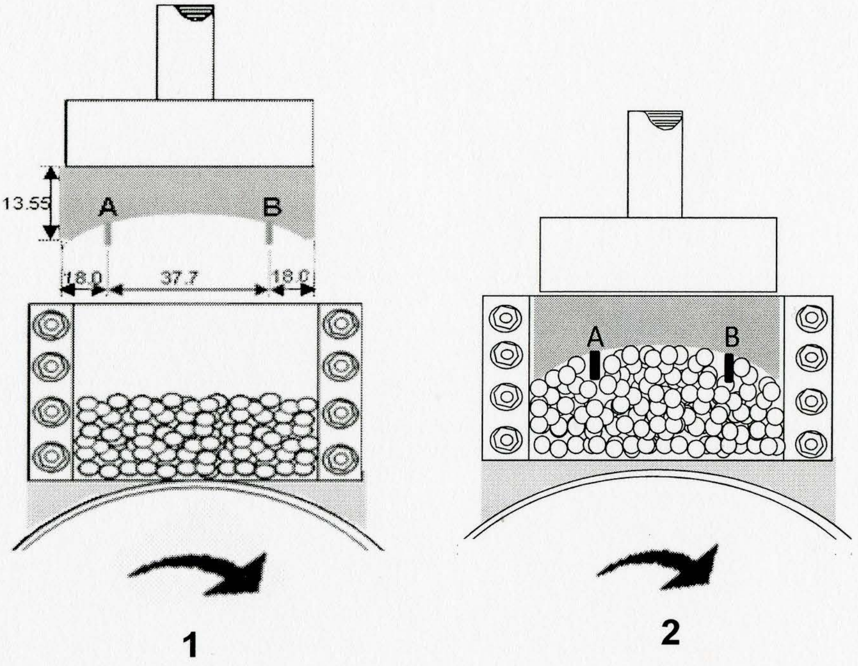

Figure 4.15 Experiment set up for the measurement; 1) shows the locations of the two thermocouples, and 2) shows the two thermocouples after applying force. A and B represents the thermocouple tips

Experimental studies by Moysey (Ph.D. thesis, 2007) have shown that for particle sizes of 6mm and below there will be no difference in the measured temperature at a thermocouple, whether situated in the interstitial region of a bed of plastics or embedded within a particle.

4.3.1 LLDPE solid bed temperature

a. At a temperature of 50°C for drum and 80°C for solids chamber.

The average temperature at points A and B as a function of time are shown in Figure 4.16. The error bars shown in the figure represent the standard deviation in the measurements over three repeated runs. The temperature curves for both points showed no change in temperature over the first two minutes which indicated that the pellets close to the plunger were still cold. The temperature of both points increased steadily with time. However, temperatures measured at point B were higher than those measured at point A. The trend was more pronounced towards the end of the test. The highest average recorded temperatures for point A and B were 48.27±0.38 °C and 50.83±0.31 °C, respectively. The highest temperature difference between point A and B was 2.77±0.11°C recorded at 17 minutes.

Quite interestingly, pellet circulation within the bed was observed by the video recording over the course of the test. The pellets close to the drum surface followed the direction of rotation towards the advancing wall (i.e. wall closest to point B) and then were pushed up towards the plunger. Eventually the solids in the chamber completed a circulating loop. Pellet motion was also seen in the center of the solid bed (i.e its core). The flow field observed is indicated qualitatively in Figure 4.17 with the inclusion of directional arrows overlaid upon an image of the circulating solids bed. The observed circulation of pellets is believed to be the reason of the temperature difference between point A and B. No melting or pellet deformation was observed at the end of the test.

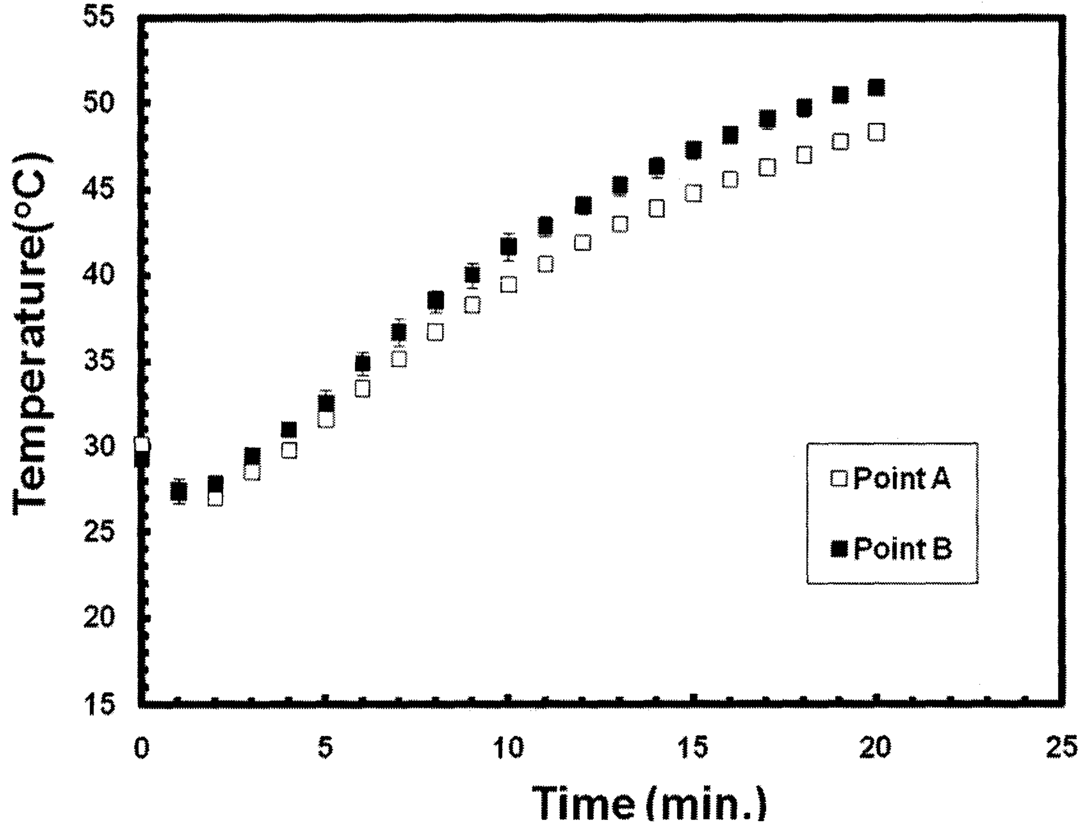

Figure 4.16 LLDPE temperature curves of point A and B at drum speed of 100RPM (solid chamber at temperature of 80°C drum temperature 50 °C)

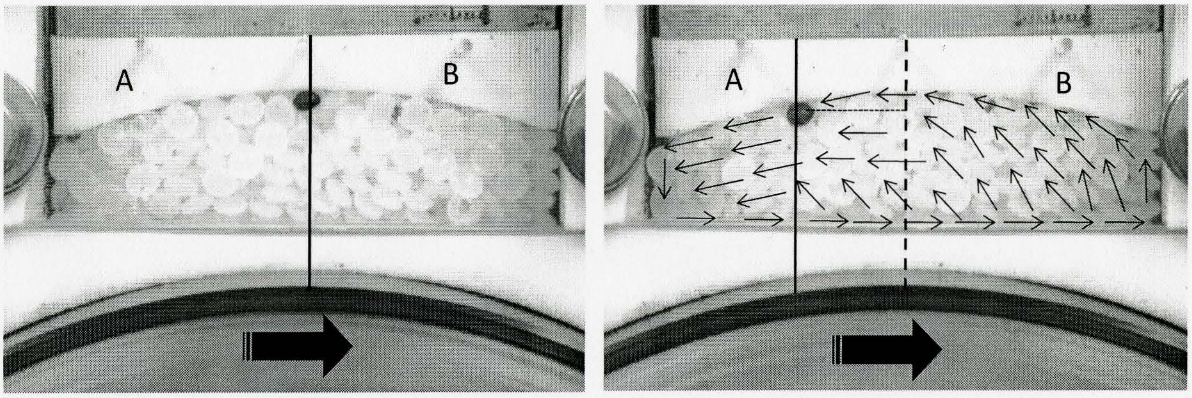

0 sec

After 60 sec

Figure 4.17 LLDPE particle motion in solid chamber at temperature of 50 °C drum and 80°C for solids chamber and drum speed of 100 RPM. The arrows represent the direction of motion. Black pellet was included in the chamber to trace the motion of the bed.

b. At temperature of 80°C for both drum and solids chamber.

The drum temperature was increased from 50°C to now 80°C in this section and once again the average temperature profiles at points A and B were plotted versus time, are shown in Figure 4.18. Similar to the previous results, a difference in temperature between the two points was observed. The highest temperatures recorded were 58.97±0.59°C for point A and 61.23±0.47°C for point B within the LLDPE bed. The maximum temperature difference between the two points was 4.17±0.07°C recorded at 14 minutes. The difference was once again attributed to observations of pellets exhibiting circulation but now at higher speed compared to the 50°C drum condition. At the end of the experiment no melting was observed, although some flakes (resin fragments) were seen on the drum surface. These flakes are probably the result of abrasive erosion created by the drum motion and the high drum temperature. The high drum temperature softened the sample and made it easy to deform.

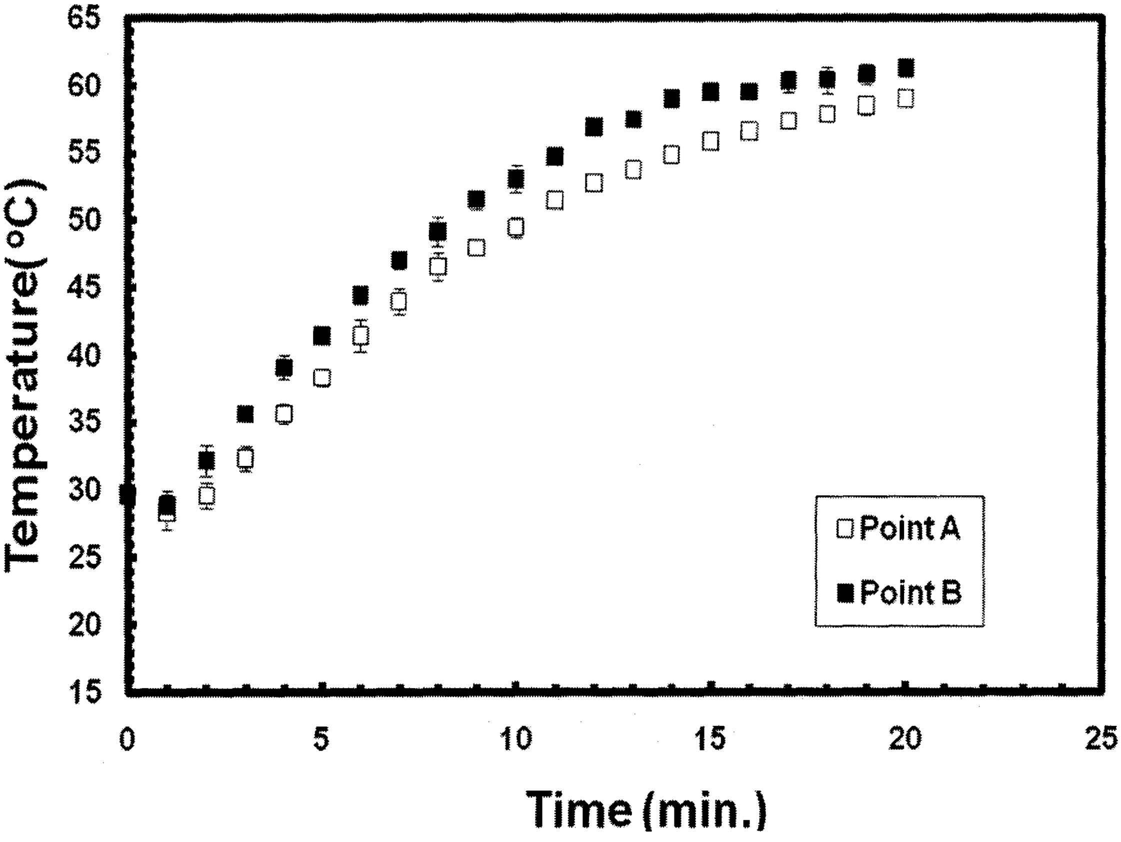

Figure 4.18 LLDPE temperature curves at points A and B for a drum speed of 100 RPM (drum and solids chamber at temperature of 80°C)

c. At a drum temperature of 110°C and solids chamber of 80°C

The average temperatures at points A and B as a function of time are shown in Figure 4.19. For the first 13 minutes, the average temperature recorded at point B was higher than at point A, though after the first five minutes into the test variance in the measurement made it difficult to state whether there was any significant difference in the temperature between these two locations. The larger standard deviation above 5 minutes was attributed to the high rate of pellet circulation observed during the experiment. The maximum temperature recorded for points A and B were 79.64±4.82°C and 79.78±3.11°C, respectively. The pellets circulation was faster than that observed at drum temperatures of 50 and 80°C. The convergence in temperatures at points A and B indicated the circulation rate now dominated over bed densification at the advancing wall. At the end of the experiments, the LLDPE sample left on the drum surface a thin melt film and high amount of flakes, as shown in Figure 4.20 (a). Also, some signs of liquid bridging between the pellets were seen, as shown in Figure 4.20(b). The reported data is based on 8 runs.

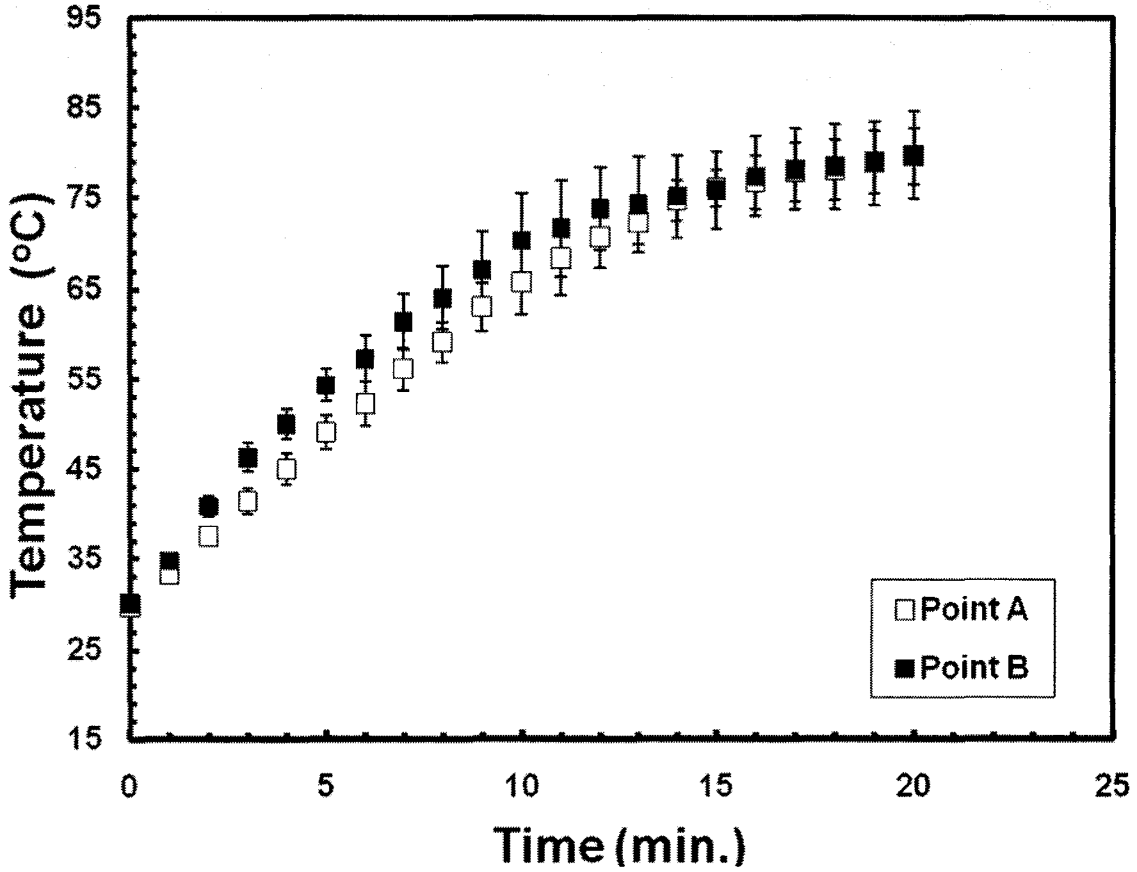

Figure 4.19 LLDPE temperature curves at points A and B for a drum speed of 100RPM (solids chamber at 80°C and drum at 110°C)

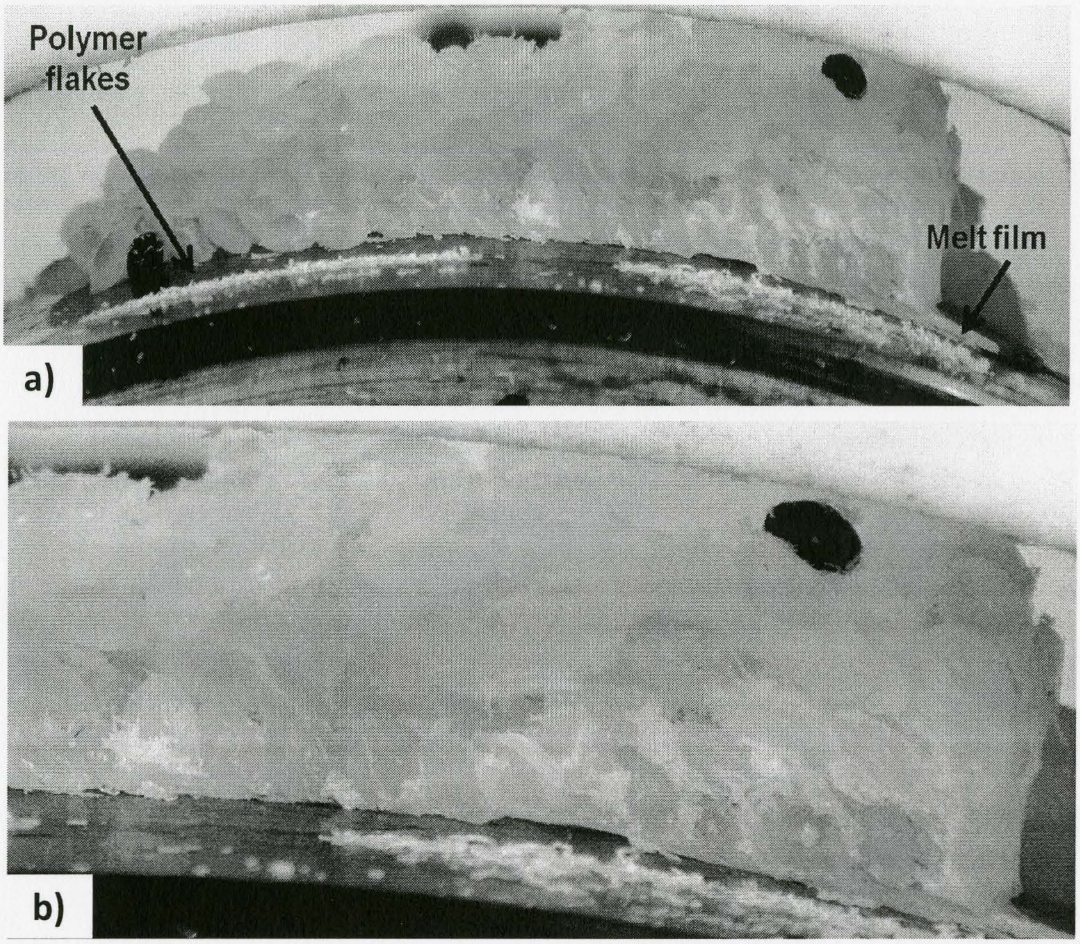

Figure 4.20 Typical condition of the LLDPE bed after run at drum speed of 100RPM and temperatures of 110°C for the drum and 80°C for the solid chamber; a) polymer flakes and the melting layer, b) the bridging between the pellets

d. Mean path velocity

Tracing the circulation path of several particles from the recorded videos at each drum temperature condition allowed quantitative determination of the mean bed circulation speed. The mean path velocity (i.e. the time taken between two designated points) is the only value stated here; however, the reader should be aware that this does not give a true representation of the tortuous path taken by any individual pellet. Contrary to the continuous streamlines seen for fluids in a lid-driven cavity, the anisotropic stress distributions typical of a dense granular bed do not allow individual particles to move along a linear path. Figure 4.21 shows the mean path velocity of LLDPE pellets within the solids chamber under an apparent pressure of 4.385kPa and for different drum temperatures. It can be seen that the pellet velocity increased with drum temperature. The pellet velocity showed large variation at 110°C indicating increased anisotropy in the stress distribution under this condition.

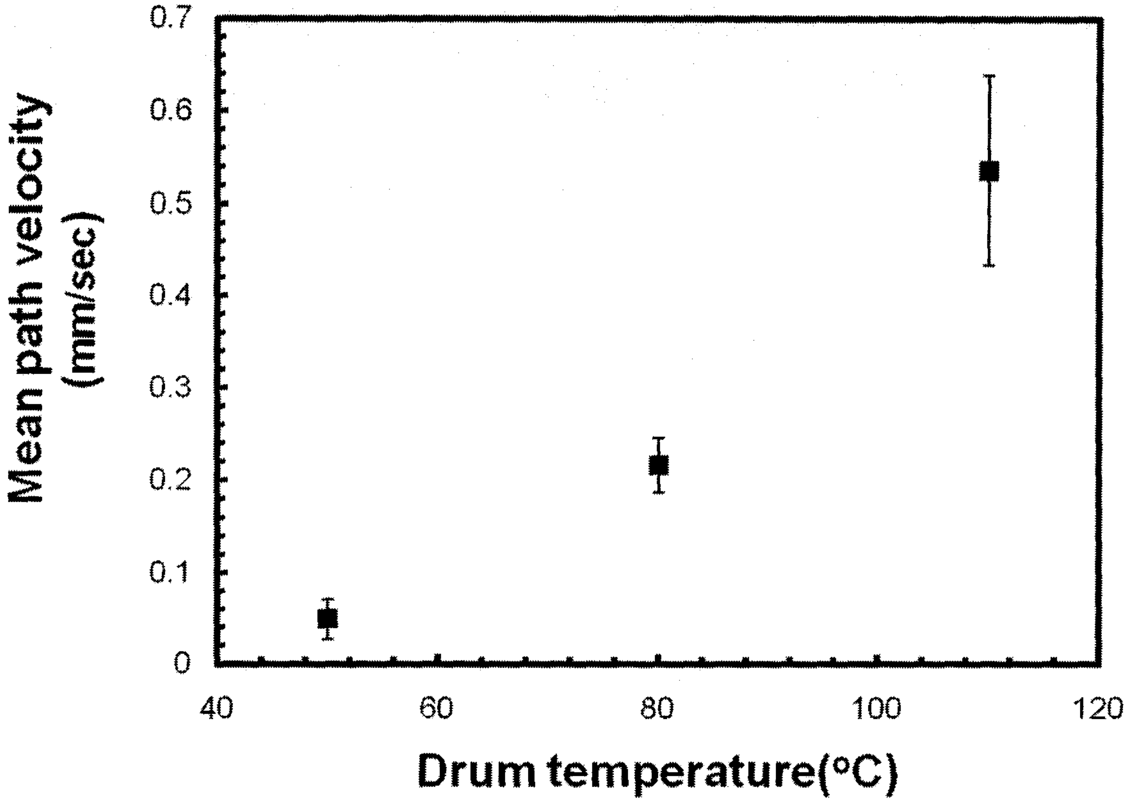

Figure 4.21 Mean path velocity of LLDPE pellets within a solid bed under an apparent pressure of 4.385kPa and at different drum temperatures.

e. Effect of compaction on the heat transfer in the LLDPE solid bed

To examine the effect of compaction on the heat transfer within the LLDPE solids bed, a series of tests were conducted under different degrees of compaction (0.01, 0.05 and 0.1 kN applied). These loads correspond to a pressure of 4.385, 21.29 and 43.85 kPa, respectively. Tests at loads higher than 0.1 kN were difficult to perform because of the upper limit on motor power. Higher loads led to an overloading of the motor and slower drum rotation. The drum and the solids chamber were maintained at 80°C and the drum speed was set at 100 RPM.

The effect of compaction on the temperature profile at points A and B are shown in Figures 4.22 and 4.23, respectively. At point A, the recorded temperatures decreased with increasing load from 4.385 to 21.29 kPa. However, further increase in load did not cause any decrease in temperature. On the other hand, temperature measurements at point B showed a continual decrease with increasing applied load.

Despite the fact that compaction of the solids led to greater contact area for heat transfer, it also reduced particle motion and results in plug flow like flow. The lowering in pellets motion led to the decrease of the measured temperature at both points.

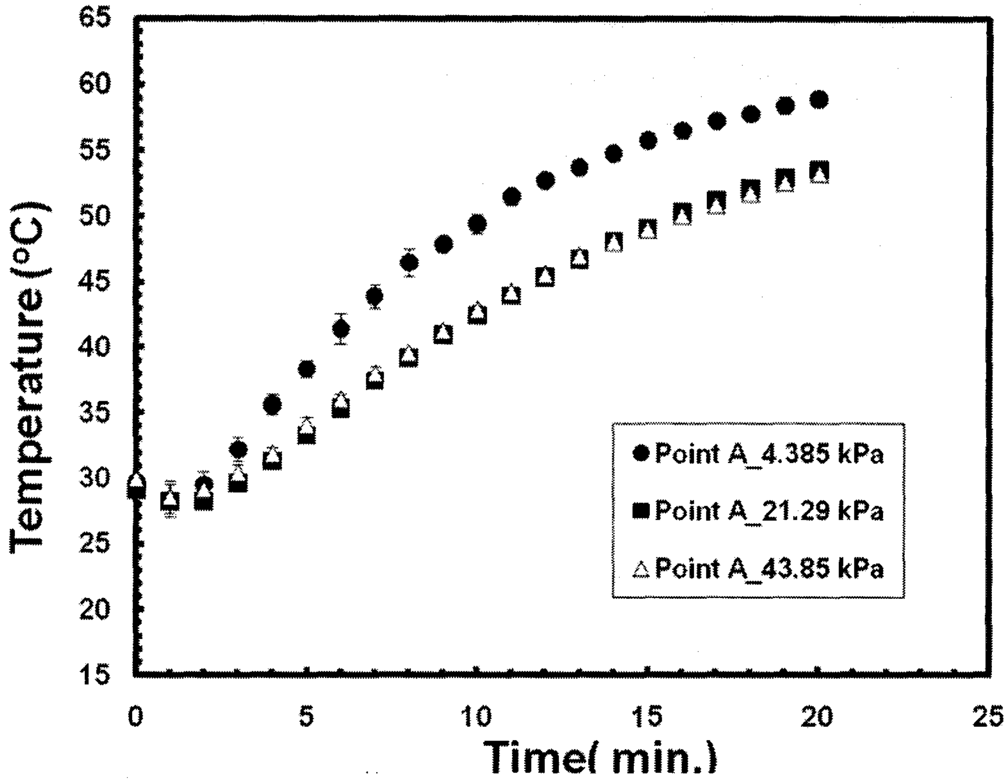

Figure 4.22 LLDPE temperature curve at point A with time at different pressures (at set temperature of 80°C for both drum and solids chamber, and drum speed of 100 RPM)

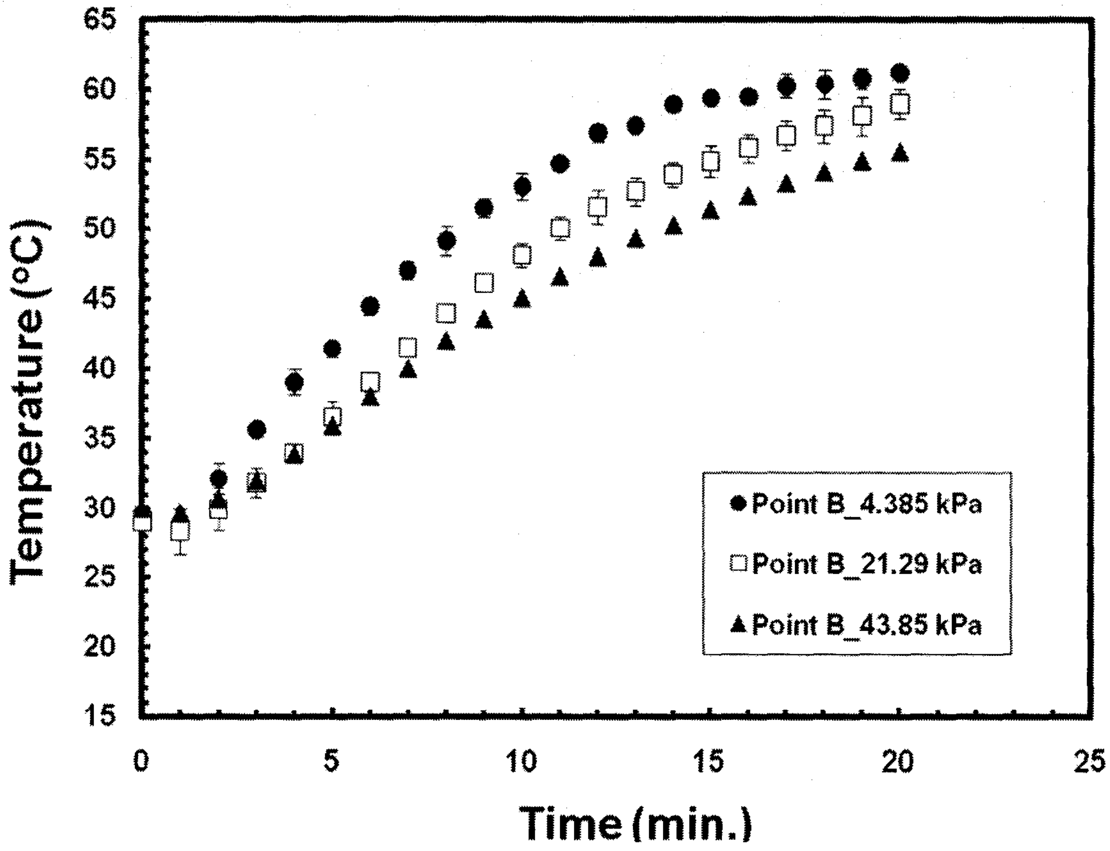

Figure 4.23 LLDPE temperature curve at point B with time at different pressures (at set temperature of 80°C for both drum and solids chamber, and a drum speed of 100 RPM)

4.3.2 PP solid bed temperature

a. Drum temperatures of 50-80°C and 80°C for the solids chamber.

Unlike the observations seen for LLDPE, PP did not show any circulation of its bed with time at these conditions. As a result, there was no difference in value between points A and B as the temperature of the bed increased over time. The temperature profiles within the bed at drum temperatures of 50°C and 80°C are shown in Figures 4.24 and 4.25, respectively. The PP bed at the end of the experiments at 80°C kept its shape. No flakes or deformation were observed at either temperature conditions.

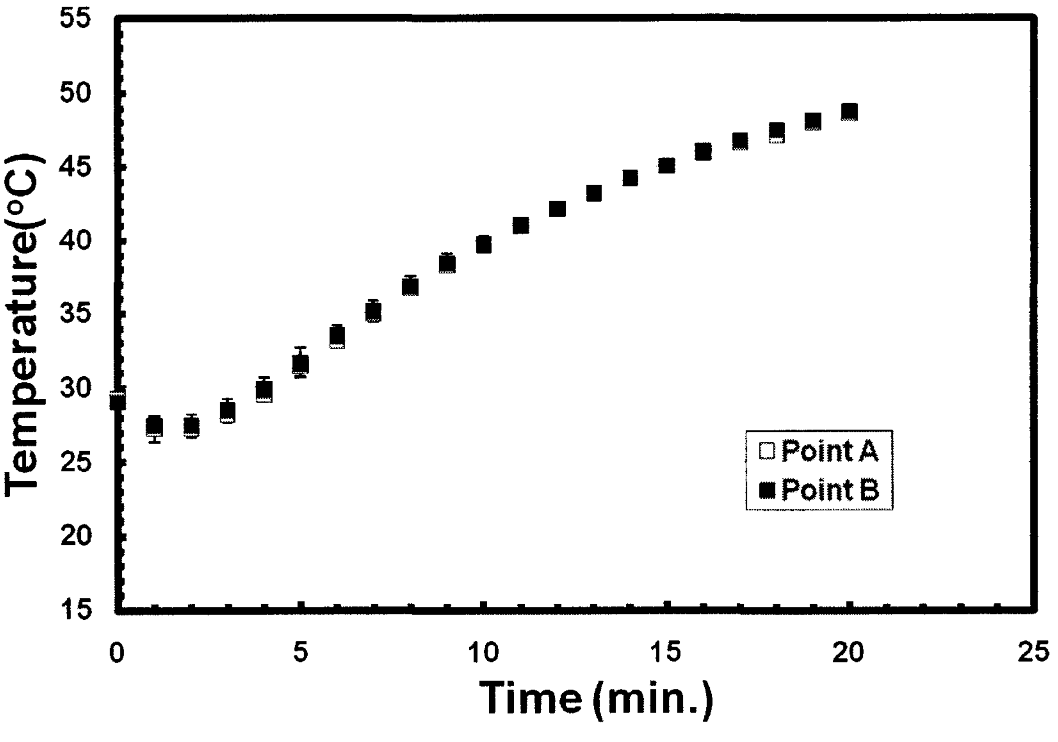

Figure 4.24 PP temperature curves at points A and B for a drum speed of 100RPM (solids chamber at temperature of 80°C and drum temperature at 50°C)

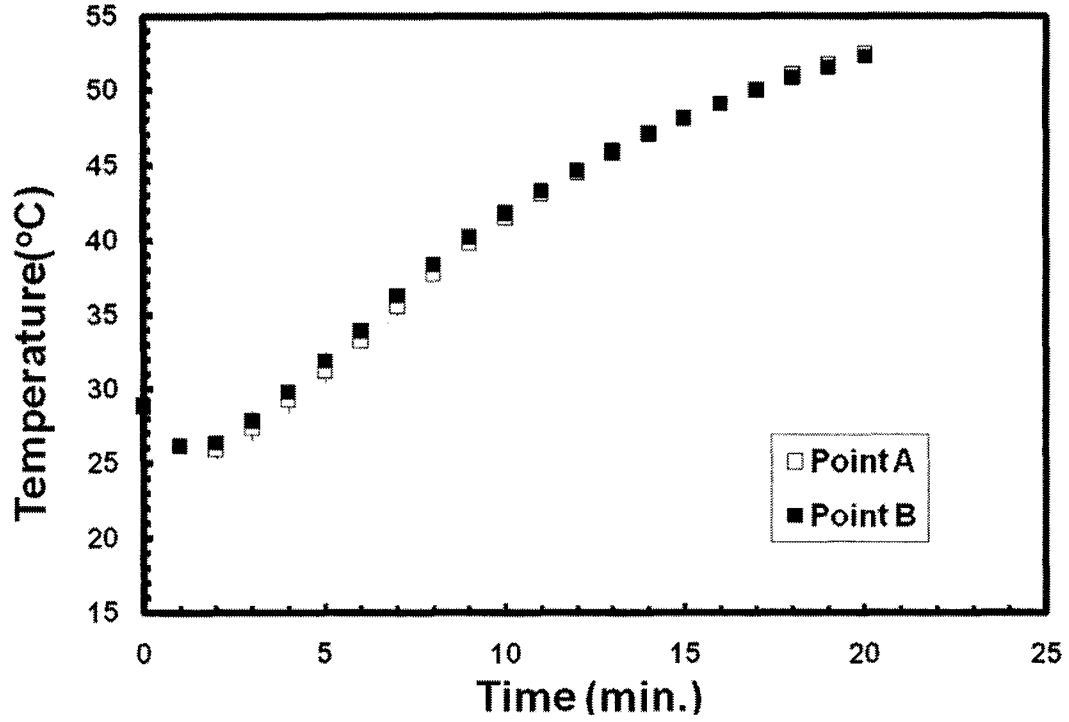

Figure 4.25 PP temperature curves of side A and B at drum speed of 100RPM (drum and solids chamber at temperature of 80°C)

b. At a drum temperature of 130°C and solids chamber of 80 °C.

The average temperature curves at points A and B as a function of time are shown in Figure 4.26. Temperature differences were observed between the two points initially (up to 4 min), but afterwards the temperature profiles overlapped. High standard deviation values were calculated for the reported data. The highest standard deviations for side B and side A were 3.65°C and 3.84°C, respectively. The temperature difference observed between points A and B during the initial five minutes was attributed to the circulation of pellets.

During the first five minutes, a relatively high pellet circulation was observed which slowed down with time afterwards. Figure 4.27 shows the average mean velocity of PP at 130 °C drum temperature. In this figure the average mean velocity for LLDPE was added for comparison purpose. It is clear from this figure that LLDPE pellets has higher average mean velocity trend compared to PP pellets.

Finally, although the set temperature of the drum was close to the melting point of PP, no pellet deformation or flakes were observed at the end of the experiment. A plausible reason for this behaviour compared to LLDPE might be the superior mechanical integrity of the material.

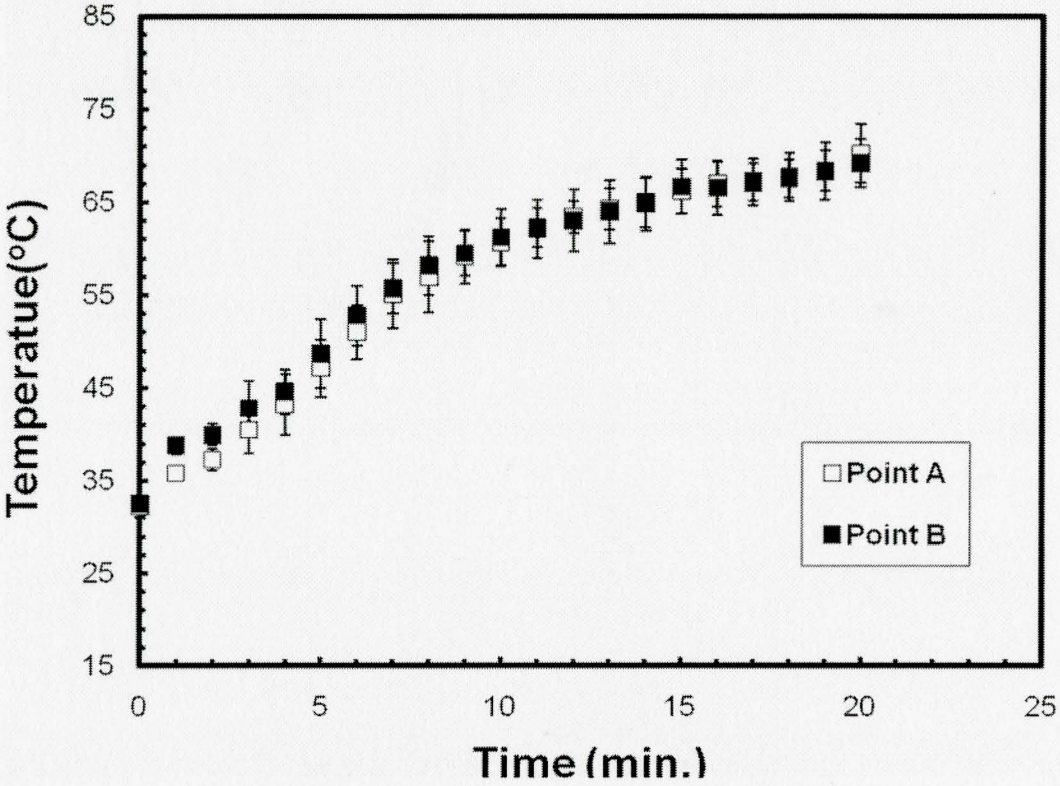

Figure 4.26 PP temperature curves of side A and B at drum speed of 100RPM (solid chamber at temperature of 80°C drum temperature 130 °C)

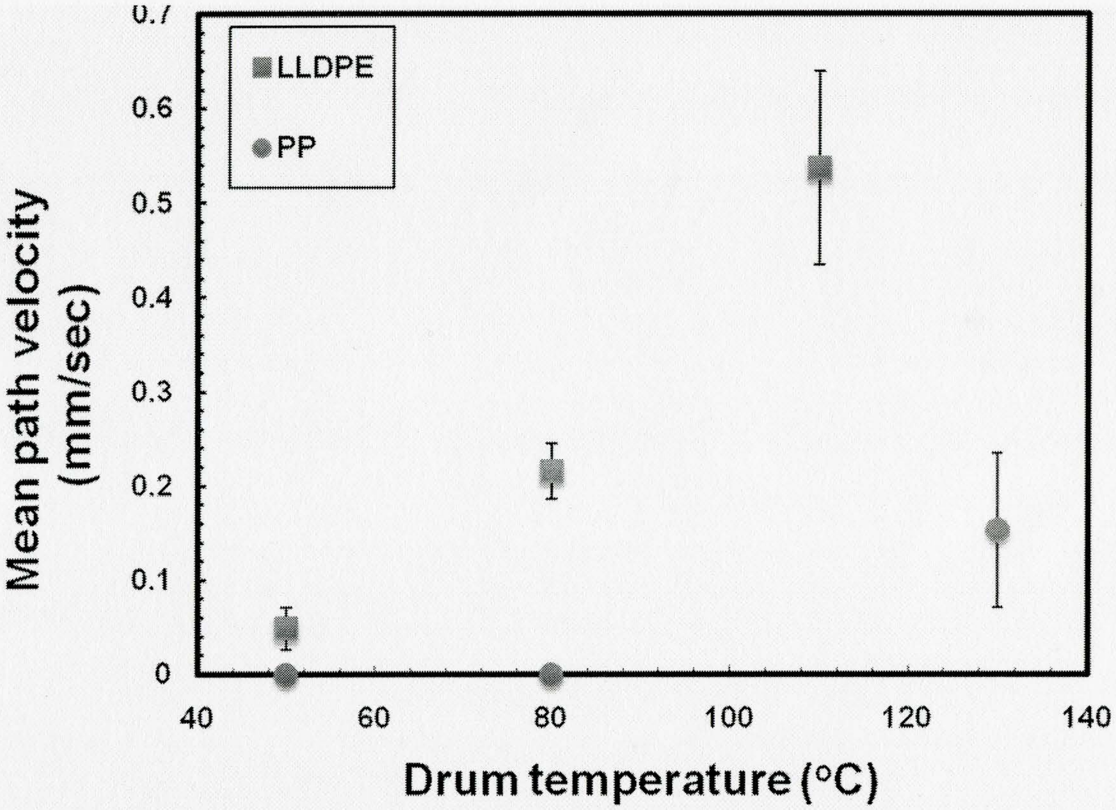

Figure 4.27 Mean path velocity of PP and LLDPE pellets within a solid bed under an apparent pressure of 4.385kPa and at different drum temperatures.

3.3 PS solid bed temperature

a. At drum temperatures of 50-80^{o}C and a solids chamber of 80^{o}C.

Figures 4.28 and 4.29 show the average temperature curves for points A and B with time for drum temperatures of 50^{o}C and 80^{o}C, respectively. No difference in temperatures was observed between the two thermocouples as the temperature of the bed increased with time. Similar to the PP experiments under the same conditions, no evidence of pellet motion was noticed during the experiment, even though the drum temperature was close to the glass transition temperature by 80°C. The sample at the end of the experiment kept its shape. No flakes formation or pellet deformation was observed.

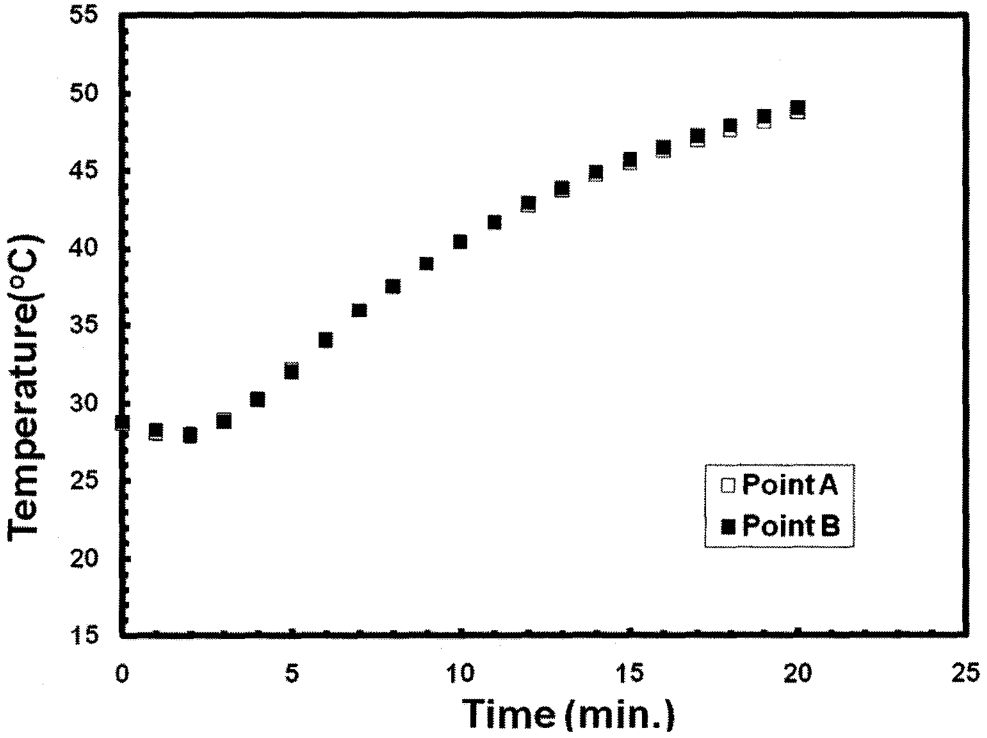

Figure 4.28 PS temperature curves ar points A and B for a drum speed of 100RPM (solids chamber at temperature of 80°C and drum temperature at 50 °C)

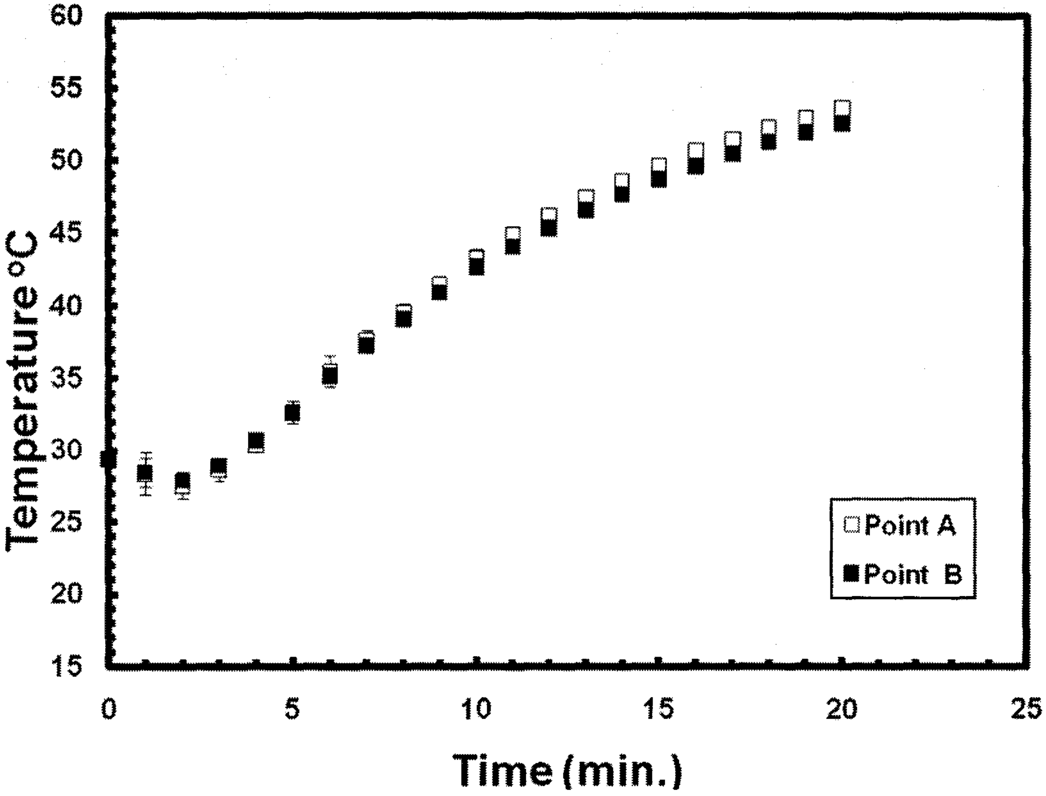

Figure 4.29 PS temperature curves at points A and B for a drum speed of 100RPM (solids chamber at temperature of 80°C and a drum temperature of 80°C)

No experiment was conducted at drum temperature condition of 130°C due to the high torque requirement on the motor for PS above its glass transition temperature.

4.3.4 Summary of the solid bed heating results for the three Polymers

Evidently, the pellet circulation noted in some experiments has an impact on the distribution of heat within a solid bed and the overall heating rate of the bed. To highlight the effect of particle circulation on the overall heating of the bed for the three resins, average temperatures were obtained from the final temperature measured at points A and B. Figure 4.30 shows the calculated averaged temperature for the three resins against the drum temperature. As seen in the figure, LLDPE bed has the highest average temperature compared to the other two resins. This is expected since LLDPE showed pellets circulation in all the experiments. When the pellet circulate, it gains heat from the hot drum and solid chamber walls surfaces which in turn exchange the heat with other pellets in the solid bed resulting in rise of the overall bed temperature.

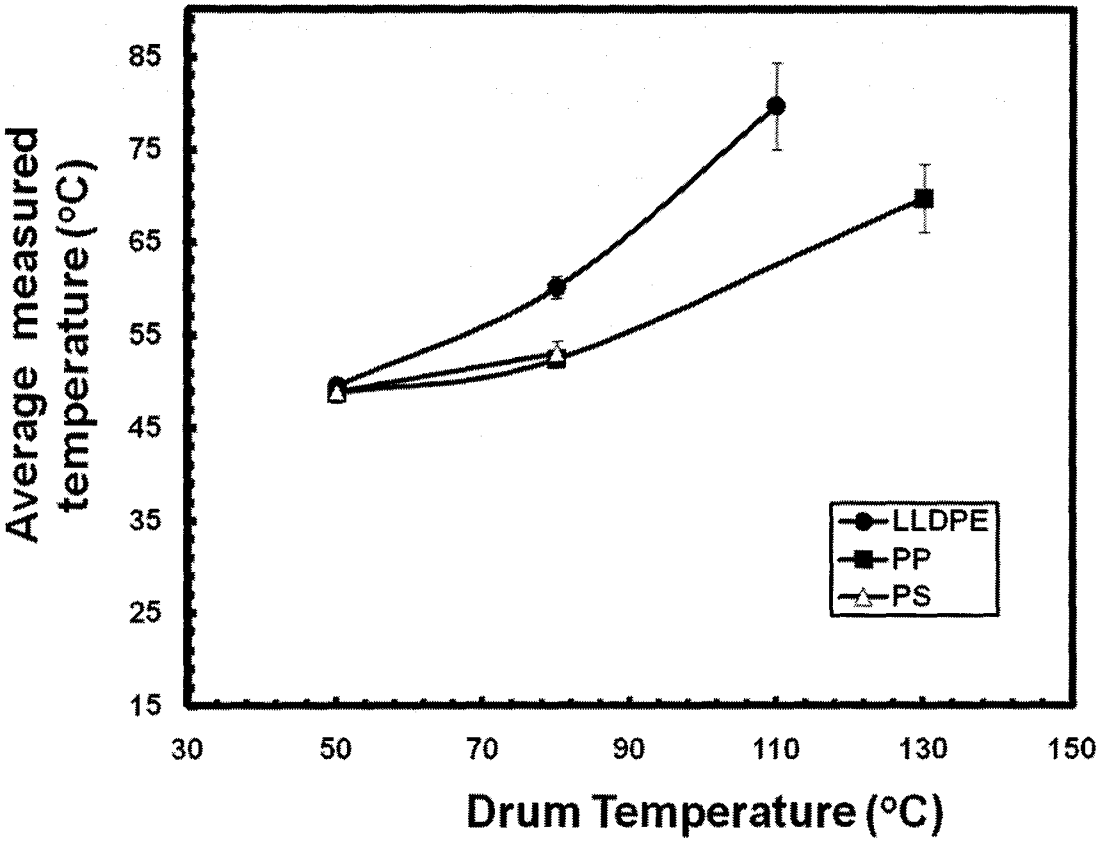

Figure 4.30 solid bed temperatures measured at end of the experiment tested at different drum temperatures (Top measurement). The lines were drawn for clarity purpose.

4.4 Effect of circulation on solid bed temperature (measurement at the center of the bed)

The previous section highlighted a never-before mentioned circulation of solids within a lid-driven cavity. While the relevance of the system to the stress field of an extruder is not clear at this moment, the finding is significant enough by itself that further experiments were warranted. In this section the temperature distribution in the solid bed was further probed by making measurements at a different location in the beds of polymers. The measurements were made by placing the two thermocouples at the mid-point for the solid bed's width and closer to the heating drum, as shown in Figure 4.31. Point C represents the core of the solid bed (i.e. center in width and height for the bed) and D represents a point close to the barrel surface. The tip of the thermocouple was at a distance of 13.92 mm from the front wall measured from the inside of the front wall. The temperature of the solids chamber and the drum were maintained at 80°C. The temperature measurements at the two points for the three polymers were compared for drum speeds of zero and 100 RPM. A 10 N load was applied which correspond to a pressure of 4.385 kPa.

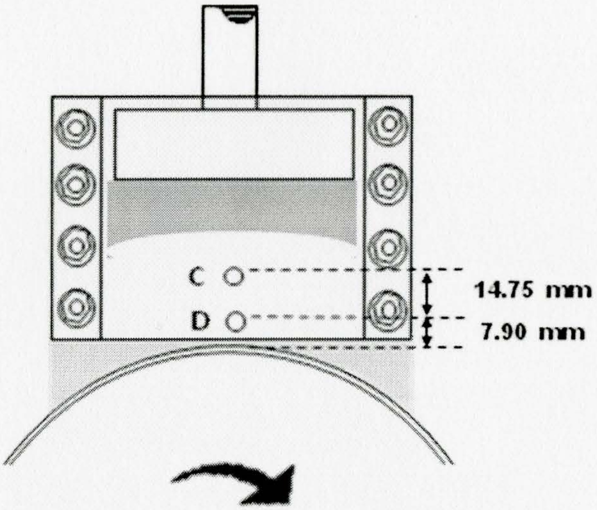

Figure 4.31 Experimental set up for the solid bed with central temperature measurements

The final recorded temperatures at point D under zero shear (no drum rotation) for the three resins are presented in Figure 4.32. We examine this data with consideration of the calculated material thermal diffusivities (neglecting interstitial fluid) calculated for LLDPE, PP and PS from Table 4.2, to be 2.13×10^{-4}, 1.88×10^{-4} and 1.18×10^{-4} mm^2/s, respectively. Based on these values, LLDPE which shows the highest thermal diffusivity was expected to demonstrate enhanced heat transfer (steeper slope) and higher final temperatures compared to PP and PS. However, the temperature profiles shown in the figure for the three resins showed little difference. The discrepancy in the predicted and observed behaviour is probably due to the plug assumption ignoring the intestinal air in the bed. These results highlight the need for considering the granular nature of the bed and the importance of using effective thermal conductivities to precisely predict heat transfer as suggested by Moysey (Ph.D. thesis, 2007).

On the other hand when the drum rotated (100 RPM), the LLDPE showed enhanced heat transfer (steeper slope) as well as higher final temperature compared to the other two resins. Figure 4.33 compares the temperature profile at point D with and without drum rotation for the three resins. It is important to recall that pellet circulation was observed for only LLDPE under these operating conditions (Section 4.4.1). The observed results are believed to be an outcome of this pellet circulation. Hence, in addition to consideration of interstitial air the dynamic particulate nature of the solid bed is also critical in predicting the heat transfer, as suggested by Moysey and Thompson (2005). Similar trends in response were observed at point C.

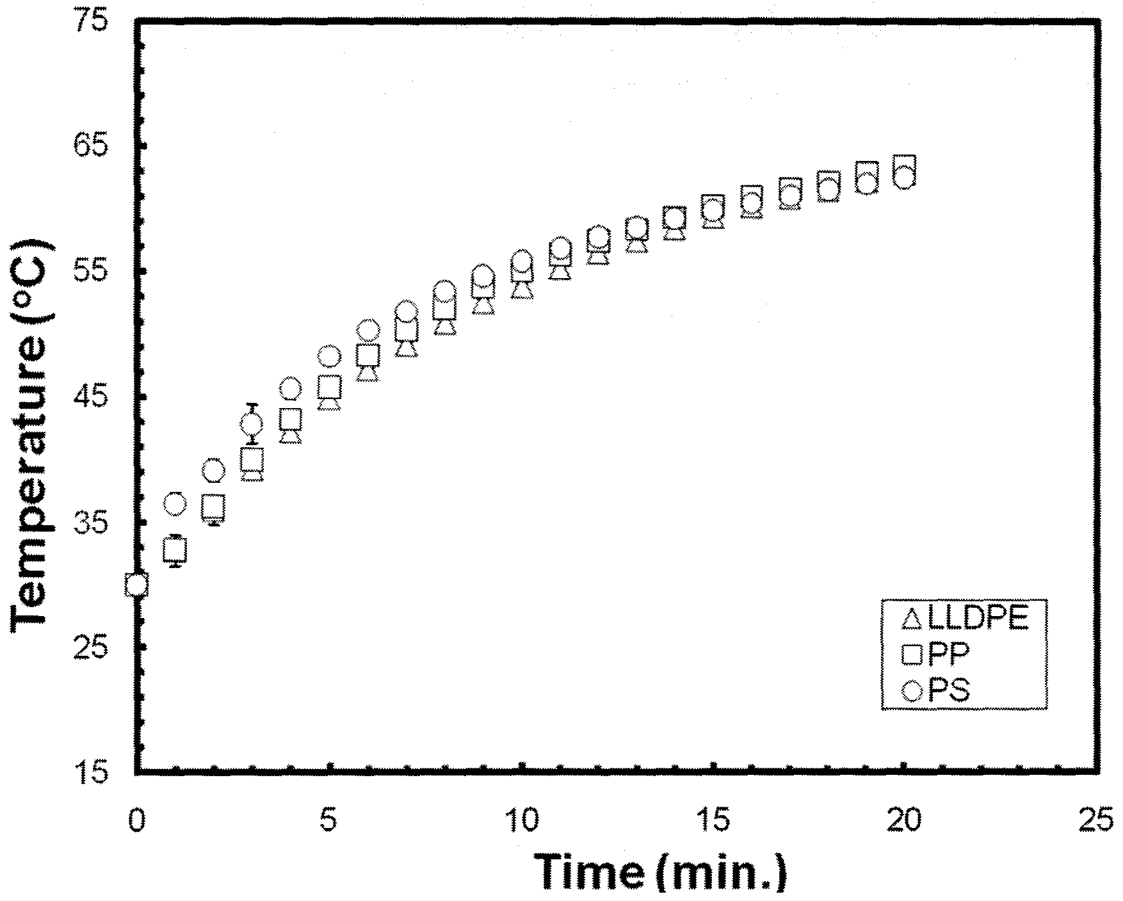

Figure 4.32 Temperature at point D for the three resins without drum rotation. Both solids chamber and drum kept at 80°C.

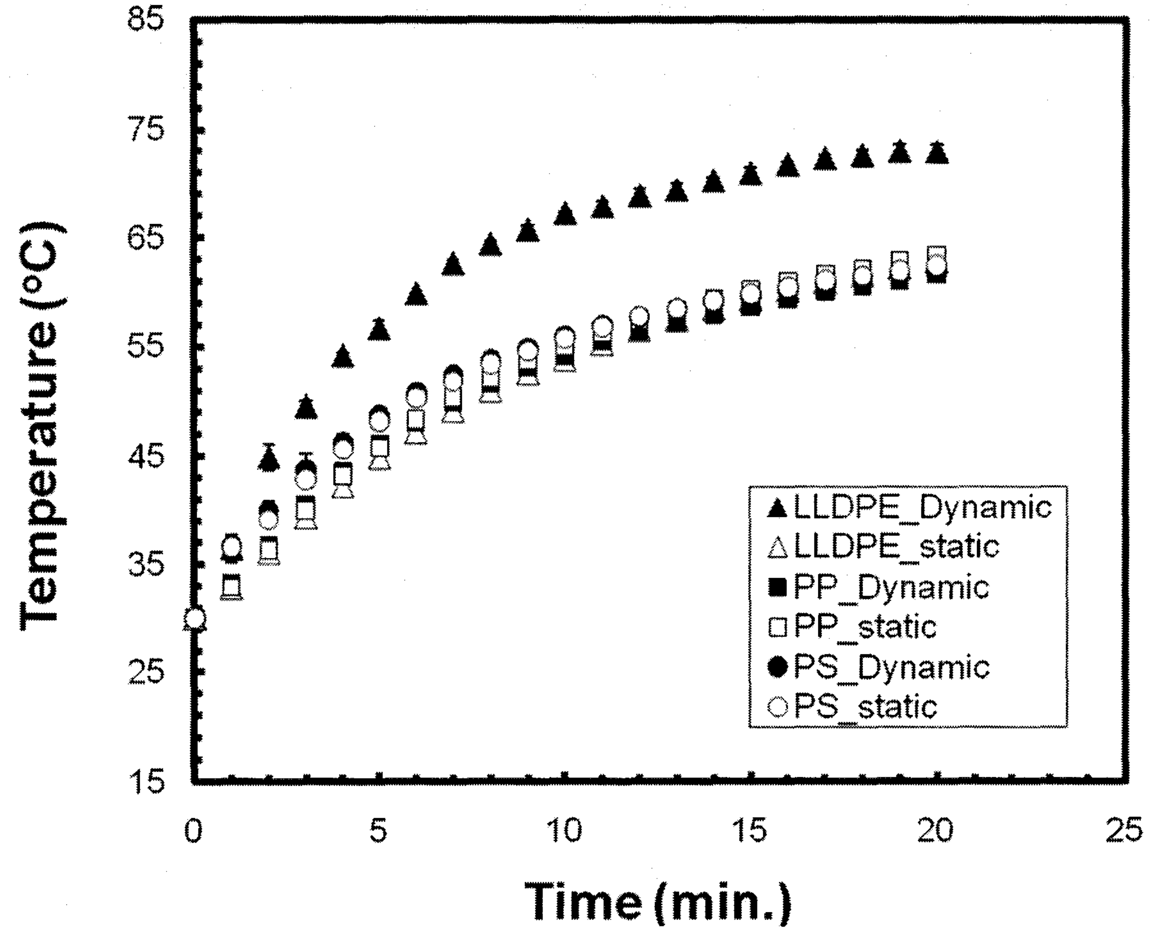

Figure 4.33 Point D temperature at end of the experiment for the three resins with and without drum rotation. Both solid chamber and drum at 80 °C.

The final temperature at points C and D for the three resins as the drum rotated are shown in Figure 4.34. Zero sample height represents a point at the drum surface .As shown in this figure, the LLDPE bed reached the highest steady-state temperature compared to the other two resins. The constant temperature gradient found for LLDPE suggests the circulating granular bed adhered to Fourier's law (conduction-dominated) while the other two resins with their stagnant beds showed a temperature gradient more indicative of convective-dominated heat transfer.

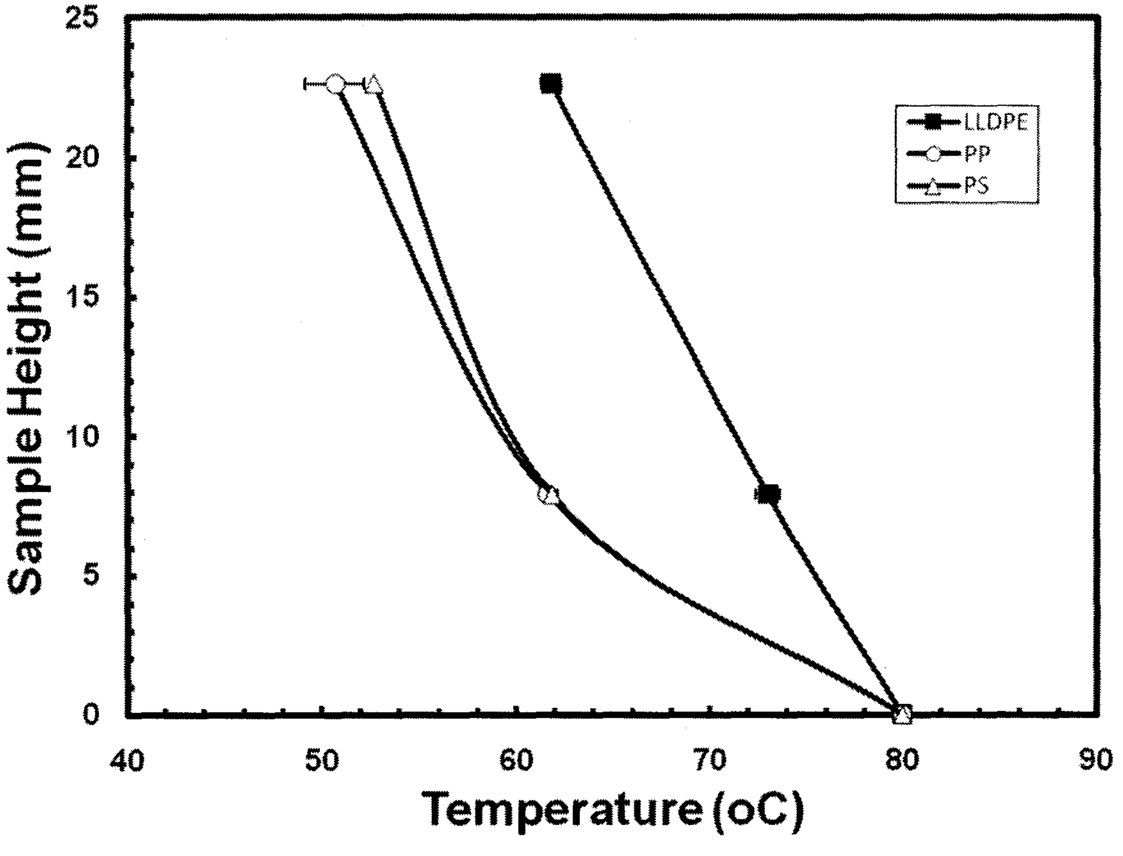

Figure 4.34 Temperature profile within the bed for the three resins at the end of the experiment at 100 RPM drum speed (drum and solids chamber at 80°C). Lines are drawn for clarity purpose

4.5 Characterizing the granular bed (direct shear test)

The experimental results discussed in the previous sections clearly show that some resins have the capacity to circulate within a lid-driven cavity and that motion can be beneficial to the heat transfer in solid bed. The results also show that the rate of temperature rise in a bed of polymer may not be significantly dictated by the thermal properties of the materials, in comparison to the modes of heat transfer.

This pellet circulation could be a result of many plausible factors such as shape and surface roughness of the pellets (which affects bulk density and friction both internal and external), physical properties of the material (Tg, mechanical strength), and the process conditions (pressure, temperature, speed). In order to create movement, the frictional resistance at the points of contact resulting from this interlocking must be overcome. The internal friction and the apparent cohesion between particles can be estimated from the direct shear test by a Jenike Shear Tester. The results of the shear test at room temperature are shown in Figure 4.35. It can be seen that normal stresses and the shear stresses showed a linear relationship for the three materials. The cohesion parameter and angle of shearing resistance (internal friction) for the three materials were determined by a linear fit to the data. The results are presented in Table 4.7. PS showed the highest angle of internal friction and apparent cohesion parameter compared to the other two resins. PP showed a higher apparent cohesion value compared to LLDPE but both had a similar angle of internal friction. These results indicate that the motion of PS pellets would be difficult to achieve compared to LLDPE and PP, at least at room temperature. Furthermore, it is expected that both the angle of internal friction and cohesion parameter would increase at higher temperatures due to enhanced cohesion resulting from softening of resin pellets.

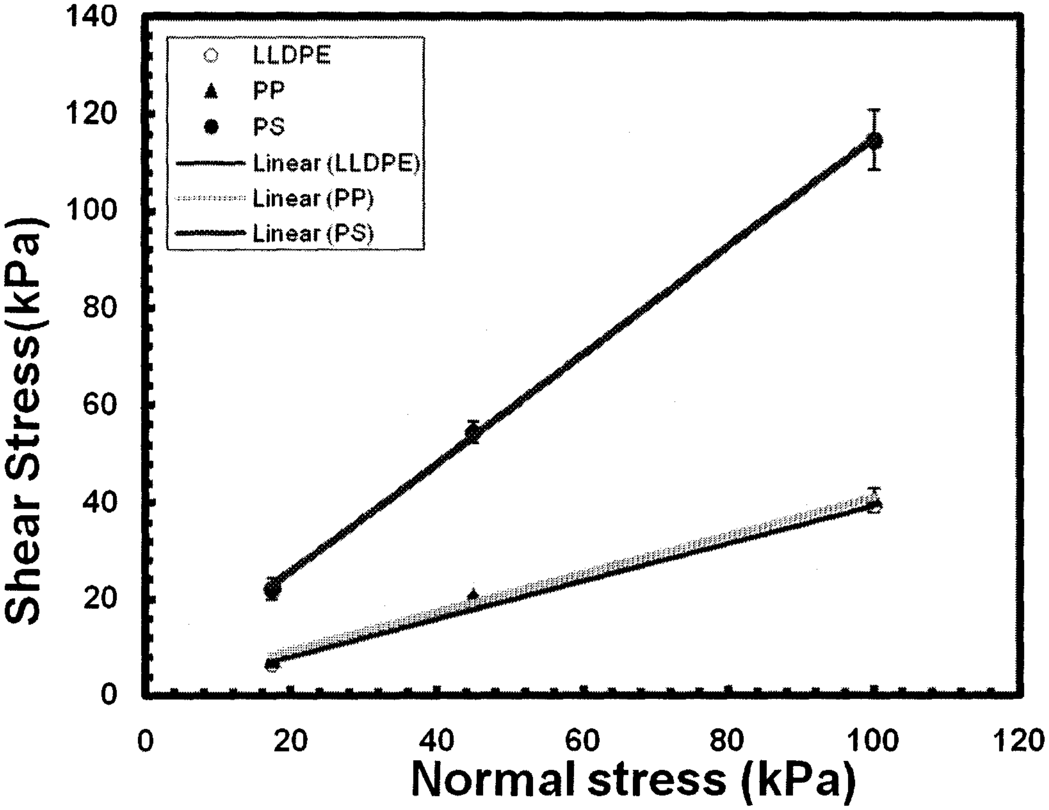

Figure 4.35 Results of direct shear cell for the three resins, Shear stress versus the normal stress at room temperature

Table 4.7 Fitted parameter from the direct shear cell test for the three resins at room temperature

Materials	Cohesion parameter (C) [kPa]	Angle of shearing resistance Φ [degrees]
PS	3.3456	48.12
PP	1.2674	21.73
LLDPE	0.2673	21.33

The other factor that can affect the pellet motion is the external friction. Circulation of LLDPE pellets observed at different drum temperatures (50, 80 and 110°C) could be a result of high external friction between the drum and the pellet. Since LLDPE showed a broad melting range beginning at 80°C (DSC curve, Section 4.1.1) the possibility of adhesion between the pellets and the drum surface were high which resulted in the pellet circulation. However, in the case of PP no circulation was observed at 50°C or 80°C of drum temperatures but upon increase of the drum temperature to 130°C there was some pellet circulation at the start of the test which then ceased on compaction. This could be a result of the low external friction between PP pellets and the drum surface. Chen et al (1977) have shown that the coefficient of external friction for PP is low (0.2) and it did not change between 100 and 135°C. Comparatively, the coefficient of external friction for PS is 0.48 and LLDPE is 0.58.

4.6 Simulation of pellet motion in a lid-driven cavity using Discrete Element Modeling (DEM)

DEM simulations (PFC^{2D}, Itasca Consulting Inc.) were carried out at different conditions with a similar geometry to the drum simulator in order to verify the feasibility of pellet circulation within the screw channel of an extruder. Simulations of a lid-driven cavity were carried out separately when the barrel rotated or screw rotated, and with or without compaction. In all cases, pellet circulation was found to occur. Figure 4.36 presents images from the simulations where the top surface is moving (represents barrel movement in case of an extruder).

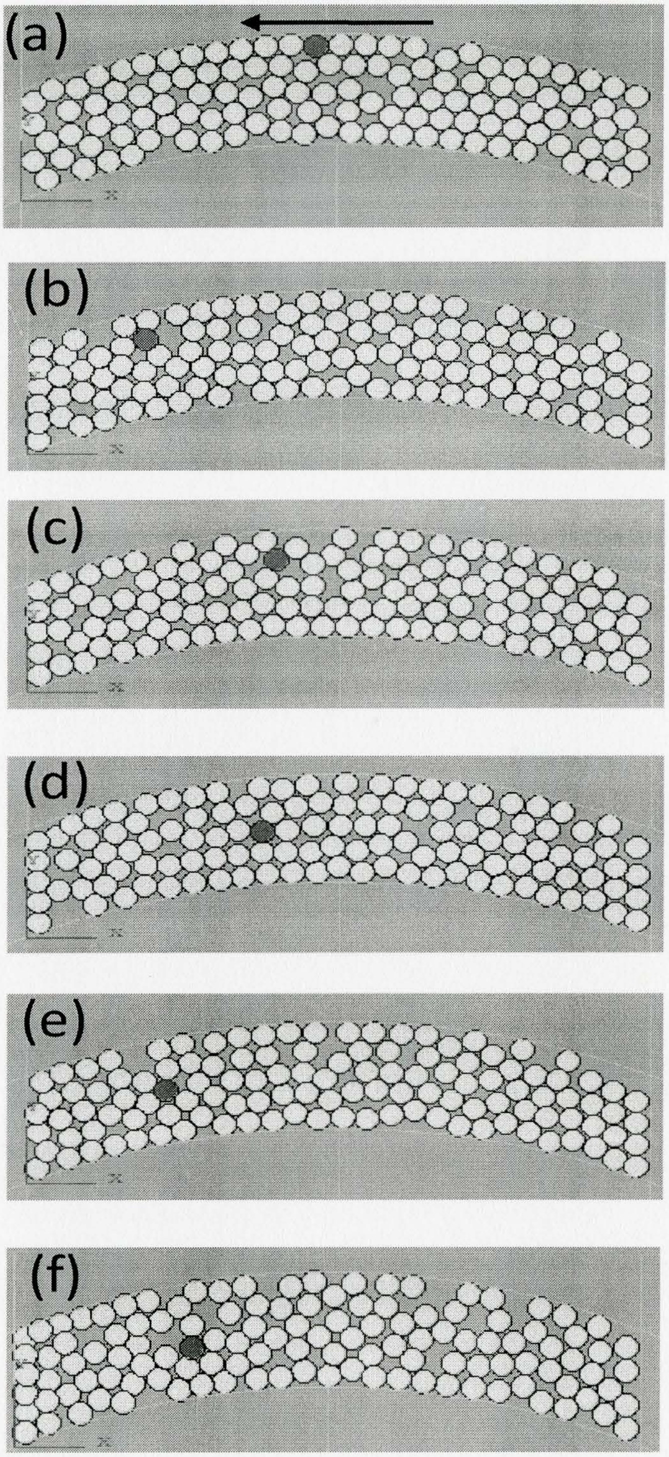

Figure 4.36 Simulation images at 100 RPM showing the solids chamber. The time in second for each image is (a) 0 ;(b) 10 ;(c) 20 ;(d) 30 ;(e) 40;(f) 50.

4.7 Simulation of heat transfer in solid bed based on plug assumption using Finite eliminate modeling (FEM)

In order to evaluate heat transfer using plug flow assumption which ignores the granular nature (intestinal air between pellets) and particle dynamics within the solid bed, finite element modeling (Finite Element Analysis, version 7.135) was conducted. A grid of 1000 nodes was used in this simulation with boundary conditions as follow; conduction from the side walls and the drum surface at temperature of 80°C and adiabatic from the plunger. Physical properties used in the simulation are same as those in Table 4.2. Figure 4.37 shows the FEM simulation results for the three resins at position of point D as in the experiment setup. For comparison experimental results obtained under static mode (Figure 4.32) were added. As shown in this figure the FEM simulation based on the continuum assumption (no consideration of the air) overestimated the heat transfer rate in the bed. This shows the importance of including the thermal properties of the air in the simulation as suggested by Moysey (Ph.D. thesis, 2007).

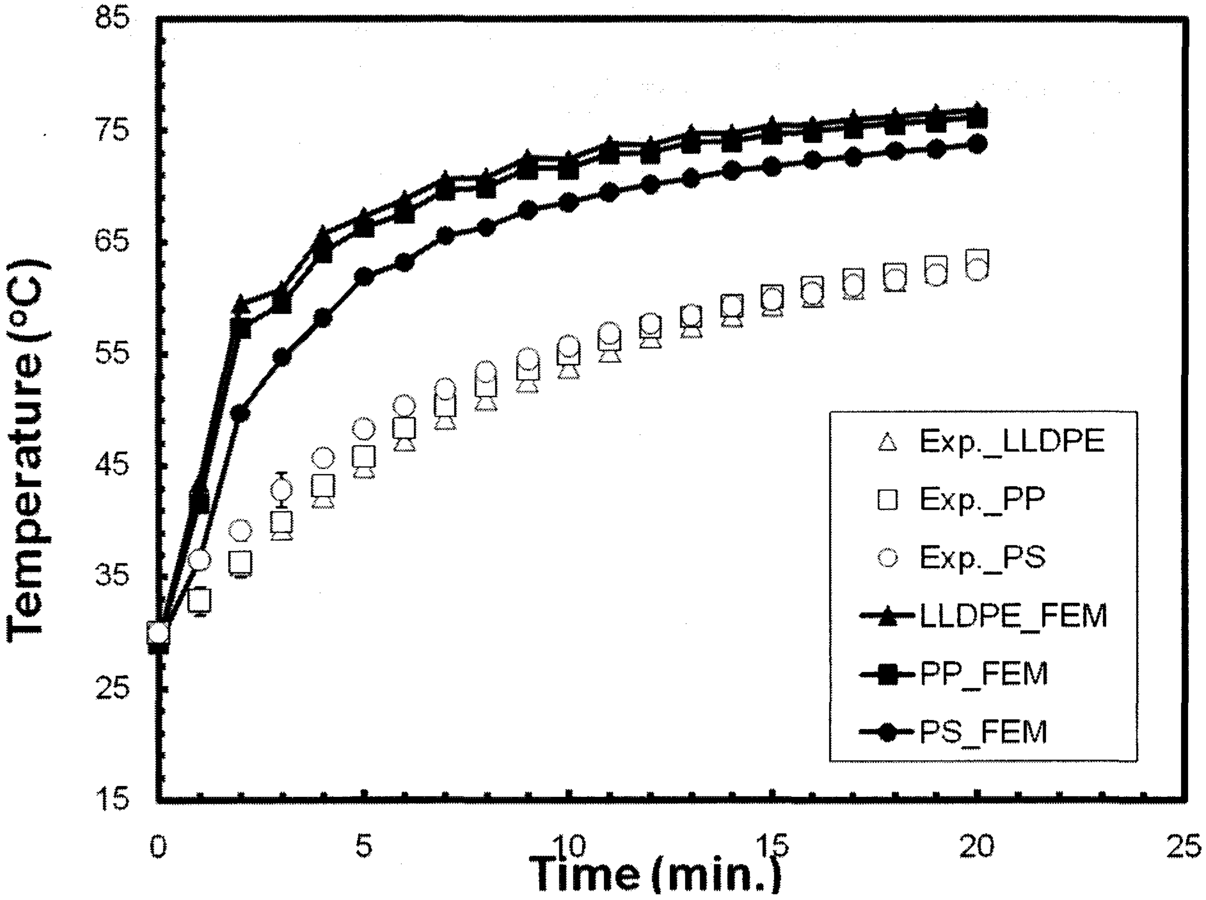

Figure 4.37 Comparison between FEM simulation and experimental results for the three reins at static mode (no drum rotation). Drum and solids chamber temperature at 80°C. Lines were drawn for clarity purpose.

4.8 Air temperature in solid chamber

We know from earlier studies conducted by Paul Moysey (Ph.D. thesis, 2007) in our research group that for stationary beds of polymer granules that most of the heat transfer is convective dominated rather than the popularly held belief for conduction. This section and the following sections further probe the modes of heat transfer in a lid-driven cavity.

A series of runs measured the air temperature inside the solid chamber in the absences of the polymer. The temperature measurements were made at 80°C (drum and solids chamber) at different drum speeds (40, 100 and 200 RPM). The height of the plunger was kept constant at 25.1 mm which was the same height as in the case of the polymer. The experimental setup was similar to those in Section 4.4 (see Figure 4.15).

The average temperature at points A and B over time while operating at a drum speed of 100 RPM are shown in Figure 4.38. As seen in this figure, the temperatures measured at point B were consistently higher than point A. However, when the drum rotations were turned off after 20 minutes, the temperature at points A and B approached a common value. The difference seen between the two points as the drum rotated suggest that the similar trend seen for the granular bed was not due to bed compaction at the advancing wall as originally thought. Similar trends for the air were observed at drum speeds of 40 and 200 RPM.

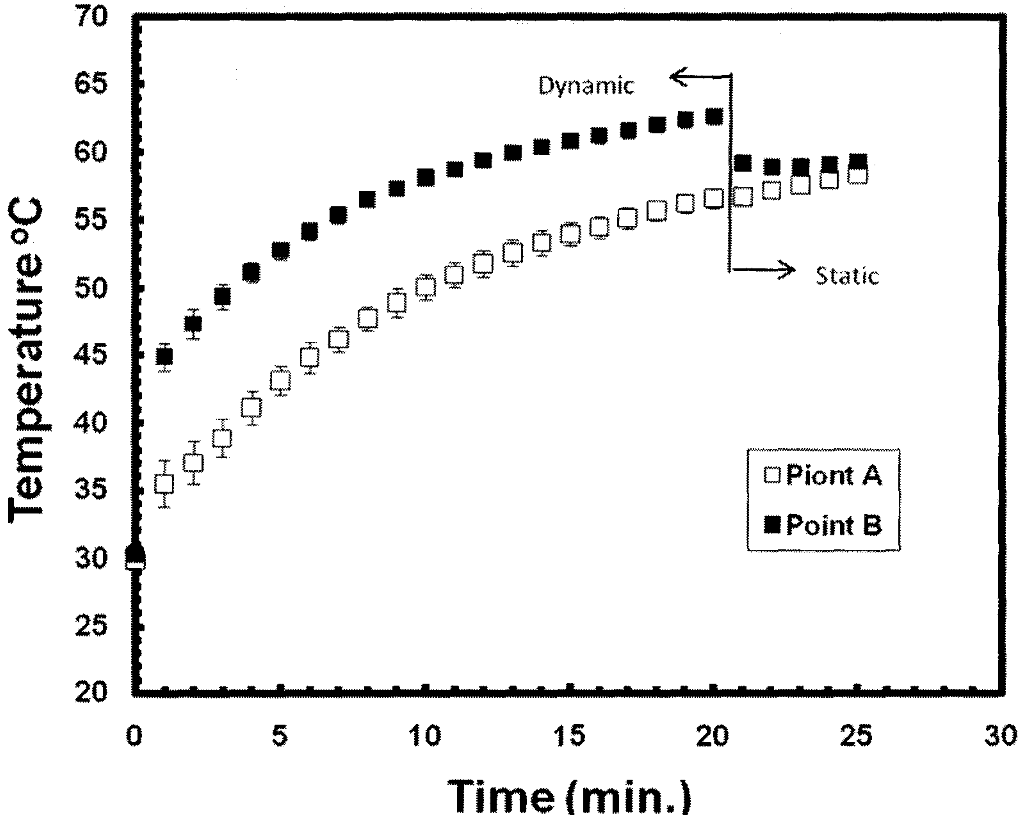

Figure 4.38 Air temperature curves at two points A and B at a drum speed of 100RPM (drum and solids chamber at temperature of 80°C)

4.9 Improving heat transfer within solid bed

a. Starve versus flood feed

The heat transfer was studied in the drum simulator when it was only partly filled with solids. Starved feeding is a highly efficient means of heat transfer in a single screw extruder and we wished to examine some of the phenomenological attributes of this operating mode. Unlike flood fed conditions in an extruder where gravity has limited influence on the movement of the solids, in starved feeding gravity strongly dictates how particles move with the screw and the system no longer resembles a lid-driven cavity. For this reason, the degree of channel starvation was held to only 10% (i.e. 90% of the chamber volume filled with solids).

LLDPE and PP at a 10% degree of chamber starvation were tested at a drum speed of 100 RPM and temperature of 80°C for both the drum and the solids chamber. The starvation percentage was controlled by the height of the plunger. Temperatures were measured from the top plate (plunger) at points A and B (refer to Figure 4.15 for configuration). Figure 4.39 shows the LLDPE bed in this starved mode as the drum turned.

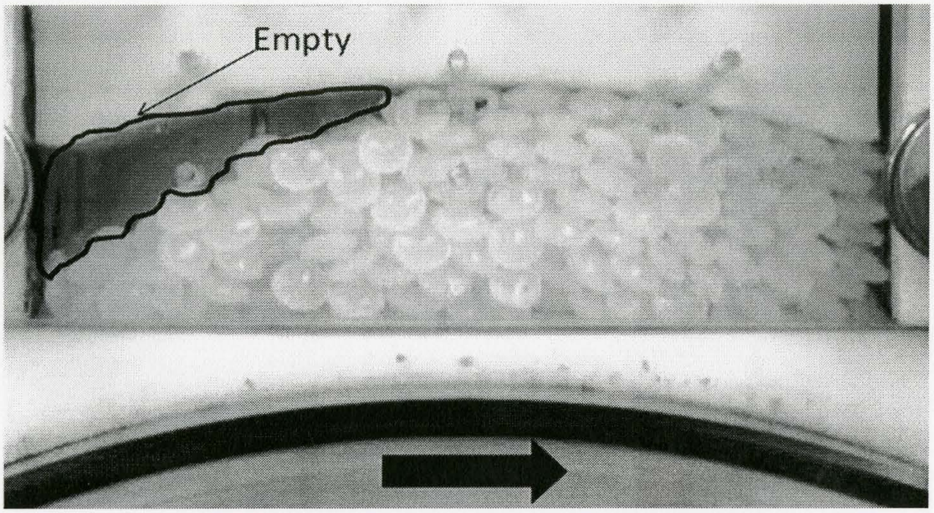

Figure 4.39 Temperature measurements under starve mode.

The temperatures at points A and B within the LLDPE bed under the starved mode showed no significant difference as reported in Figure 4.40 .The error bars, though difficult to see in the graph, overlapped for these two temperature measurements. The lack of difference is believed to be a result of the observed pellet circulation and loose nature of the bed which promoted both more interaction between the pellets and greater movement of the interstitial air. Included in this figure is temperature profile for the same two thermocouple locations under flood feed condition (Section 4.4.1). It was consistently seen that the polymer bed heated faster and reached a higher temperature for the starved mode. For PP, the solids bed once again did not circulate even under starved mode and no difference in temperature was noted between points A and B while operating under this condition, as shown in Figure 4.41. However, similar to the

LLDPE, the PP bed reached a higher temperature in starved mode compared to the flooded state.

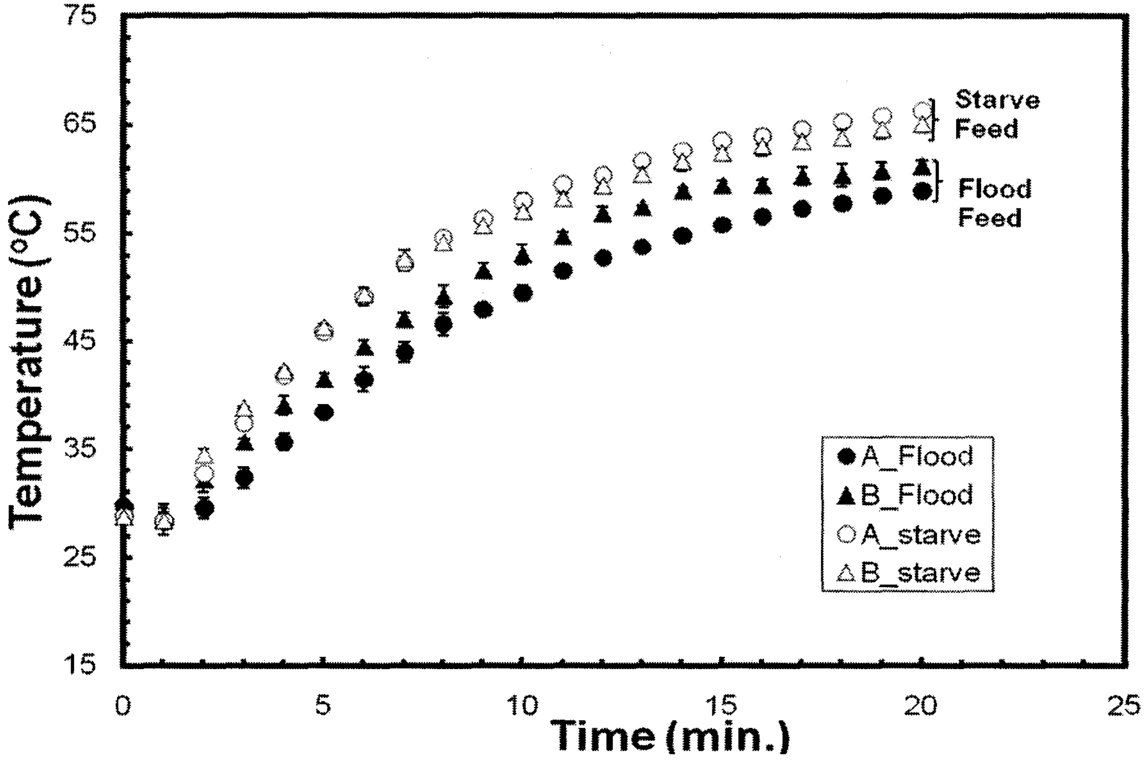

Figure 4.40 Temperature curves for 10 % starved LLDPE bed versus its flooded condition for points A and B with time. Set temperature of 80°C for both drum and solids chamber, and drum speed was 100 RPM)

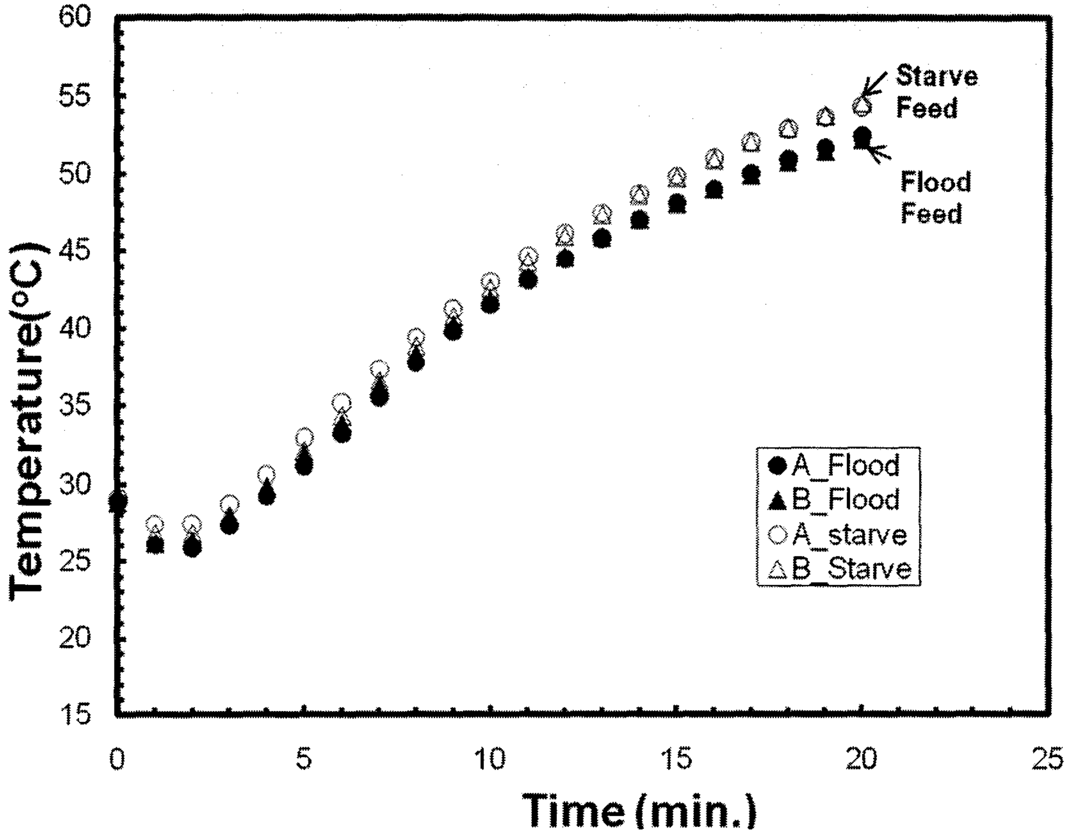

Figure 4.41 Temperature curves for 10 % starved PP bed versus its flooded condition for points A and B with time. Set temperature of 80°C for both drum and solids chamber, and drum speed was 100 RPM)

b. Forced convection

The effect of the forced convection on the heat transfer within solid bed was examined for LLDPE and PP. A hot air gun was set at a distance of 110 mm above the solid chamber inlet. The air gun was positioned at the center of the solid chamber and firmly fixed with a holder and two spots E and F were selected for the temperature measurements as shown in Figure 4.42. The air temperature at the solid chamber inlet was 133.5±1.9 °C. The drum speed was set to100 RPM and the temperature of the drum and solids chamber were 80°C.

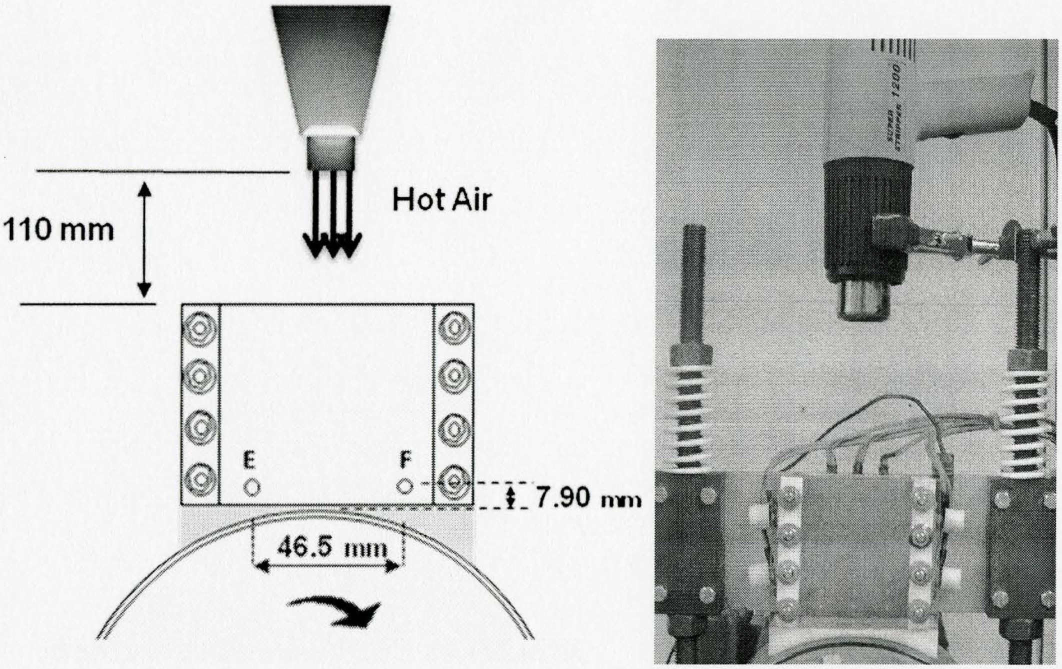

Figure 0.2

Figure 4.42 Experiment set up for forced convection condition

LLDPE temperatures at point E with and without forced convection are shown in Figure 4.43. The temperatures reported are believed to be the temperautre of pellet rather than air. As indicated by Botteril (1975) for fluidized beds, due to higher heat capacity of the pellet it is generally found that the gas gives up its heat readily to the surrounding particles and hence its temperature is always equal to the bed of particles. The air gun was switched off after ten minutes and temperature measurements were continued. AS seen in the figure, the final bed temperature (at 20 min.) at point E under the forced convection was higher by at least 10°C then temperatures attained in the absence of forced convection. Similar trends were observed for point F. In case of PP, the difference in the final bed temperature due to forced convection was 20°C measured at 20 minutes, as shown in Figure 4.44 . Both PP and LLDPE beds reached approximately the same final temperature under force convection, while the PP was more than 10°C cooler compared to LLDPE without this applied heating mode.

The varying degree of temperaure difference observed in LLDPE and PP beds as a result of forced convection is beleived to be the consequence of differences in granular bed dynamics of the materials. LLDPE pellet circulation has already been shown to improve heat transfer and hence without forced convection, its rate of heating was already better than PP. However, with both materials reaching similar final bed temperatures using forced convection, we see a mode of heat transfer which dominates the heating of the bed and can be better utilized to heat up solids in an extruder.

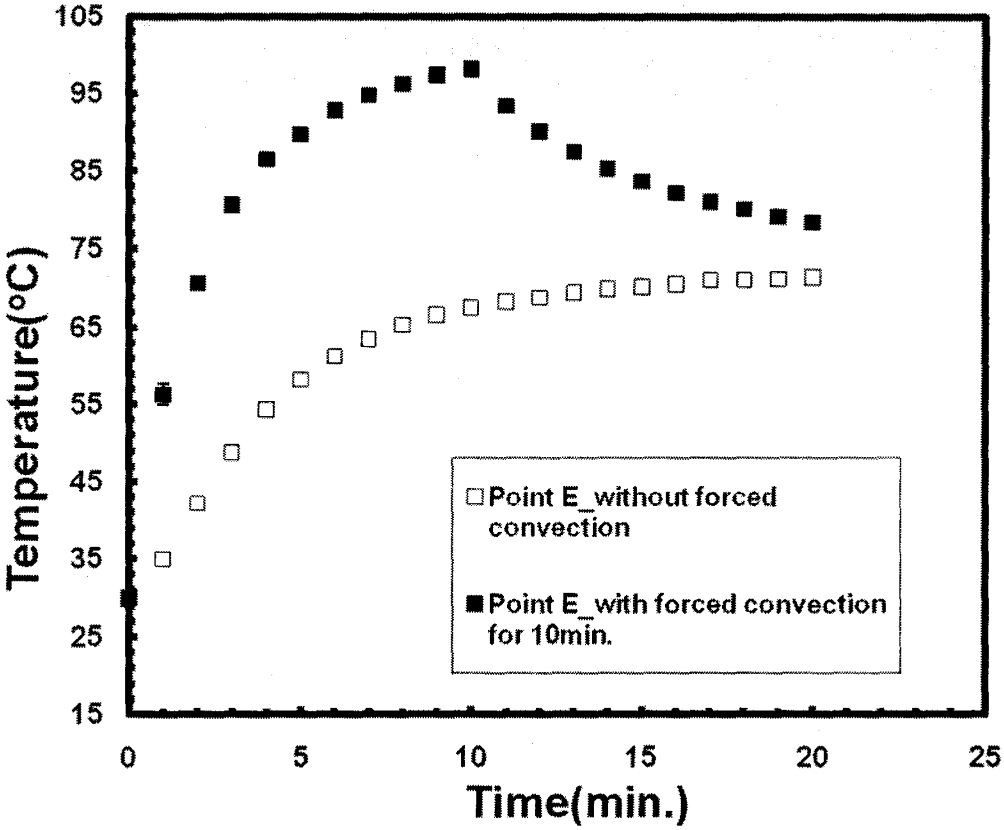

Figure 4.43 LLDPE temeprature profile for point E with and without forced convection at drum speed of 100 RPM. The solid chamber and the drum were at 80°C.

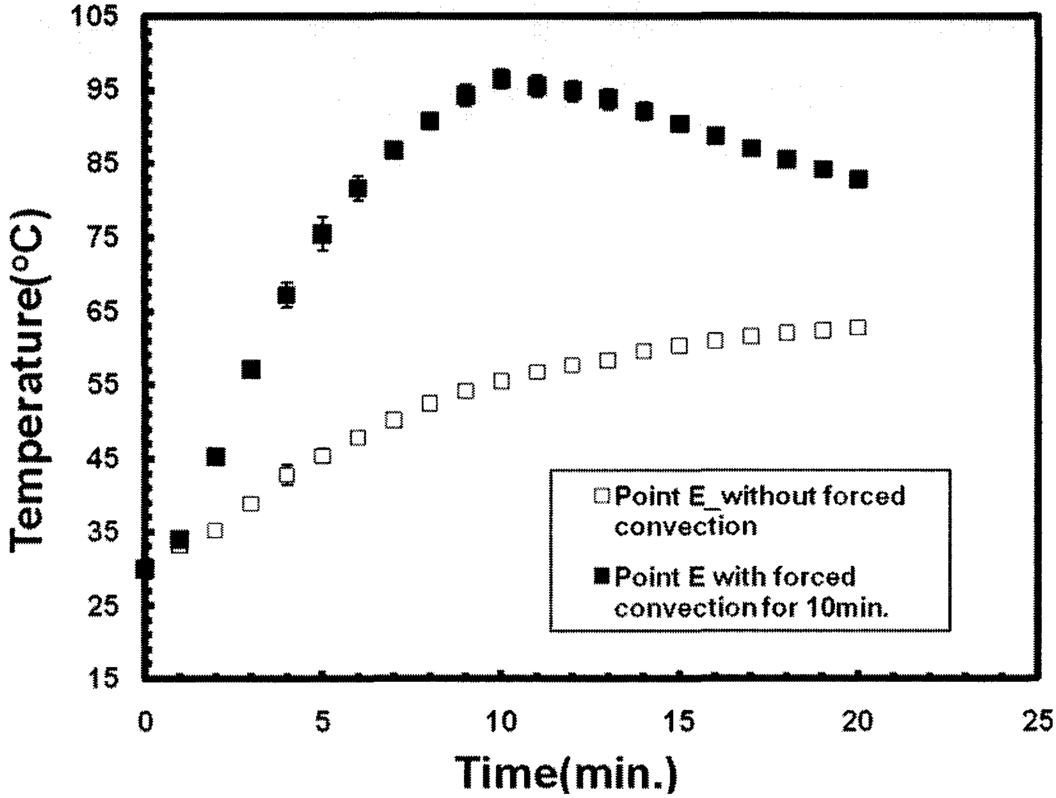

Figure 4.44 PP temeprature profile for point E with and without forced convection at drum speed of 100 RPM. The solid chamber and the drum were at 80°C.

c. Pellet shape

Temperature measurements for spherical PS with a diameter of 6.35 mm were compared to regular pellet in the drum simulator. The experiment setup was similar to that in Section 4.3 (see Figure 4.15) and both the drum and the solid chamber were at 80°C. Figure 4.45 shows the temperature curves for spherical PS versus PS pellets at drum speed of 100 RPM. It can be seen from the figure that the temperatures for PS bed with spherical shaped particles was higher than cylindrical ones. This is believed to be a combined result of the sphere circulation and rolling of spheres about their own axis which was observed in case of the PS spheres. The motion of the spheres provided distributive mixing contributions to the heat transfer, enhancing the rate of heat transfer within the bed despite the lower contact conduction due to the smaller area (point contact) in contact with the heated surface compared to cylindrical pellets. Further, there is good air circulation around which is a result of the uniform shape of the spheres. At the end of the experiments, the PS sample showed large deformation of the spheres, as shown in Figure 4.46, which was not seen in the case of PS pellets. The extent of deformation calculated from the number of the deformed spheres to the non-deformed ones was 33.64 %. This can be related to the small contact area which created high shear stress at the external surface of the sphere. The small contact area could be also beneficial to PED contributions since the transmitted pressure would result in higher normal forces at the contact points for the spheres.

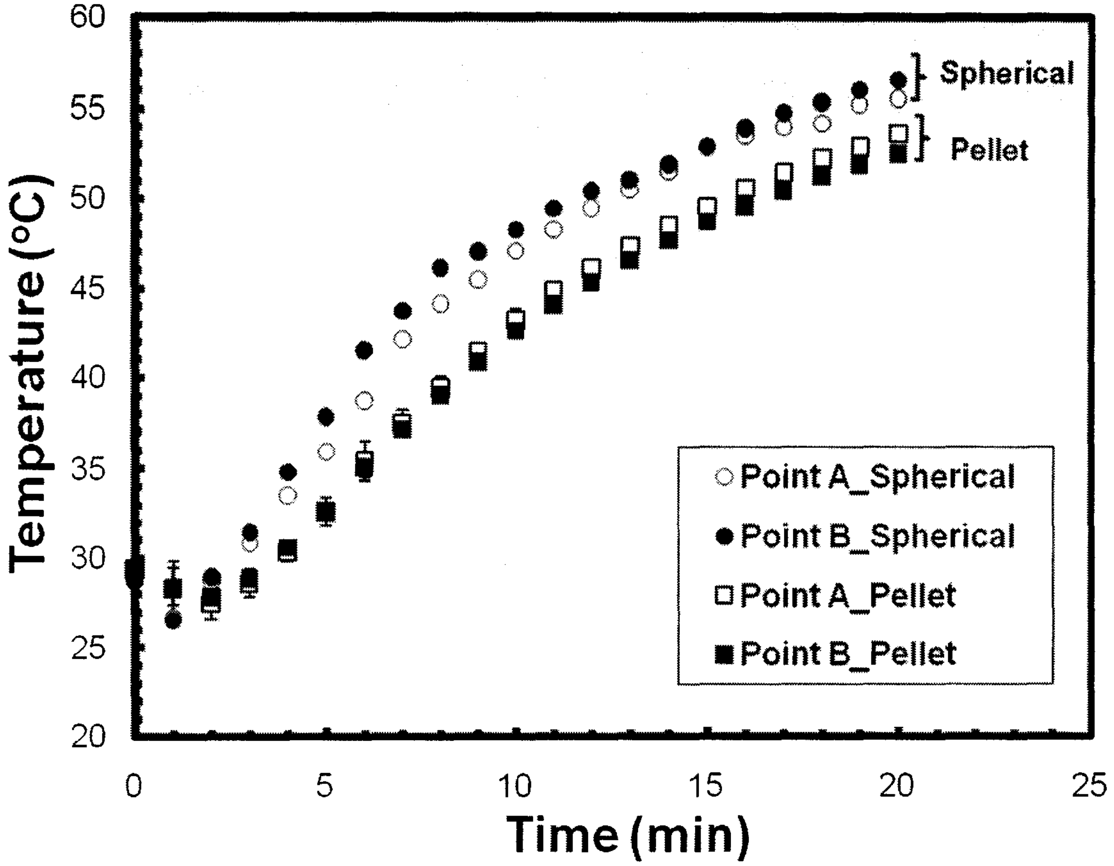

Figure 4.45 PS spheres temperature profile of compared to PS pellet at drum and solid chamber of 80°C. Drum speed was 100 RPM

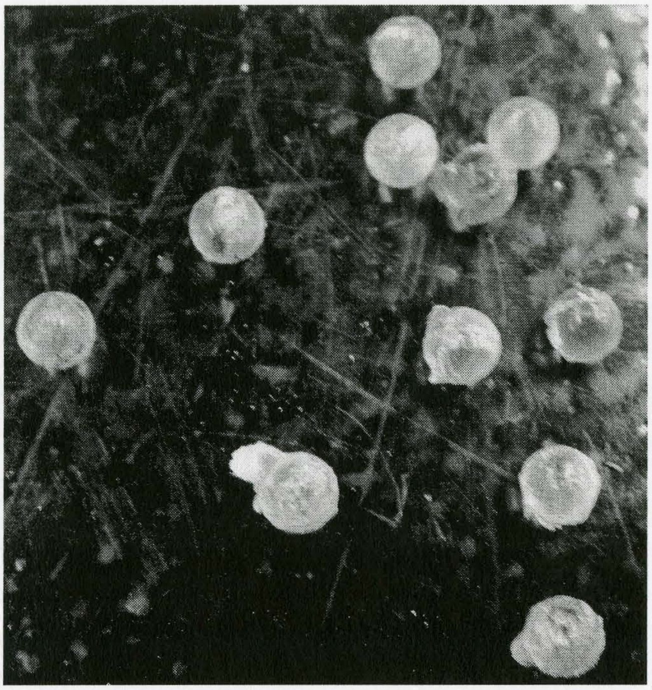

Figure 4.46 PS spheres at the end of the experiment. Drum and solids chamber were at temperature of 80 °C and drum speed of 100 RPM

Chapter 5

5. Conclusions and recommendations

5.1 Conclusion

A new device was designed and built to model the radial compressive stresses and shear stresses on a solid bed of plastics similar to the environment within the screw channel of a single screw extruder. This device enables the user to visualize the nature of the solids bed under different experiment conditions through the transparent wall. Also, the device provides ways to explore the heat transfer in a solids bed under different conditions by embedding thermocouples from the top or through the front wall. From a practical point of view, experimental measurements of solids bed heat transfer within a rotating screw, particularly cross channel, as the bed moves down the length of the solids conveying zone are impossible to perform.

The heat transfer experiments for the selected materials in the drum simulator have shown that LLDPE has more efficient heat transfer compared to PS and PP. This efficient heat transfer is believed to be a result of pellet circulation within LLDPE bed observed under all test conditions investigated. The pellet circulation was found to increase with increasing drum temperature at similar drum speed. The influence of pellet circulation on heat transfer of the bed was further evaluated by performing additional experiments under static (no drum rotation) and dynamic (with drum rotation) modes at set temperature of 80°C for drum and solids chamber. Temperatures within the bed were monitored by embedded thermocouples. The final temperatures of the three materials (PP, PS and LLDPE) were comparable for the static mode. However, in the dynamic mode (i.e. drum rotation) only LLDPE showed enhanced heat transfer (steeper temperature gradient with respect to time) as well as higher final temperature (10°C difference between the static and dynamic mode). For PP and PS no difference in heat transfer was observed between the static and dynamic modes.

The influences of starved feeding and forced convection on heat transfer within the solid bed for PP and LLDPE were subsequently investigated. Starved feeding was found to improve the heat transfer as well as the final temperature achieved within the bed. Both LLDPE and PP bed reached a higher temperature in starved fed mode compared to the flooded state. Forced convection was also found to improve the heat transfer within the bed. In case of PP, the difference in the final bed temperature due to forced convection was 20°C higher compared to no forced convection state. Both PP and LLDPE beds reached approximately the same final temperatures under forced convection, while the PP was more than 10°C cooler compared to LLDPE in the absence of forced convection. This difference was once again attributed to the pellet circulation observed in only the LLDPE bed. However, with both materials reaching similar final bed temperatures using forced convection, we see a mode of heat transfer which dominates the heating of the bed and can be better utilized to heat up solids in an extruder.

The influence of the shape of the particle on the heat transfer within a solid bed was studied. Improved heat transfer and higher final temperatures were attained within the PS bed with spherical particles compared to cylindrical pellets. This is believed to be a combined result of the sphere circulation and rolling of spheres about their own axis observed in case of PS spheres.

The results found in this study suggest that the common assumption of the solid plug flow in extrusion over-estimates the heat transfer by ignoring the importance of the granular nature of the bed. According to the solid plug assumption, no relative motion exists between pellets and thermophysical properties dominate heat transfer. However, the results shown in this study showed that neither assumption is particularly true.

5.2 Recommendation and future work

Although the designed device was a useful tool in this study, several improvements could be made. One of the limitations of the device was its inability to conduct melting experiments under shear due to leakage of the melt under compaction and high motor load. To overcome the leakage problem, modification to the sealing design between the solid chamber and the drum is needed. Also for the high motor load a more powerful motor is needed. Another important modification to this device is the addition of a better measuring method for the torque on the drum which in turn would provide valuable information about the friction between the test materials and the drum. The AC motor does not allow for true determination of torque from its measured load amperage.

The heat transfer experiments were conducted at two points in all experiments. It would be more informative to have more than two points for the temperature measurements to show the temperature profile across the bed. Also, it would be more accurate and efficient to have a data acquisition system for temperature recording rather than the existing hand-held monitor.

Finally, heat transfer through the solid bed is strongly affected by the type of the polymer, the size and the shape of the pellet. Therefore, there is a need to investigate the heat transfer within solids bed of different polyethylene grades (i.e LDPE and HDPE) which was not examined in this study. There is a need to further investigate heat transfer within spherical shaped granules of PP and LLDPE.

References

Altinkaynak, Atakan, Mahesh Gupta, Mark A. Spalding, and Sam L. Crabtree. 2007. An experimental study on shear stress characteristics of polymers in single-screw extruders. In Society of plastics engineers annual technical conference: Plastics encounter at ANTEC 2007;394-398.

Argento, C., D. Bouvard. 1996. Modeling the effective thermal conductivity of random packing of spheres through densification. International Journal of Heat and Mass Transfer 39, no. 7 (05) : 1343-50.

Barr, Robert. 1981. solid-bed melting mechanism: the first principle of screw design. Plastics Engineering 37: 37-41.

Bellehumeur, C. T., M. K. Bisaria, and J. Vlachopoulos. 1996. Experimental study and model assessment of polymer sintering. Polymer Engineering and Science 36, no. 17: 2198-2207.

Bellehumeur, C. T., J. Vlachopoulos. 1998. Polymer sintering and its role in rotational molding. In Part 1 (of 3)1112-1115. Atlanta, GA, USA: Soc Plast Eng, Brookfield, CT, USA.

Bellehumeur, CÔeline T., J. Vlachopoulos, and McMaster University. Dept. of Chemical Engineering. 1997. Polymer sintering and its role in rotational molding.

Botterill, J. S. M.. Academic Press, 1975,Fluid-bed heat transfer : gas-fluidized bed behaviour and its influence on bed thermal properties

Buonanno, G., A. Carotenuto. 1997. Effective thermal conductivity of a porous medium with interconnected particles. International Journal of Heat and Mass Transfer 40, no. 2: 393-405.

Buonanno, G., A. Carotenuto, G. Giovinco, and L. Vanoli. 2003. Effective thermal conductivity of rough spheres packed bed. In 2003 ASME summer heat transfer conference ;251-256.

Campbell, Gregory A., Zirong Tang. 2004. Solid bed melting in single screw extruders - an alternative first order mechanism. In ANTEC 2004 - 162-166.

Campbell and Nagarajan, 1995, Small and Staples Solids conveying in low friction and starve fed extruders , ANTEC, ,268-278

Chaudhary, Bharat I., Elizabeth Takacs, and John Vlachopoulos. 2002. Ethylene copolymers as sintering enhancers and impact modifiers for rotational molding of polyethylene. Polymer Engineering and Science 42, no. 6: 1359-1369.

Chaudhary, Bharat I., Elizabeth Takacs, and John Vlachopoulos. 2001. Processing enhancers for rotational molding of polyethylene. Polymer Engineering and Science 41, no. 10: 1731-1742.

Chung, C. I., W. J. Hennessey, and M. H. Tusim. 1977. FRICTIONAL BEHAVIOR OF SOLID POLYMERS ON A METAL SURFACE AT PROCESSING CONDITIONS. Polymer Engineering and Science 17, no. 1: 9-20.

CI, CHUNG. 1970. new ideas about solids conveying in screw extruders. 26, no. 5: 32-44.

C. Cheng, Extrusion characteristics of polypropylene, ANTEC 1988,34-37

Craig, R. F. 1997. Soil mechanics. London ; New York: E & FN Spon.

Del Pilar Noriega, Maria, Tim A. Osswald, and Nicola Ferrier. 2004. In line measurement of the polymer melting behavior in single screw extruders. In ANTEC 2004 ;154-161.

Darnell and Mol, 1956 ; Solids conveying in extruders, SPE Journal, pp. 20–29.

Edmondson, I. R. 1., R. T. 1. Fenner. 1975. Melting of thermoplastics in single screw extruders. Polymer 16, no. 1 (01) : 49-56.

Francis, P. J. J., R. Joseph, and K. E. George. 1997. Starved extrusion for the improvement of mechanical properties of rubber vulcanizates. Journal of Elastomers and Plastics 29, no. 2: 148-162.

Fuhua, Z., C. Liqing, and W. Naiyi. 1989. Studies on theory of single screw plasticating extrusion. part 1. physical model of extrusion. In ANTEC 89 ;90-92.

Gale, Martin. 1997. Compounding with single-screw extruders. Advances in Polymer Technology 16, no. 4: 251-262.

Gogos, Costas C., Zehev Tadmor, and Myung H. Kim. 1998. Melting phenomena and mechanisms in polymer processing equipment. Advances in Polymer Technology 17: 285-305.

Gogos, Costas G., Bainian Qian. 2002. Plastic energy dissipation during compressive deformation of individual polymer pellets and polymer particulate assemblies. Advances in Polymer Technology 21, no. 4: 287-298.

Gogos, Costas, Mustapha Abbaoui, Batara Sianturi, and Jisheng Shen. 1985. ON THE MELTING OF A COMPRESSED POLYMER BED IN AN ANNULAR CELL. ANTEC85 ;65-68.

Gonzo, E. E. 2002. Estimating correlations for the effective thermal conductivity of granular materials. Chemical Engineering Journal 90, no. 3 (12/28) : 299-302.

Gonzo, E. E., J. C. Gottifredi. 1983. Rational Approximations Of Effectiveness Factor And General Diagnostic Criteria For Heat And Mass Transport Limitations. Catalysis Reviews - Science and Engineering 25, no. 1: 119-140.

Hahnfeld and Dalke, 1985,Encyclopaedia of polymer science and engineering volume ,16,styrene polymer,

Hwang, Chii-Guang, James M. McKelvey. 1989. Solid bed compaction and frictional drag during melting in a simulated plasticating extruder. Advances in Polymer Technology 9: 227-251.

Hyun, K. S., M. A. Spalding. 1989. Bulk density of solid polymer resins as a function of temperature and pressure. In ANTEC 89 - 47th annual technical conference of SPE72-74. New York, NY, USA: Publ by Soc of Plastics Engineers, Brookfield Center, CT, USA.

Incropera, Frank P., and Frank P. Incropera. 2007. Fundamentals of heat and mass transfer. Hoboken, NJ: John Wiley.

Isherwood, D. P., R. N. Pieris, and J. Kassatly. 1984. EFFECT OF METERED STARVE FEEDING ON THE PERFORMANCE OF A SMALL EXTRUDER. Journal of Engineering for Industry, Transactions ASME 106, no. 2: 132-136.

Jin, Zhiming, Furong Gao, and Fuhua Zhu. 2004. An experimental study of solid-bed break-up in plasticization of a reciprocating-screw injection molding. Polymer Engineering and Science 44, no. 7: 1313-1318.

Jin, Zhi-Ming, Fu-Hua Zhu, and Fu-Rong Gao. 2003. Solid-bed break-up in injection moulding. Zhongguo Suliao/China Plastics 17, no. 2: 94.

Kontopoulou, M., J. Vlachopoulos. 2001. Melting and densification of thermoplastic powders. Polymer Engineering and Science 41, no. 2: 155-169.

Kruder , 1985,Emulsion polymerization to fibbers ,Encyclopaedia of Polymer Science and Engineering, vol. 6, John Wiley & Sons, New York

Lee, Kee Y., Chang D. Han. 1990. Analysis of the performance of plasticating single-screw extruders with a new concept of solid-bed deformation. Polymer Engineering and Science 30, no. 11: 665-676.

Lin, Y. Y., C. Y. Hui, and A. Jagota. 2001. The role of viscoelastic adhesive contact in the sintering of polymeric particles. Journal of colloid and interface science 237, no. 2: 267-282.

Marzocchella, A., U. Arena, A. Cammarota, and L. Massimilla. 1991. Break-up of cylindrical clusters of solid particles under gravity flow in a two-dimensional column. Powder Technology 65, no. 1-3: 453-460.

Maddock, B. H. 1959, A visual analysis of flow and mixing in extruder screws,SPE J, 15, 383

McKelvey, James M., Samuel Steingiser. 1978. IMPROVED PROCESSING WITH METERED-STARVED FEEDING OF EXTRUDERS. Plastics Engineering 34, no. 6: 45-49.

Mohan Rao, S., H. L. Toor. 1987. Heat transfer from a particle to a surrounding bed of particles. Effect of size and conductivity ratios. Industrial & Engineering Chemistry Research 26, no. 3 (03) : 469-74.

Mohan Rao, S., H. L. Toor. 1984. HEAT TRANSFER BETWEEN PARTICLES IN BEDS. In Heat transfer - 1984. AIChE sponsored session papers accepted for presentation at the 22nd national heat transfer conference.23,294-298.

Mohan Rao, S. 1., H. L. 1. Toor. 1987. Heat transfer from a particle to a surrounding bed of particles. Effect of size and conductivity ratios. Industrial & Engineering Chemistry Research 26, no. 3 (03) : 469-74.

Molerus, O. 1997. Heat transfer in moving beds with a stagnant interstitial gas. International Journal of Heat and Mass Transfer 40, no. 17 (10) : 4151-9.

Mount III, Eldridge M. 2005. A review of melting mechanisms in single screw extrusion. In Society of plastics engineers annual technical conference 2005, ANTEC 2005;289-295.

Mount, E. M. I., J. G. Watson, and C. I. Chung. 1979. NEW PLASTICATING MODEL AND EXPERIMENTAL VERIFICATION FOR SOLID POLYMERS AT PROCESSING CONDITIONS. American Society of Mechanical Engineers, Applied Mechanics Division, AMD : 176-180.

Moysey, P. A., M. R. Thompson. 2007. Determining the collision properties of semi-crystalline and amorphous thermoplastics for DEM simulations of solids transport in an extruder. Chemical Engineering Science 62, no. 14: 3699-3709.

Moysey, P. A., M. R. Thompson. 2007. Solids compaction and conveying in a single-screw extruder by discrete particle modeling. In Society of plastics engineers annual technical conference: Plastics encounter at ANTEC 2007;424-428.

Moysey, P. A., M. R. Thompson. 2006. Plastic contact mechanics and its impact on DEM simulations of solds transport in extruders. In Society of plastics engineers annual technical conference 2006, ANTEC 2006;882-886.

Moysey, P. A., M. R. Thompson. 2004. Investigation of solids transport in a single-screw extruder using a 3-D discrete particle simulation. Polymer Engineering and Science 44, no. 12: 2203-2215.

Moysey, P. A. 1., M. R. 1. Thompson. 2007. Determining the collision properties of semi-crystalline and amorphous thermoplastics for DEM simulations of solids transport in an extruder. Chemical Engineering Science 62, no. 14: 3699-709.

Moysey, P. A. 1., M. R. 1. Thompson. 2005. Modelling the solids inflow and solids conveying of single-screw extruders using the discrete element method. Powder Technology 153, no. 2 (05/16) : 95-107.

Moysey, P. A. 1., M. R. 1. Thompson. 2004. Investigation of solids transport in a single-screw extruder using a 3-D discrete particle simulation. Polymer Engineering and Science 44, no. 12 (12) : 2203-15.

Moysey, "Discrete Element Simulation of the Solids Conveying Zone of a Single-Screw Extruder", Ph.D. thesis, McMaster University, 2007

Pokluda, Ondrej, Celine T. Bellehumeur, and John Vlachopoulos. 1997. Modification of Frenkel's model for sintering. AICHE Journal 43, no. 12: 3253-3256.

Qian, Bainian, Costas G. Gogos. 2000. Importance of plastic energy dissipation (PED) to the heating and melting of polymer particulates in intermeshing co-rotating twin-screw extruders. Advances in Polymer Technology 19, no. 4: 287-299.

Qian, Bainian, David B. Todd, and Costas G. Gogos. 2003. Plastic energy dissipation and its role on heating/melting of single-component polymers and multi-component polymer blends. Advances in Polymer Technology 22: 85-95.

Qian, Bainian, David B. Todd, and Costas G. Gogos. 2003. Plastic energy dissipation and its role on heating/melting of single-component polymers and multi-component polymer blends. Advances in Polymer Technology 22, no. 2: 85-95.

Qian, Bainian, David B. Todd, and Costas G. Gogos. 2003. Plastic energy dissipation and its role on heating/melting of single-component polymers and multi-component polymer blends. Advances in Polymer Technology 22, no. 2: 85-95.

Qiu, D. Q. 1., P. 1. Prentice. 1998. Influence of pressure on bulk density of polymer solid granules at different temperatures. Advances in Polymer Technology 17, no. 1: 23-36.

Rao, S. M., H. L. Toor. 1984. Heat transfer between particles in packed beds. Industrial and Engineering Chemistry, Fundamentals 23, no. 3 (08) : 294-8.

Rauwendaal, Chris. 2005. Recent advances in barrier screw design. Plastics, Additives and Compounding 7, no. 5: 36-39.

Rauwendaal, Chris. 2001. Polymer extrusion. Cincinnati, OH: Hanser Gardner Publications.

Rauwendaal, Chris. 1996. Comparison of two melting models. Advances in Polymer Technology 15, no. 2: 135-144.

RC, DONOVAN. 1971. THEORETICAL MELTING MODEL FOR PLASTICATING EXTRUDERS. 11, no. 3: 247-57.

Riley, G. S. 1., G. R. 1. Mann. 1972. Effects of particle shape on angles of repose and bulk densities of a granular solid. Materials Research Bulletin 7, no. 2 (02) : 163-70.

Spalding, M. A., K. S. Hyun. 1995. Coefficients of dynamic friction as a function of temperature, pressure, and velocity for several polyethylene resins. Polymer Engineering and Science 35, no. 7: 557.

Spalding, M. A. 1., Kun Sup Hyun1, and K. R. 1. Hughes. 1997. Stress distribution in solid polymer compacts. Journal of Reinforced Plastics and Composites 16, no. 13: 1231-41.

Spalding, Mark A., Kun S. Hyun, Donald E. Kirkpatrick, and Steven R. Jenkins. 1995. Coefficients of dynamic friction and the mechanical melting mechanism for vinylidene chloride copolymers. In Part 1 (of 3)260-267. Boston, MA, USA: Soc of Plastics Engineers, Brookfield, CT, USA.

Spalding, Mark A., Donald E. Kirkpatrick, and Kun S. Hyun. 1993. Coefficients of dynamic friction for low density polyethylene. Polymer Engineering and Science 33, no. 7: 423-430.

Spalding, Mark A., Donald E. Kirkpatrick, and Kun S. Hyun. 1993. Coefficients of dynamic friction for low density polyethylene. Polymer Engineering and Science 33, no. 7: 423-430.

Sundstrom, D. W. 1978. SOFTENING RATES FOR POLYSTYRENE UNDER SHEAR CONDITIONS. Polymer Engineering and Science 18, no. 5: 422-426.

Syrjala, S. 1. 2000. A new approach for the simulation of melting in extruders. International Communications in Heat and Mass Transfer 27, no. 5 (07) : 623-34.

Smith, A. Neil, "Melting behaviour of polyethylenes synthesized with Ziegler-Natta and constrained geometry catalysts" Thesis (M.A.Sc.) -- McMaster University department of chemical engineering ,Canada(1999)

Tadmor Zehev, Ilan Duvdevani, Imrich Klein 1967,Melting in plasticating extruders theory and experiments, polymer engineering and science (p 198-217)

Tadmor, Zehev, and Costas G. Gogos. 2006. Principles of polymer processing. Hoboken, N.J.: Wiley-Interscience.

Tehranian, F. 1., M. A. Abdou, and M. S. Tillack. 1994. Effect of external pressure on particle bed effective thermal conductivity. In Sixth international conference on fusion reactor materials (ICFRM-6) 885-90.

Thompson, M. R., G. Donolan, and J. P. Christiano. 2000. Melting mechanism of a starved-fed single-screw extruder for calcium carbonate filled polyethylene. Polymer Engineering and Science 40, no. 9: 2014-2026.

Tinson, Arthur R., “A study of the surface tension of polymer melts and its role in particle coalescence for rotational molding” Thesis (M.A.Sc.) -- McMaster University department of chemical engineering ,Canada(2004).

Vargas, Watson L., J. J. McCarthy. 2002. Conductivity of granular media with stagnant interstitial fluids via thermal particle dynamics simulation. International Journal of Heat and Mass Transfer 45, no. 24: 4847-4856.

Vargas, Watson L., J. J. McCarthy. 2002. Stress effects on the conductivity of particulate beds. Chemical Engineering Science 57, no. 15: 3119-3131.

Vargas, Watson L., J. J. McCarthy. 2001. Heat conduction in granular materials. AICHE Journal 47, no. 5: 1052-1059.

Vlachopoulos, J., D. Strutt. 2003. Polymer processing. Materials Science and Technology 19, no. 9: 1161-1169.

Vlachopoulos, J., David Strutt. 2004. The role of rheology in polymer extrusion. In Extrusion minitec and conference: From basics to recent developments107-132

White, James L., H. Potente, and U. Berghaus. 2003. Screw extrusion : Science and technology. Munich ; Cincinnati: Hanser.

Yusuf, Rahel, Morten C. Melaaen, and Vidar Mathiesen. 2005. Convective heat and mass transfer modeling in gas-fluidized beds. Chemical Engineering and Technology 28, no. 1: 13-24.

Yagi, D. Kunii: ,1957,Studies on the Effective Thermal Conductivities in Packed Beds. A.I.Ch.E. Journal 3, p.373

Zhu, F., A. C. -. Wong, R. Liu, and T. Liu. 1997. Breakup of solid bed in melting zone of single screw extruder. Part 2 - strength of solid bed and experimental results. Plastics, Rubber and Composites Processing and Applications 26: 343-350.

Zitzenbacher,G and G. R. Langecker 2005,A New Plasticating Model for Amorphous and Semi-crystalline Polymers in Single Screw Extruders ,International Polymer Processing, Page 360-368